


**NGU Report 2010.030**

**HeatBar Final Report 2010  
Basement characterization  
Barents Sea and Svalbard**



Report no.: 2010.030		ISSN	Grading: Open	
Title: HeatBar Final Report 2010, Basement Heat Generation and Heat Flow in the western Barents Sea - Importance for hydrocarbon systems				
Authors: Christophe Pascal, Niels Balling Cécile Barrère, Børre Davidsen, Jörg Ebbing, Harald Elvebakk, Melanie Mesli, David Roberts, Trond Slagstad and Bjørn Willemoes-Wissing			Client: Statoil ASA NFR	
County: Finnmark			Commune: Kautokeino, Båtsfjord	
Map-sheet name (M=1:250.000) Vadsø, Nordreisa			Number of pages: 91      Price (NOK): Map enclosures:	
Fieldwork carried out: 2006-2009	Date of report: 30.11.2010	Project no.: 3127.00	Person responsible: 	
<p>Summary:</p> <p>The HeatBar project aimed to determine the relative proportion of heat originating in the basement of the western Barents Sea and, as such, followed the methodologies and scientific approach developed in the course of the 2005-2008 Kontiki Project. We proposed to shed new lights on the thermal state of the basins of the western Barents Sea by (1) determining the heat flow and the relative content in heat-producing elements of the basement onshore northern Norway, (2) building 3D structural models of the basement offshore based on extensive geophysical information and (3) building 3D thermal models of the basins offshore. The present report summarises the work accomplished in the framework of the project since 2006.</p> <p>The onshore basement in Finnmark has been extensively sampled for geochemical analyses and the new heat-production data shows, in general, higher values for the Caledonian nappes (i.e. 1-2 <math>\mu\text{W}/\text{m}^3</math>) than for the Precambrian basement (i.e. <math>\sim 0.1 \mu\text{W}/\text{m}^3</math>). Six drillholes have been logged in Finnmark and Svalbard and, when available, core material has been used for measuring thermal conductivities. We obtained convincing results only for two of the boreholes. Results from the Vuoddašjav'ri borehole, Central Finnmark, suggest a steady-state heat flow value of <math>\sim 40 \text{ mW}/\text{m}^2</math>. In contrast, we derived a steady-state heat flow value of <math>\sim 80 \text{ mW}/\text{m}^2</math> for the Sysselmannbreen borehole on Svalbard. Results from the very first datings of offshore basement samples are also presented. Dense gravity and magnetic datagrids constrained by available seismics have been used to determine the nature of the basement underlying offshore sedimentary basins and to build 3D structural models. Finally, we used the geophysical crustal model together with available thermal constraints in order to build a 3D thermal model of the SW Barents Sea. Although absolute temperature and heat flow values remain unconstrained, two first-order conclusions can be drawn. Firstly, subcrustal temperatures appear to increase when approaching the continent-ocean boundary. The most robust result of the modelling is the strong control that basement topography exerts on the heat flow pattern, maxima and minima being predicted at basement highs and sedimentary basins respectively. Our modelling suggests that a difference of up to <math>\sim 20 \text{ mW}/\text{m}^2</math> can exist depending on basement topography. It is thus recommended that variation of basement heat flow according to basement topography is used instead of assuming constant basement heat flow in basin modelling studies.</p>				
Keywords: Geofysikk (Geophysics)	Kontinentalsokkel (Continental shelf)	Tolkning (Interpretation)		
Varmestrøm (Heat flow)	Magnetometri (Magnetometry)	Berggrunnsgeologi (Bedrock geology)		
Petrofysikk (Petrophysics)	Gravimetri (Gravimetry)	Fagrapport (Scientific report)		



## CONTENTS

1	INTRODUCTION .....	7
2	THERMAL LOGGING IN 2009.....	9
	2.1 Introduction .....	9
	2.2 Vuoddašjav'ri.....	9
	2.3 Bidjovagge, Dh 2008-01 .....	14
3	HEAT FLOW DETERMINATIONS IN FINNMARK AND SVALBARD .....	19
	3.1 Introduction .....	19
	3.2 Thermal conductivity measurements.....	20
	3.3 Båtsfjordfjellet.....	20
	3.4 Vuoddašjav'ri.....	26
	3.5 Longyearbyen (CO <sub>2</sub> -Dh1 drillhole).....	29
	3.6 Sysselembreen, Svalbard.....	33
	3.7 Conclusions .....	38
4	RADIOGENIC HEAT PRODUCTION .....	39
	4.1 Introduction .....	39
	4.2 Sources of heat production data .....	39
	4.3 Radiogenic heat production rates of Norwegian bedrock .....	40
	4.4 Summary of previous work .....	40
	4.5 Heat production vs. lithology, composition and tectonic setting .....	41
	4.5.1 Lithology and chemical composition .....	41
	4.5.2 Tectonic setting .....	46
	4.6 Heat production vs. age and metamorphic grade .....	48
	4.6.1 Age .....	48
	4.6.2 Metamorphic grade (crustal depth) .....	48
	4.7 Heat production in Finnmark, northern Norway .....	49
5	GEOCHRONOLOGICAL STUDIES OF OFFSHORE BASEMENT SAMPLES .....	53
	5.1 Overview .....	53
	5.2 Results .....	54
6	3D DENSITY AND MAGNETIC CRUSTAL CHARACTERISATION OF THE SOUTHWESTERN BARENTS SHELF .....	57
	6.1 Introduction .....	57
	6.2 Modelling concept.....	58
	6.3 Data .....	60
	6.3.1 Petrophysical data .....	61
	6.3.2 Geometric constraints from seismic experiments .....	61
	6.4 Modelling results.....	65
	6.4.1 Modelled densities.....	65
	6.4.2 Modelled susceptibilities.....	65
	6.4.3 Depth to top basement.....	69
	6.4.4 Depth to the crust-mantle boundary .....	70
	6.5 Basement characterisation and basin characteristics.....	72
	6.5.1 Onshore .....	73
	6.5.2 Coastal area .....	73
	6.5.3 COT = elongated marginal zone .....	73
	6.5.4 Central zone.....	73
	6.5.5 Eastern and northern zones .....	74
	6.6 Conclusion.....	74
7	3D THERMAL MODELLING OF THE SW BARENTS SEA.....	75

7.1	Introduction .....	75
7.2	Modelling strategy .....	75
7.3	Modelling results .....	77
7.4	Summary .....	80
8	CONCLUSIONS .....	81
9	REFERENCES .....	82
10	APPENDIX A.....	90

# 1 INTRODUCTION

Understanding heat flow variation in sedimentary basins is of vital importance for the success of petroleum exploration campaigns. While oil industry has invested much in understanding the thermal input related to lithospheric thinning, it appears that comparatively little has been done on the subject of heat flow from different basement types. In 2004, Statoil and NGU decided to establish the Kontiki Project (Continental Crust and Heat Generation In 3D, Olesen et al. 2007) to improve the knowledge on the varying heat flow on the Norwegian continental shelf. Kontiki was terminated in 2007 and the HeatBar Project is a sister project aiming to apply a similar approach to the western Barents Sea area.

Approximately half of the heat flow in thermally-relaxed sedimentary basins (i.e. older than 60 Myr) originates in the crystalline basement while the other half comes from the mantle (e.g. Ritter et al. 2004). The heat production within the crystalline basement depends on the content of radioactive elements such as potassium, uranium and thorium. The content of these elements shows a wide variation within the mainland crystalline basement of Norway. Partly due to a lack of systematic data compilation, the knowledge of the basement rock composition below the Norwegian continental shelf is very poor or almost non-existing in large areas.

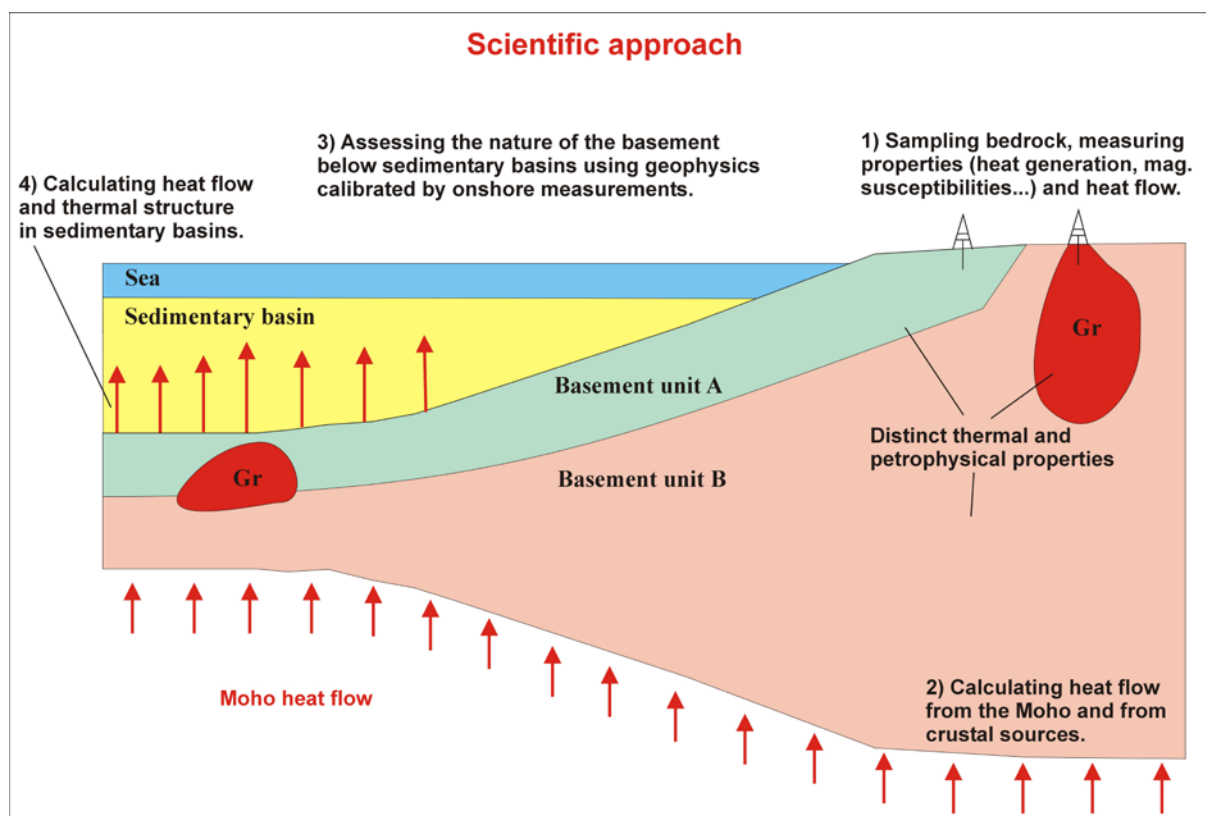


Figure 1.1. The Kontiki and HeatBar scientific approach.

Relatively acidic rocks of the Precambrian gneisses and granites generate more heat than intermediate-mafic rocks within the Caledonian nappes and high-grade metamorphic units (e.g. the Lofoten gneiss complex). The latter rock units are representative for middle and lower crust. While mafic rocks within underplated bodies and other mafic igneous rocks

provide a transient heat pulse at the time of emplacement, they have a low radioactive heat production. Assuming a constant heat production from the continental crust in basin modelling studies offshore Norway and other basins in the world will lead to considerable errors in the calculation of the temperature regime in sedimentary basins. Analysis of offshore and onshore well data is a fundamental step to obtain detailed input for heat flow and thermal gradients.

The present project aims at compiling lithochemical information on basement rocks in northern Norway with emphasis on characterizing the U, Th and K content (Fig. 1.1). Geophysical information such as seismic, aeromagnetic, and gravity data will, together with well penetrations of basement, provide a basis for extending this information below the offshore sedimentary basins. The Geological Survey of Norway (NGU) holds complete gravity and aeromagnetic databases from the whole of the Norwegian mainland and offshore areas in addition to detailed information on the mainland bedrock geology. The onshore-offshore geophysical interpretations will also be constrained by geochemical analysis and age dating of basement core samples obtained from offshore exploration wells. Finally, the whole set of informations helps to constrain 3D thermal models of the offshore basins. This report presents the final results of the HeatBar project, preliminary but complementary results can be found in Pascal et al. (2008).



## 2 THERMAL LOGGING IN 2009

Harald Elvebakk, NGU

### 2.1 Introduction

Thermal logging was carried out in two boreholes in Finnmark in 2009. A 767 m deep borehole was drilled close to the lake Vuoddašjav'ri between Kautokeino and Karasjok. At Bidjovagge a 391 m borehole was logged. This hole was drilled in 2008 by a mineral prospecting company, IGE Nordic. NGU got access to this borehole. Table 2.1 shows borehole data. The logging was carried out 03.07.09 – 08.07.09 by Harald Elvebakk, NGU.

**Table 2.1. Borehole data.**

Borehole	North wgs 84	East wgs 84	Zone	masl	Logging date	Incl.	Diam (cm)	Depth (m)
Vuoddašjav'ri	7696752	382955	35 W	357	03.07.09	Vertical	6.0	767
2008-01 Bidjovagge	7688793	558671	35 V	608	08.07.09	77 <sup>0</sup>	6.0	391

Besides temperature, these parameters were logged: water conductivity, natural gamma radiation, resistivity (SHN and LON), seismic velocity (P- and S-wave), pH and Eh.

The Water Quality Sonde (WQS), Robertson Geologging ltd. with high resolution sensors was used for the temperature measurements, see below.

#### WQS

Parameter	Range	Accuracy	Resolution	Time constant
Pressure	0 – 2000 dbar	0.05 %	0.0015 %	50 ms
Temperature	-1 – 50 °C	0.005 °C	0.001 °C	50 ms
Conductivity				
Salt water	0 – 64 mS/cm	0.005 mS/cm	0.001 mS/cm	50 ms
Fresh water	0 – 6400 µS/cm	1 µS/cm	0.1 µS/cm	50 ms
Oxygen	0 – 50 ppm	0.1 ppm	0.01 ppm	3 s
pH	0 – 14 pH	0.01 pH	0.001 pH	3 s
Redox potential	+/- 1000 mV	1 mV	0.1 mV	3 s
Nitrate, NO <sub>3</sub>	0 – 100 mg/l			

#### TCN

Parameter	Range	Accuracy
Temperature	0 – 70 °C	0.5 °C
Conductivity	0 – 50,000 µS/cm	+/- 2.5 % at 500 µS/cm
Natural Gamma	50 mm x 25 mm NaI scintillation crystal	

### 2.2 Vuoddašjav'ri

Figures 2.1 and 2.2 show the borehole location close to the lake Vuoddašjav'ri. The borehole was drilled to 767 m depth. The cores showed highly crushed rock below 700 m. The logging tools stopped at 675 m depth and 100 m of the borehole was not logged.



below 300 m) the gradient is ca 11 °C/km. On the 20 m interval gradient there are some local variations which can be caused by water inflow or changes in the thermal conductivity.

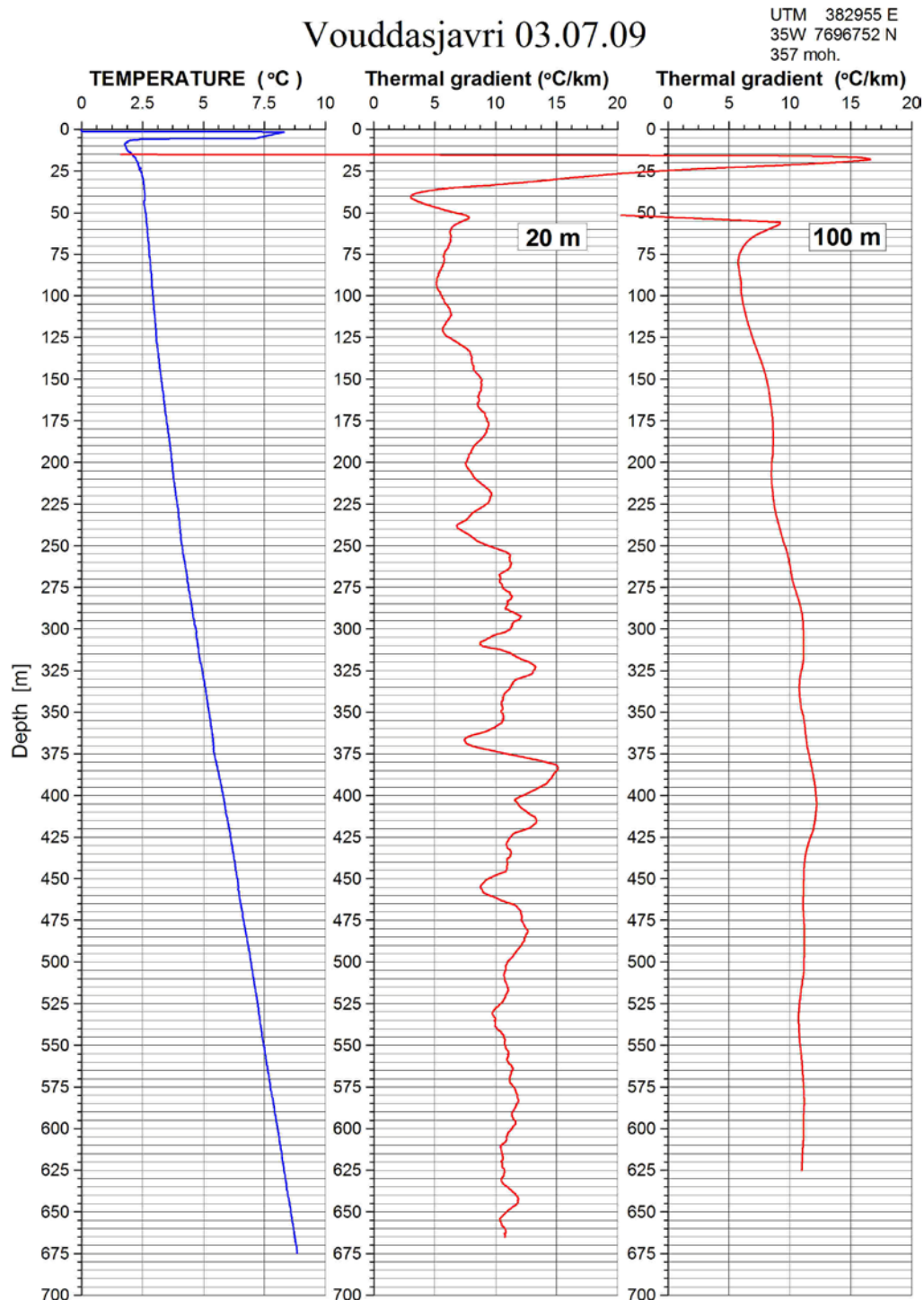


**Figure 2.3. Temperature and thermal gradient in the Vouddasjavri drill hole.**

Figure 2.4 shows temperature, water conductivity, natural gamma radiation, resistivity and seismic velocities (P- and S-wave). Water conductivity is low and constant. Very low conductivity in the upper 25 m is probably caused by open fractures and water inflow.

## Vuoddasjavri, Kautokeino

UTM 591632 E  
35V 7828977 N  
357 masl.

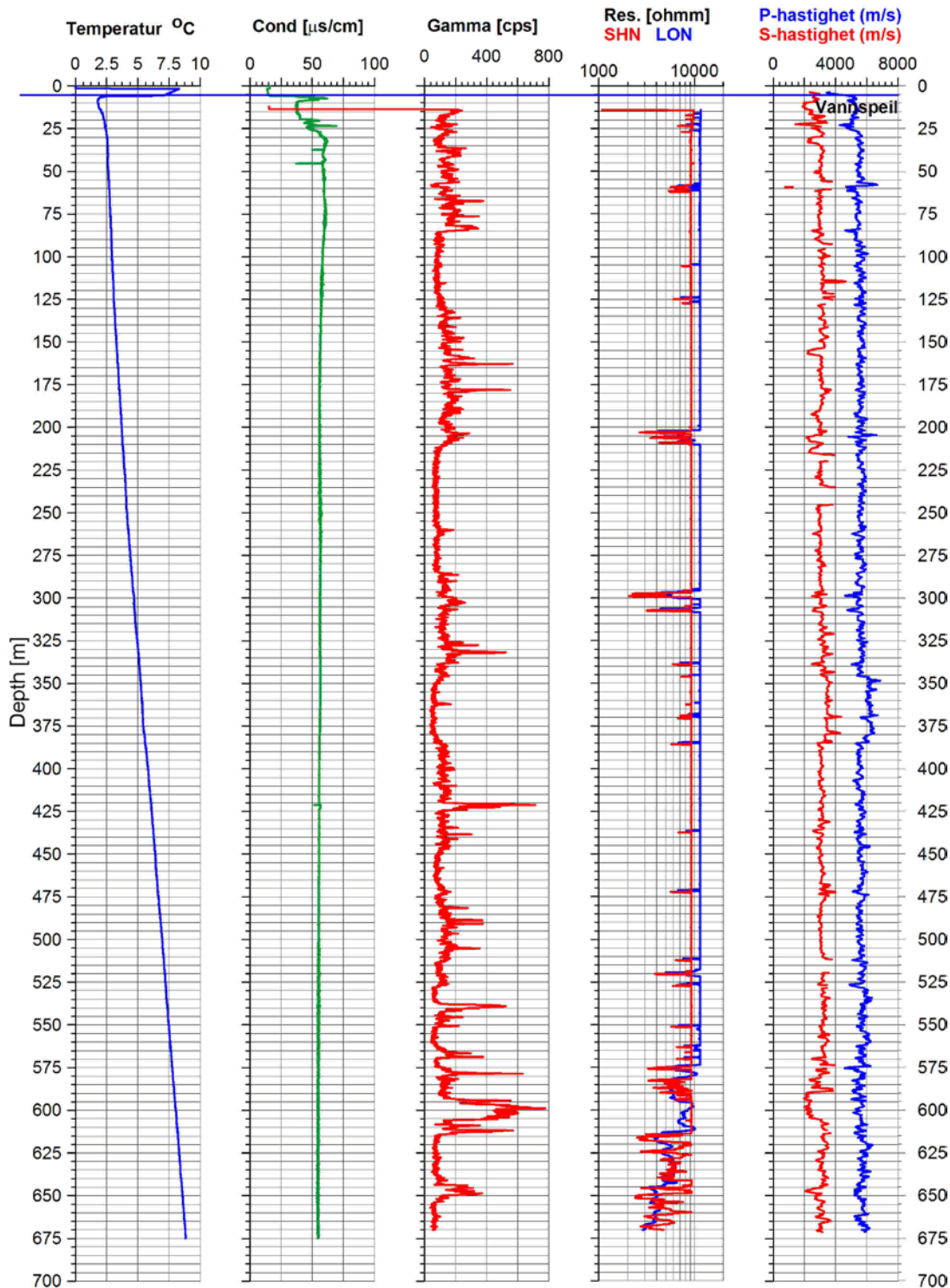


**Figure 2.4.** Vuoddasjav'ri borehole. Temperature, conductivity, natural gamma, resistivity and seismic velocity (P-and S-wave).

The natural gamma log correlates well with the lithological units. The lowest gamma radiation (below 100 cps) is seen in amphibolites while gneisses produce radiations of 150 – 200 cps. Some high radiation peaks (600 – 800 cps) are probably caused by pegmatite veins

and granitic gneisses containing radioactive minerals or an increased content of feldspar (40K).

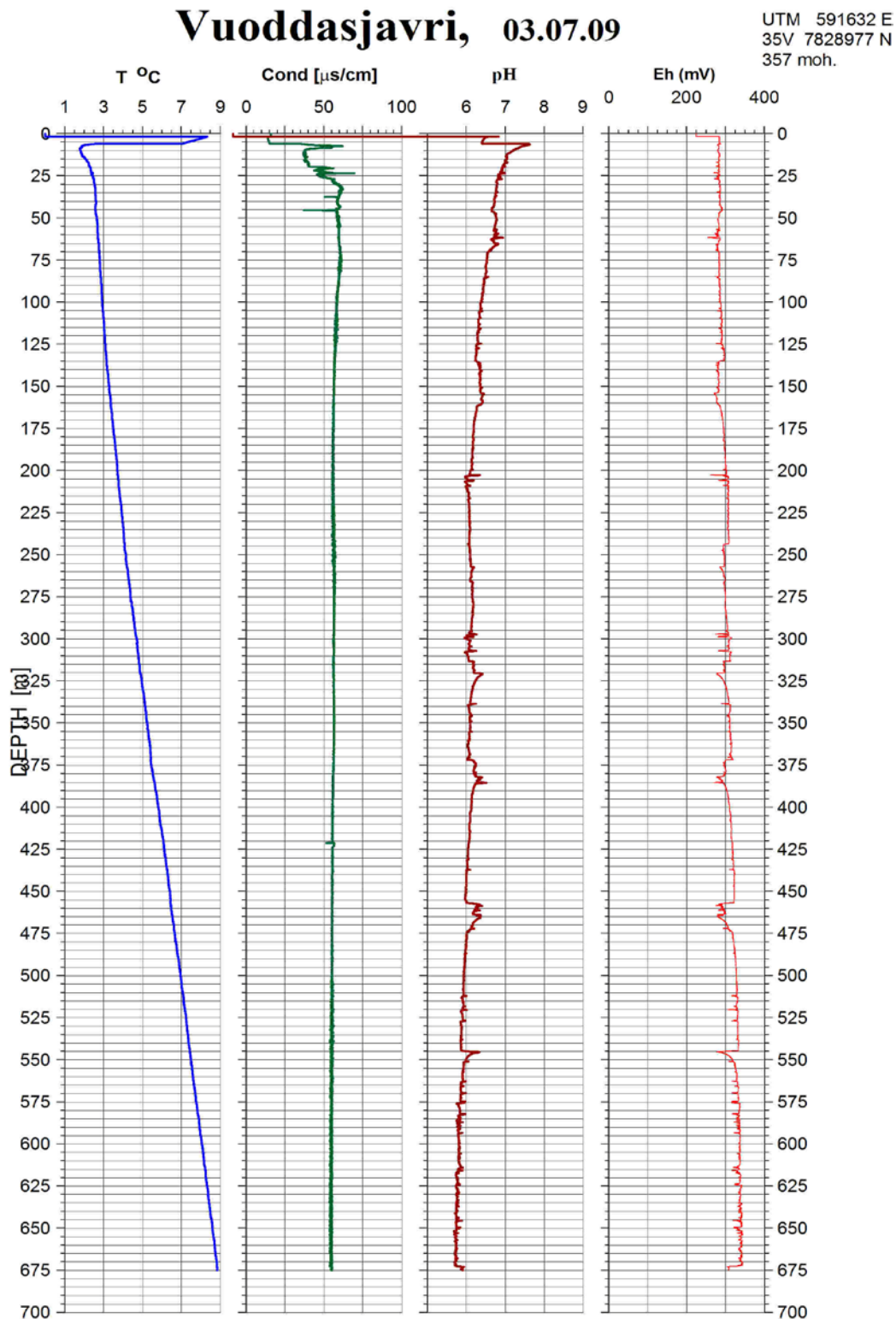


**Figure 2.5. Vuoddasjav'ri borehole. Temperature, conductivity, pH and Eh.**

Electrical resistivity in the gneisses and the amphibolites is very high (> 10.000 ohm.m). The RG resistivity sonde can measure resistivity values up to 10.000 ohm.m. Consequently the

resistivity log follows a straight line along the 10.000 ohm.m level. However, some low resistivity areas can be observed and are probably caused by fractured rock. Below 575 m depth the rock seems to be highly fractured as reflected by the low resistivity. The seismic P-velocity is about 5500 m/s both in gneiss and amphibolite. Low P-velocity correlates with low resistivity and fractured zones. Figure 2.5 shows temperature, water conductivity, pH and Eh.

### 2.3 Bidjovagge, Dh 2008-01

Figures 2.6 and 2.7 show the borehole location at Bidjovagge. The borehole was drilled to 391 m depth. The main rock types are gabbro and felsites. Parts of the borehole contain sulphides and graphite. Thanks to Boye Flood and Geologiske Tjenester AS for sharing the geological log.



Figure 2.6. Overview map and borehole location at Bidjovagge.



Figure 2.7. Bidjovagge Dh 2008-01, logging.

Dh 2008-01, Bidjovagge 08.07.09

UTM 558593 E  
35W 7688671 N  
608 masl.

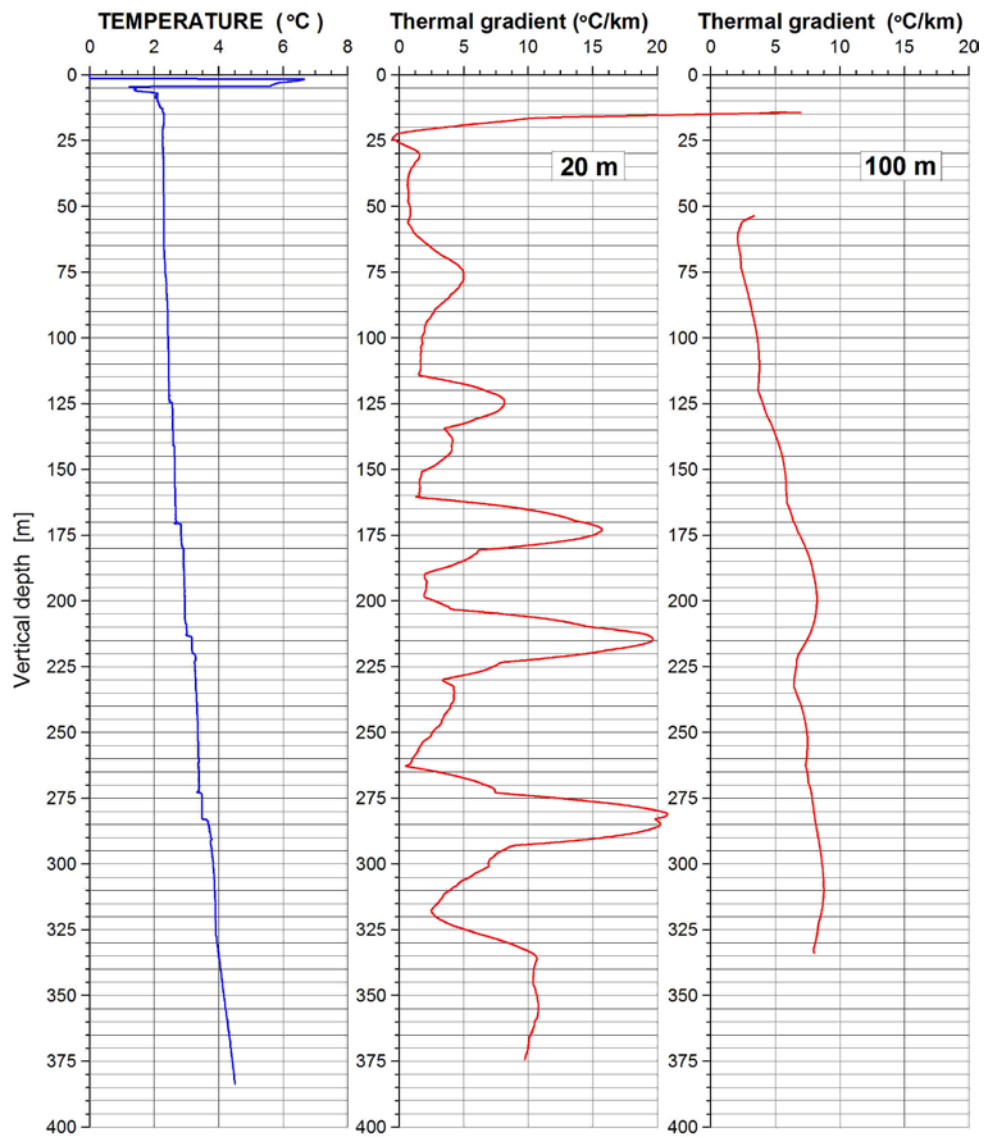


Figure 2.8. Dh 2008-01, Bidjovagge. Temperature and thermal gradient.

Figure 2.8 shows the temperature log and the thermal gradient in Dh 2008-01, Bidjovagge. The bottom temperature at 383.6 m vertical depth is 4.5 °C. The thermal gradient is low, 7-8 °C/km. There are several changes (increase) in the temperature which is clearly seen on the 20 m interval gradient curve. Most likely these changes are caused by water inflow in the borehole. A neighbour borehole was artesian with water flowing out on the surface.

Figure 2.9 shows temperature, conductivity, natural gamma, resistivity, and seismic velocity in Dh 2008-01, Bidjovagge. The temperature log is described in the previous section. The water conductivity is high and increase even more in the deepest part of the borehole. There is abundant graphite and metal sulphides in the rock in this area and this could influence water conductivity.

The gamma log clearly indicates two main rock types. Gabbro and metagabbro have very low and constant gamma radiation, 30 – 50 cps. In the felsites the gamma radiation is much higher, 200 - 250 cps. The radiation is anyway variable and peaks of 1600 cps are observed at 300 m depth.

The resistivity is high in the gabbro, up to 10.000 ohm.m. Inside the gabbro there might be several schlieren of pyrite, chalcopyrite and graphite lowering the resistivity to almost zero. In the felsites the resistivity is below 100 ohm.m and most of the sulphides and graphite are found in this type of rock.

The P-velocities in gabbros and felsites are 6200 m/s 5400 m/s respectively. Variations (decrease) in the velocity might be caused by fractures.

Figure 2.10 shows temperature, water conductivity, pH and Eh.



# Dh 2008-01 Bidjovagge

UTM 558593 E  
35W 7688671 N  
608 masl.

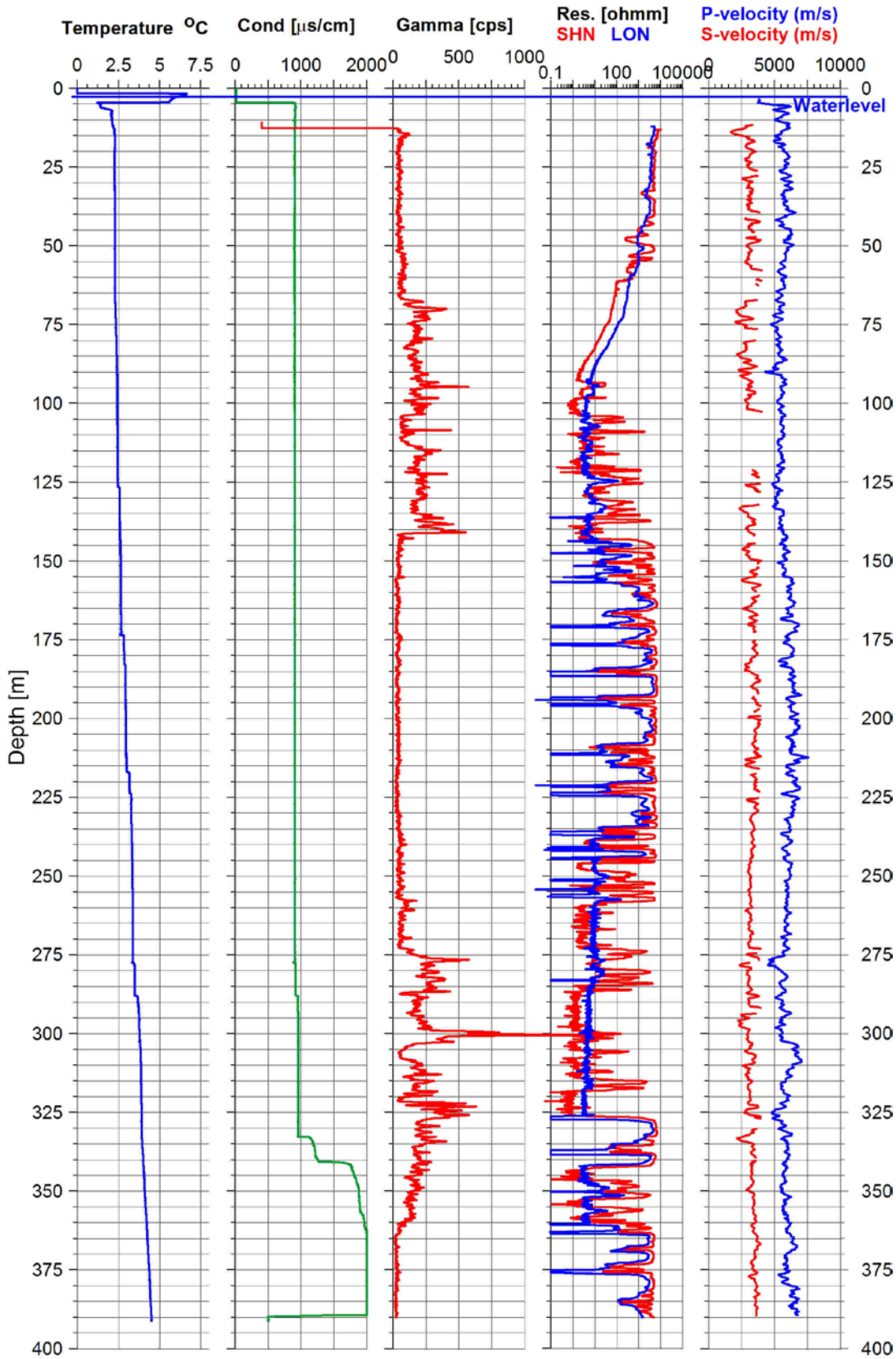


Figure 2.9. Dh 2008-01, Bidjovagge. Temperature, conductivity, natural gamma, resistivity and seismic velocity (P-and S-wave).

# Dh 2008-01, Bidjovagge

UTM 558671 E  
35V 7688793 N  
608 masl.

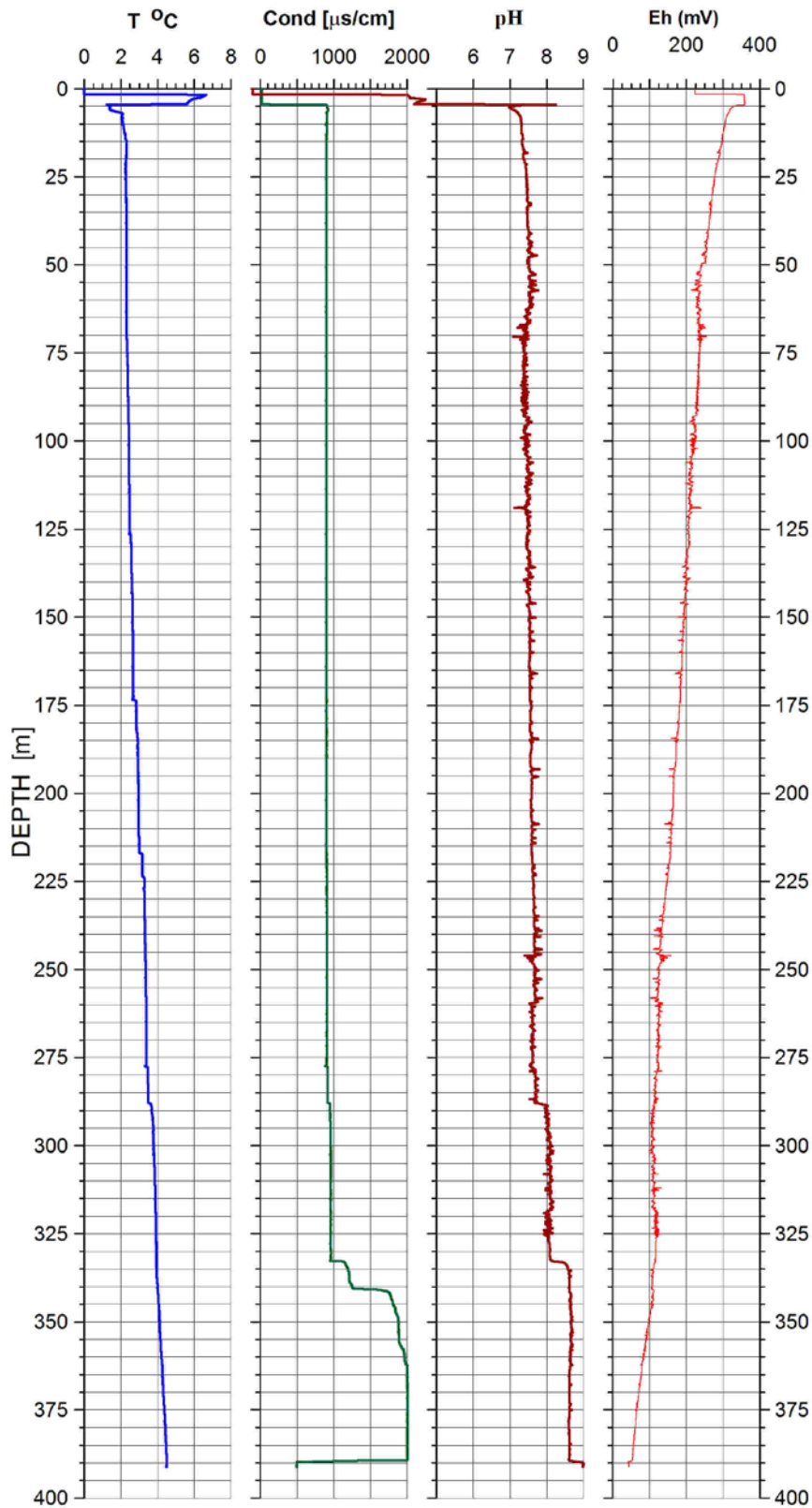


Figure 2.10. Dh 2008-01, Bidjovagge. Temperature, conductivity, pH and Eh.

### 3 HEAT FLOW DETERMINATIONS IN FINNMARK AND SVALBARD

Christophe Pascal, Harald Elvebakk, Melanie Mesli & Bjørn Willemoes-Wissing, NGU  
Niels Balling, University of Aarhus, Denmark

#### 3.1 Introduction

In the course of the HeatBar project we studied four drillholes for heat flow calculations in Finnmark (Fig. 3.1, Table 3.1). Two of them were drilled and cored during the project (i.e. Båtsfjordfjellet and Vuoddašjav'ri) whereas the two remaining ones were drilled for mining exploration purposes (i.e. Bjørnevatn and Bidjovagge). Unfortunately, the two mining boreholes showed very noisy temperature logs and no core material was available from them (Pascal et al. 2008 and Fig. 2.8) hampering any attempt to calculate reliable heat flow values.

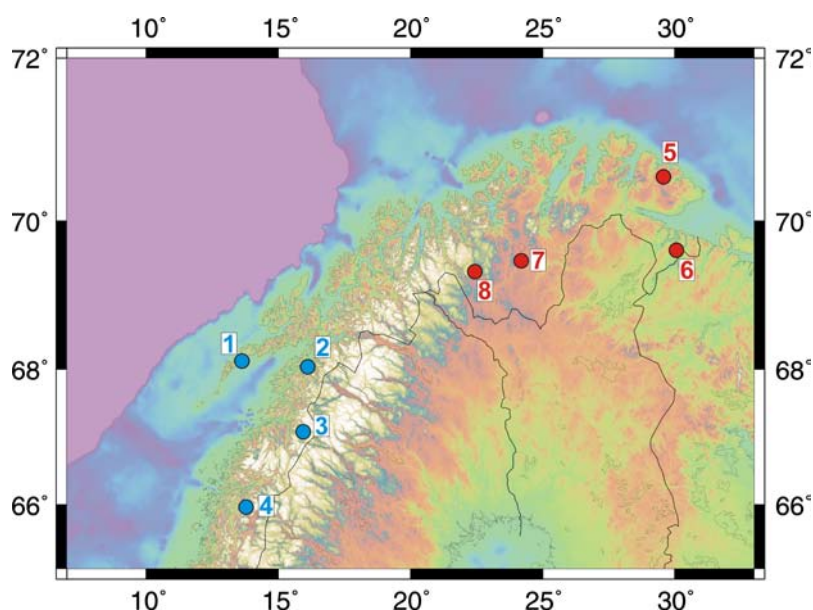


**Figure 3.1.** Heat flow sites in northern Norway: blue and red dots represent Kontiki (Olesen et al. 2007) and HeatBar boreholes respectively. 1) Leknes, 2) Drag, 3) Sulitjelma, 4) Bleikvassli, 5) Båtsfjordfjellet, 6) Bjørnevatn 7) Vuoddašjav'ri and 8) Bidjovagge.

**Table 3.1.** Drillholes studied in the HeatBar project.

Site	UTM Zone	Coord. <sup>1</sup>	Elevation (m)	TD (m) <sup>2</sup>	Dip (°) <sup>3</sup>
Bidjovagge	35V	558671 7688793	608	384	77
Bjørnevatn	36V	384849 7729422	125	384	48
Båtsfjordfjellet	35V	591632 7828977	331	592	90
Longyearbyen (CO <sub>2</sub> _Dh1)	33X	512445 8684766	4	440	89
Sysselmannbreen	33X	524562 8617240	423	1035	88
Vuoddašjav'ri	35W	382955 7696752	357	675	90

<sup>1</sup>WGS84

<sup>2</sup>Logged depth

<sup>3</sup>From horizontal

In the framework of other collaborative projects, NGU also measured temperatures in two recently drilled boreholes on Svalbard (Elvebakk 2008, Elvebakk et al. 2008, Table 3.1) where core samples were made available for thermal conductivity measurements. In this chapter we summarise the heat flow studies carried out during the HeatBar project and present its final results.

### 3.2 Thermal conductivity measurements

Thermal conductivity of rock samples is measured with a transient method described in detail in Kalskin Ramstad et al. (2008). A constant heat flow is induced to the top of the samples. The heat mechanism is radiation and the heat source, with a constant temperature of  $300 \pm 2^\circ\text{C}$ , is placed 10 mm above the top surface of the sample. The sample is insulated at all its other faces. Temperature is measured at the base of the sample. Thermal diffusivity ( $\kappa$ ) is estimated from the temperature – time plot, and the thermal conductivity ( $k$ ) is calculated from thermal diffusivity, measured density ( $\rho$ ) and assumed specific heat capacity ( $c_p$ ) of the sample:

$$k = \rho c_p \kappa \quad (3.1)$$

The theory of this method is described in Carslaw & Jaeger (1959) and Middleton (1993). Quality controls are carried out by measurements on the standard material Pyroceram 9606. The apparatus at NGU was improved in December 2005 and the error of the thermal diffusivity measurements is now within  $\pm 5\%$ .

### 3.3 Båtsfjordfjellet

The Båtsfjordfjellet borehole was drilled in December 2005 by the Finnish company SMOY. The borehole was cored from top to bottom and reached 800 m TD, additional information is given in Table 3.1. The borehole was logged for the first time August 26<sup>th</sup> 2006 and appeared to be blocked at ~592 m depth. We logged again the well August 26<sup>th</sup> 2007 three weeks before SMOY attempted to re-open and deepen the well. Unfortunately the borehole collapsed at ~620 m depth September 27<sup>th</sup> 2007.

Logged temperatures in the well appeared to be extremely low, reaching  $4^\circ\text{C}$  at ~600 m depth and a minimum value of  $1.75^\circ\text{C}$  at ~100m (Fig. 3.2). Accordingly the thermal gradient is also low varying from negative values above 100 m depth to  $6^\circ\text{C}/\text{km}$  on average in the deepest parts. In more detail strong variations of the thermal gradient (i.e. from 1 to  $13^\circ\text{C}/\text{km}$ , Fig. 3.2.) are seen below 400 m depth. These are probably the result of water circulation through small fractures and/or drastic changes in thermal conductivity.

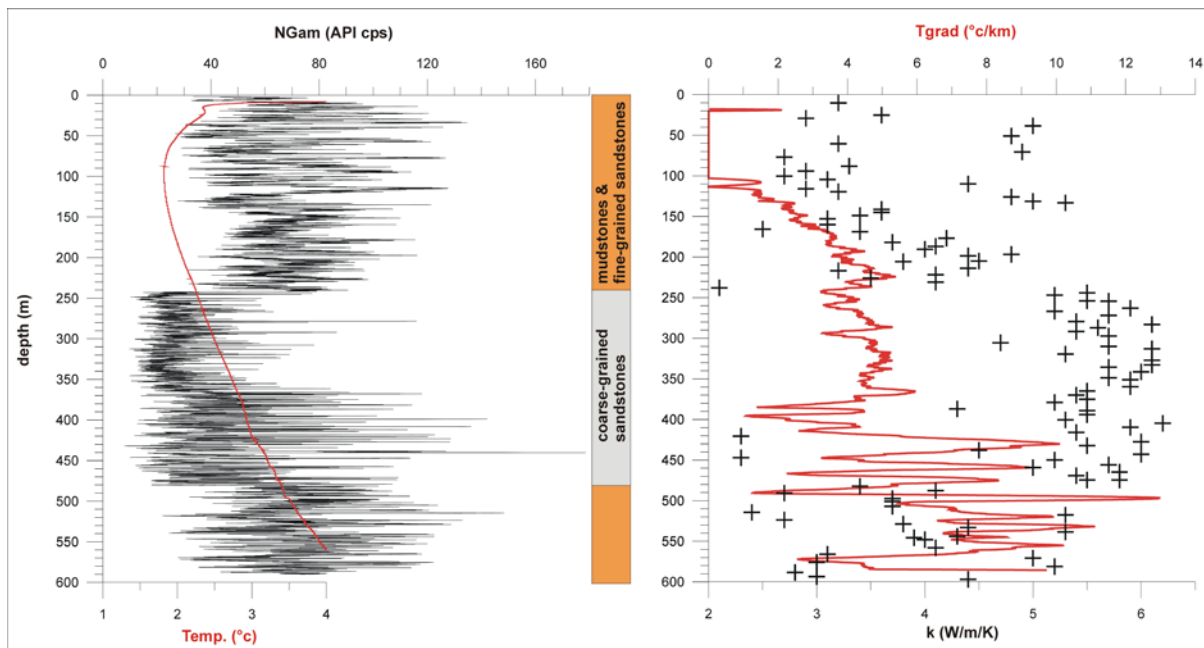


**Figure 3.2.** *Båtsfjordfjellet: a) Temperature profile superimposed on the gamma log and simplified lithostratigraphic column. b) Computed thermal gradient (least-squared on a 10 m moving window) and measured thermal conductivities on core material.*

Thermal conductivity values are extremely scattered and range from 2 to 6 W/m/K (Figs. 3.2 and 3.3a). Two groups of values can however be isolated. In the depth ranges 0-240 m and 480-600 m, conductivity values are scattered but fall most frequently in between 3 and 4 W/m/K (Fig. 3.2). In the depth range 240-480m, conductivity values are extremely high and better clustered around a mean value of 5.5 W/m/K. Those changes in thermal conductivity find their counterparts in changes in number of gamma countings and variations in bulk lithology (Figs. 3.2 and 3.3b). The upper and lower parts of the well penetrate mudstones and siltstones alternating with fine-grained sandstones whereas the central part exhibits almost exclusively medium to coarse grain sandstones. The higher content in radioactive elements and lower thermal conductivity of more shaly layers with respect to quartz-dominated ones explains the observed differences in the gamma log and measured thermal conductivities. Finally the extremely high thermal conductivities recorded for the sandstones of Båtsfjordfjellet is explained by their loss in porosity, conductivity values approaching the one of pure quartz (i.e.  $\sim 7$  W/m/K, Brigaud & Vasseur 1989).

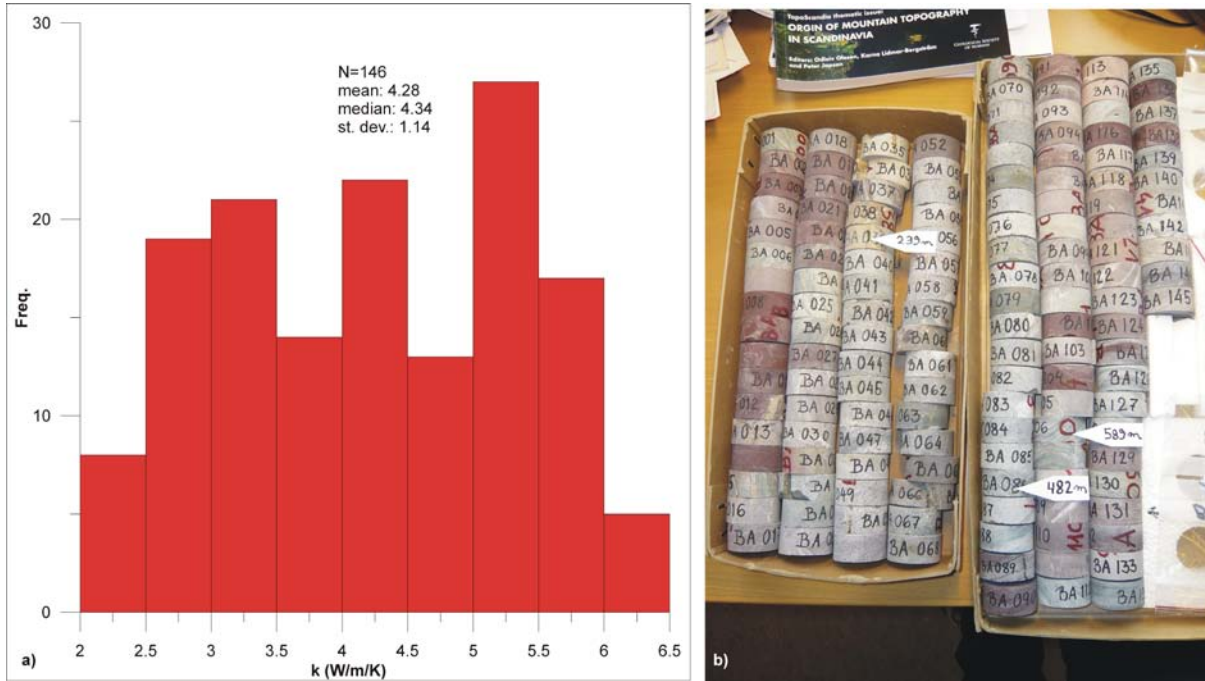


**Figure 3.3.** *Båtsfjordfjellet a) Distribution of thermal conductivity values as measured from core material at different depths (see also Fig. 3.2). b) Core samples used for thermal conductivity measurements. Note the almost complete lack of reddish rocks (i.e. mudstones) between 239 and 482 m depth. Note as well coarser grain sandstones for the same depth interval.*

In order to detect eventual departures from steady-state thermal conditions in the wells, we used the "Bullard Method" (Bullard 1939). The Bullard Method is based on the concept of thermal resistance expressed as:

$$R(z_i) = \Delta z_i / k_i \quad (3.2)$$

where  $k_i$  is the thermal conductivity of the rocks located in the depth interval  $\Delta z_i$ .

Temperature at depth  $z$  can be written as a function of heat flow and thermal resistance (for a detailed description of the method see e.g. Beardsmore & Cull 2001):

$$T(z) = T_0 + \sum_{i=1}^N q(\Delta z_i) \cdot R(z_i) \quad (3.3)$$

where  $q(\Delta z_i)$  is the heat flowing through the depth interval  $\Delta z_i$ ,  $N$  the number of depth intervals in between the surface and depth  $z$  and  $T_0$  mean temperature at the surface.

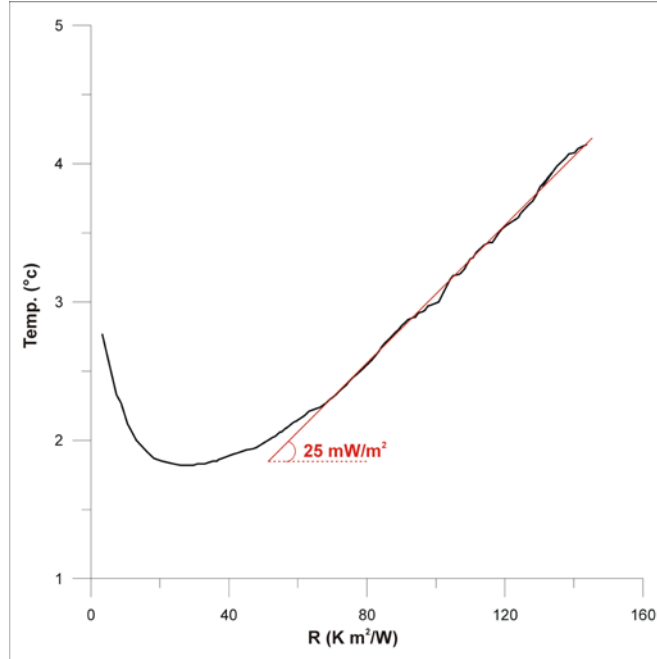


**Figure 3.4.** *Båtsfjordfjellet: computed heat flow using the Bullard-plot technique,  $R$  represents thermal resistance.*

Temperature versus thermal resistance plots are consequently called Bullard plots. From equation (3.2) it is implicit that if the heat flow is constant through the whole depth section sampled by the well (i.e. steady-state thermal conditions apply), the corresponding Bullard plot should be a line and the slope of the line should give the value of this constant heat flow. However, if heat flow variations occur in the well (i.e. the thermal field is not in equilibrium whatever the reasons are) the corresponding Bullard plot is non-linear. The obtained Bullard plot indicates that heat flow increases gradually with depth and reaches a stable value of  $\sim 25$   $\text{mW/m}^2$  (Fig. 3.4). Our previous analyses show that heat flow becomes stable below  $\sim 300$  m depth (Pascal et al. 2008).

This latter heat flow value appears much too low to represent a thermal steady state and calls for further corrections. An obvious strong disturbance, resulting in a typical “hook-shape” temperature profile (Fig. 3.2), is related to Quaternary paleoclimatic variations. Heat flow disturbances due to varying surface temperatures through time were calculated using the semi-analytical formula (derived from e.g. Powell et al. 1988):

$$\Delta q(z) = \sum_{i=1}^N \Delta q(t_i, z) = \sum_{i=1}^N k \Delta T_i \frac{\exp\left(\frac{-z^2}{4\kappa t_i}\right)}{\sqrt{\pi\kappa t_i}} \quad (3.4)$$

where  $k$  and  $\kappa$  are respectively thermal conductivity and diffusivity as determined from our laboratory measurements (NGU analysekontrakt 2006.0368) and  $\Delta T_i$  is instantaneous surface temperature change at time  $t_i$  BP. Based on inversion of temperature data from the nearby Kola ultradeep drillhole, Rath & Mottaghy (2007) estimated the magnitude of surface temperature changes to be in the range of 4 to 7° C at the beginning and the end of the last glacial period (i.e. Weichselian,  $\sim 10^5$ - $10^4$  BP). We applied these values in our tentative corrections assuming a drop and rise in temperatures at  $10^5$  and  $10^4$  BP respectively (Fig. 3.5). In addition, we used two sets of values for the thermal properties of the rocks (i.e. thermal conductivity and diffusivity), representing the two lithological end members

penetrated in the well, i.e. coarse-grained sandstones and mudstones/fine-grained sandstones (Fig. 3.2 and 3.3), and constrained from our laboratory measurements.

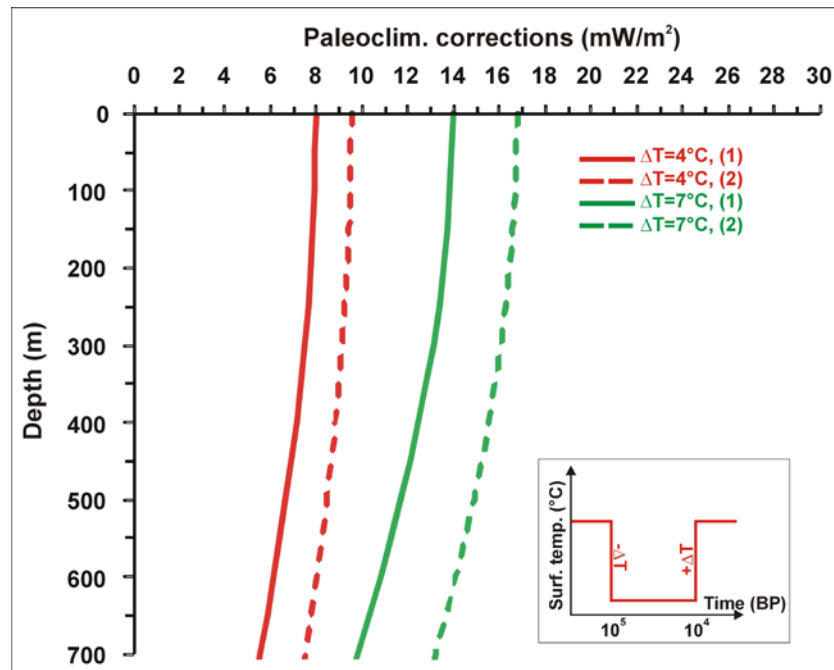


**Figure 3.5.** *Båtsfjordfjellet: tentative paleoclimatic corrections using two simplified paleoclimatic models and two sets of rock thermal properties: (1)  $k=3.73$  W/(m.K) and  $\kappa= 1.64 \cdot 10^{-6}$  m<sup>2</sup>/s and (2)  $k=5.42$  W/(m.K) and  $\kappa= 2.42 \cdot 10^{-6}$  m<sup>2</sup>/s .*

Our simulations suggest that  $\sim 7$  to  $\sim 16$  mW/m<sup>2</sup> should be added to heat flow values determined below 300 m depth in the well (Fig. 3.5), resulting in corrected values ranging from  $\sim 32$  to  $\sim 41$  mW/m<sup>2</sup>. Noteworthy the value of 16 mW/m<sup>2</sup> represents an unlikely uppermost bound in the range of permissible paleoclimatic corrections, suggesting that acceptable corrected values fall merely below 40 mW/m<sup>2</sup> and suggesting, in turn, that other factors might disturb temperatures in the borehole.



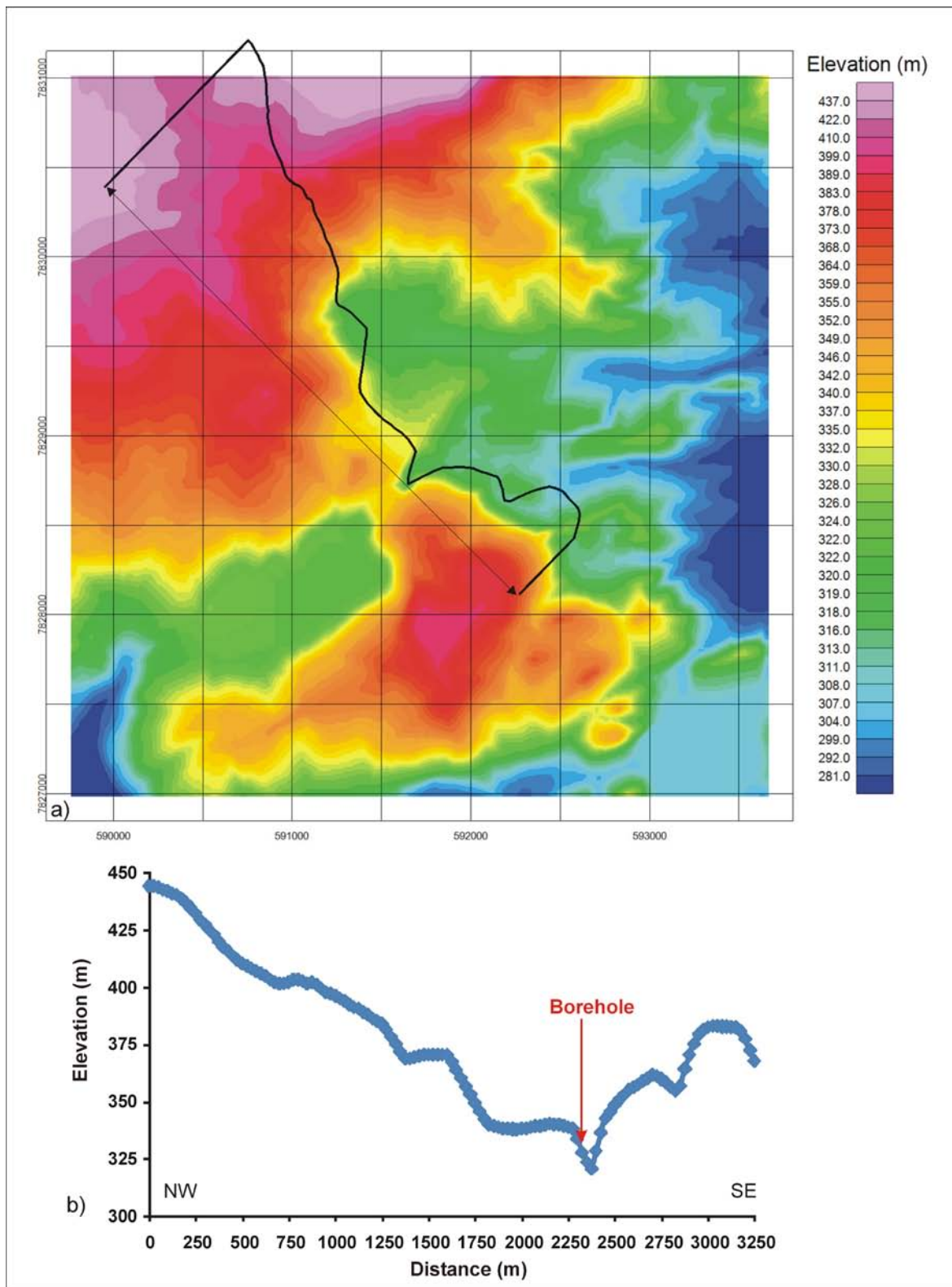


**Figure 3.6.** a) Topography of Båtsfjordfjellet (grid 5x5 km, UTM 35N WGS84). b) NW-SE topographic profile crossing approximately at the location of the borehole and parallel to the steepest slopes. Note the very gentle relief with average slopes of less than 3°.

Gentle relief prevails in the vicinity of the Båtsfjordfjellet borehole (Fig. 3.6). We estimated that the average dip of the steepest slopes having typical dimensions for eventually influencing the temperature field deep in the well (i.e. hundreds to thousands of metres) is below 3°. Such a gentle topography is expected to produce a heat flow disturbance of less than 10% at the surface (Lachenbruch 1968) and negligible below 300m depth. However, the elevation of Båtsfjordfjellet with respect to the surroundings is expected to produce a topographic head for ground water flow as demonstrated in the case of the Kola ultradeep borehole (Mottaghy et al. 2005). We suggest that the anomalously low heat flow values at Båtsfjordfjellet are diagnostic of undected large-scale ground water circulation and that no reliable steady-state value can be estimated at the present-day.

### 3.4 Vuoddašjav'ri

The Vuoddašjav'ri borehole was drilled in Central Finnmark (Figs. 2.1 and 3.1) for the purposes of the HeatBar Project. Drilling took place from May 14<sup>th</sup> until June 15<sup>th</sup> 2008. The borehole was drilled vertically in Archean gneisses with an initial target depth of 800 m but drilling operations stopped at ~720 m TD after having encountered a major fault zone.

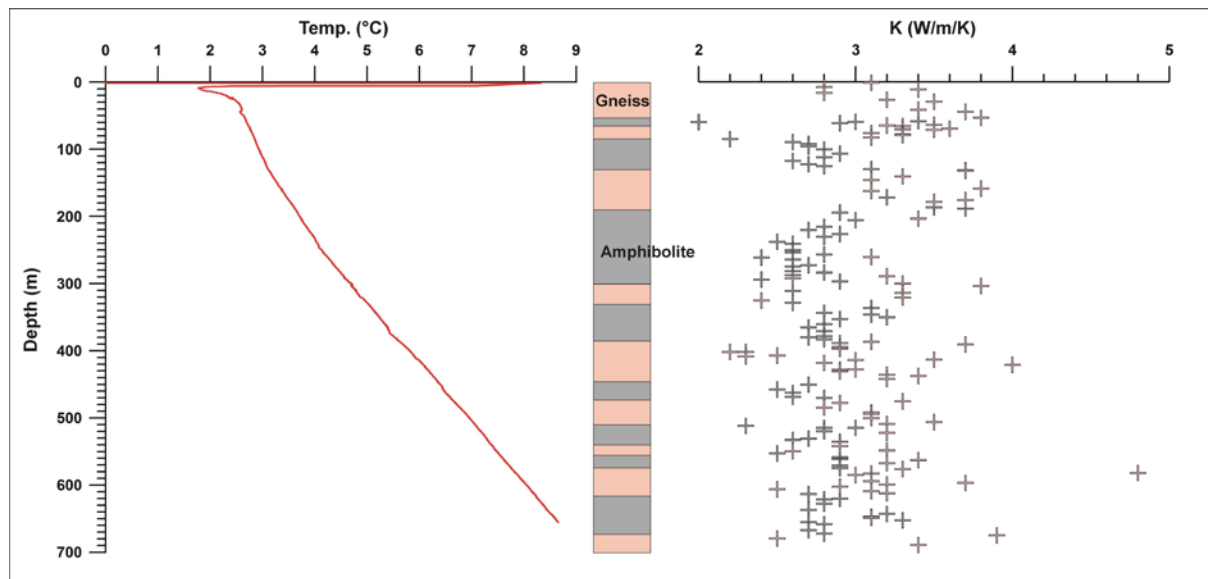


**Figure 3.7.** *Vuoddašjav'ri: temperature log, simplified geological log and thermal conductivities measured on core samples; grey and pink symbols represent amphibolites and gneisses respectively .*

The drillhole was logged more than one year later (see chapter 2). In order to avoid eventual problems related to the highly fractured bedrock of the fault zone, we decided to restrict the logging to the depth interval from 0 to 675 m (Fig. 3.7). The obtained temperature profile shows the typical convex shape and some sharp but spatially restricted bifurcations (Fig. 3.7). We measured thermal conductivities on 165 samples from core material, comprising mainly gneisses and amphibolites and occasionally pegmatites (Figs. 3.7 and 3.8). Our measurements resulted in a relatively narrow range of values where amphibolites and gneisses present

average thermal conductivities of 2.8 and 3.2 respectively (Fig. 3.8) in good agreement with values found in the literature (Clauser & Huengens 1995).

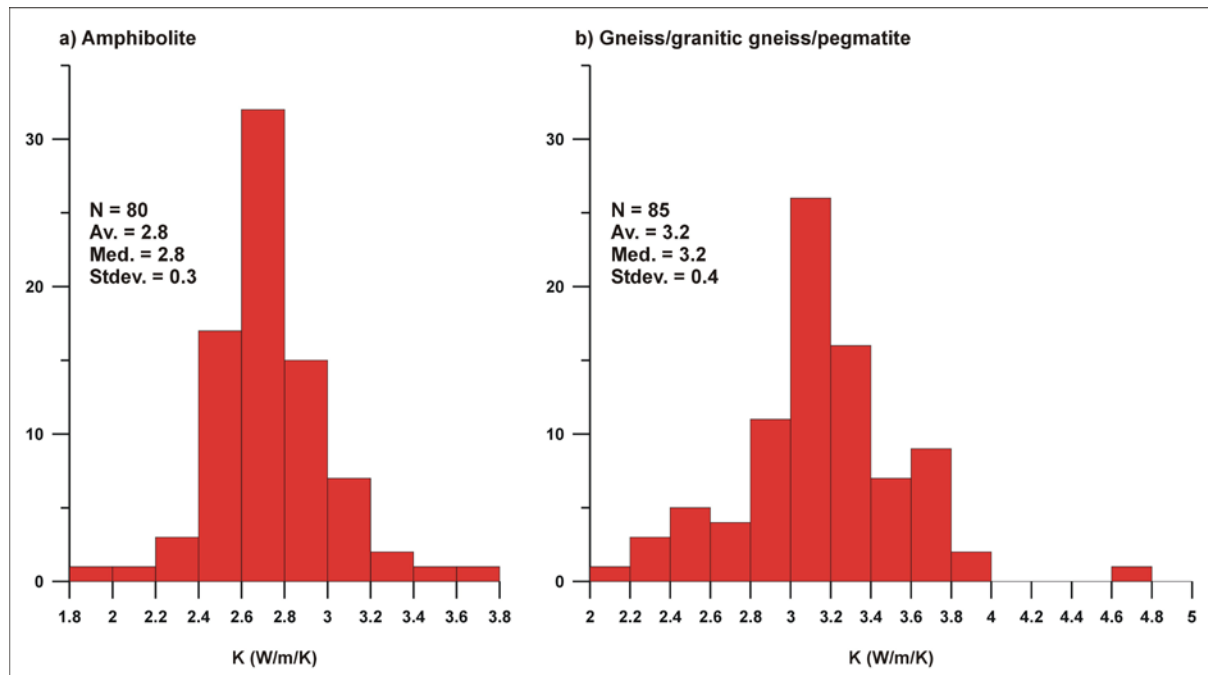


**Figure 3.8.** *Vuoddašjav'ri: statistical distributions of thermal conductivities measured on core samples and separated according to lithology.*

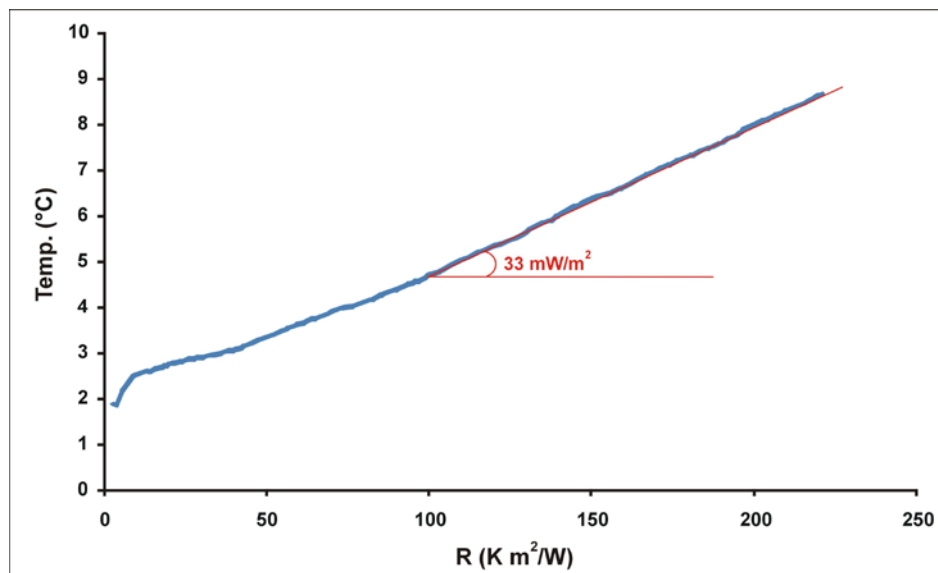


**Figure 3.9.** *Vuoddašjav'ri: computed heat flow using the Bullard-plot technique, R represents thermal resistance.*

With the data at hand we carried out a “Bullard-plot” analysis (Fig. 3.9). The obtained Bullard plot shows a reasonably stable slope for the deepest parts of the logged interval and suggested a heat flow value of 33 mW/m<sup>2</sup>. In detail, heat flow values become relatively constant from 300 m depth downwards (Fig. 3.10). A departure of ~3 mW/m<sup>2</sup> can be seen at

~400 m in the filtered heat flow profile (i.e. red curve in Fig. 3.10). This minor departure is probably related to drastic but spatially restricted changes in thermal conductivity as no clear signals related to an open fracture are seen in the resistivity log at corresponding depths (Fig. 2.4).

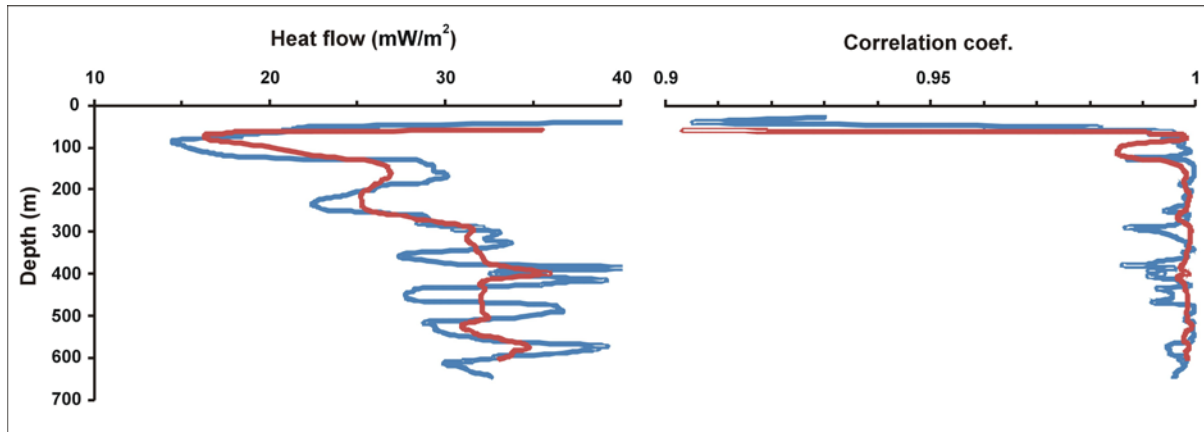


**Figure 3.10.** *Vuoddašjav'ri: variation of heat flow vs depth. Heat flow profiles are constructed by computing series of regression lines for the Bullard plot showed in Fig. 3.9. and plotting their respective slopes vs depth. The number of points used to calculate regression lines and their corresponding correlation coefficients is 9 (25) for the blue (red) heat flow profile .*

Finally, we carried out paleoclimatic and topographic corrections. We followed a correction procedure for paleoclimatic disturbances similar to the one previously described for the Båtsfjordfjellet drillhole and used two paleoclimatic models (see Fig. 3.5). Our computations suggest a positive heat flow correction ranging from 5 to 10 mW/m<sup>2</sup> for the 300-670 m depth range (Fig. 3.11). In turn topographic corrections appear to be modest and result in a negative correction comprised between -2 and -1 mW/m<sup>2</sup> for the corresponding depth interval (Fig. 3.12). In summary, the results suggest a steady-state heat flow value of ~40 mW/m<sup>2</sup> in agreement with values commonly measured in Archean cratons (Nyblade & Pollack 1993).

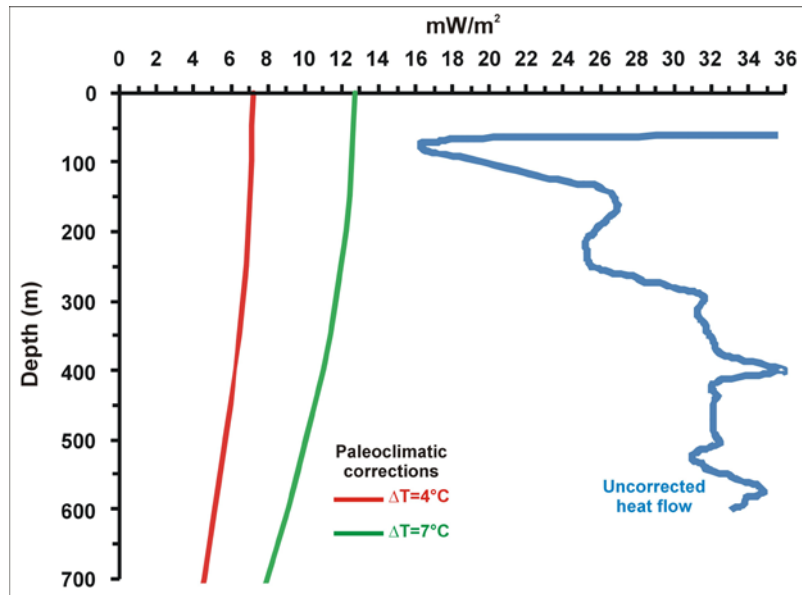


Figure 3.11. Vuoddašjav'ri: tentative paleoclimatic corrections using two simplified paleoclimatic models (see box in Fig. 3.5). Rock thermal properties are  $k=3 \text{ W/(m.K)}$  and  $\kappa=1.29 \cdot 10^{-6} \text{ m}^2/\text{s}$ .

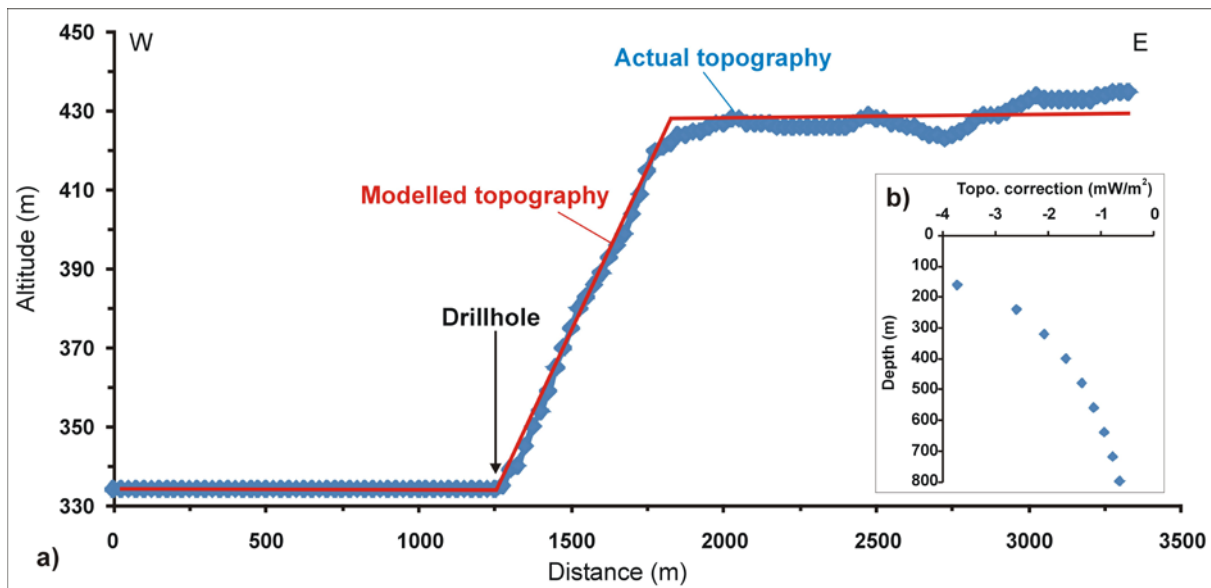
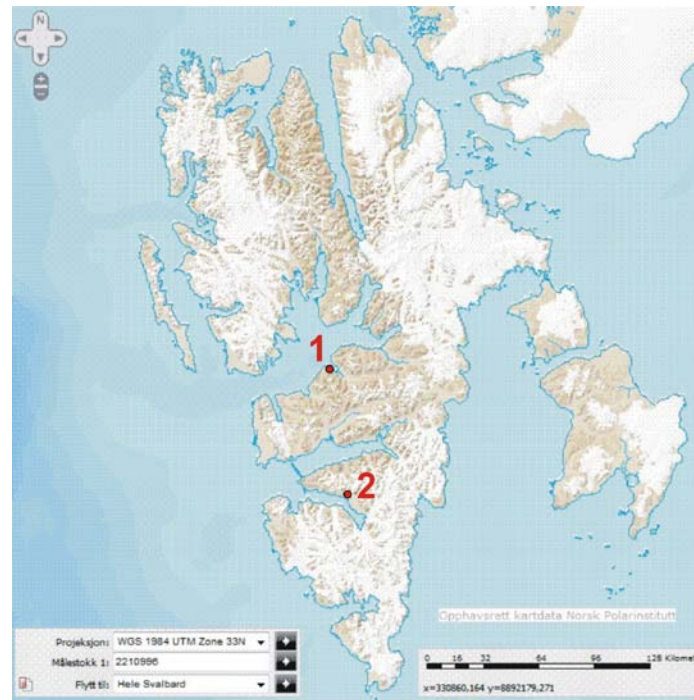


Figure 3.12. Vuoddašjav'ri: topographic corrections. a) Topography and location of the drillhole, b) corrections computed by means of 2D numerical modelling and using the simplified topographic profile depicted in red.

### 3.5 Longyearbyen (CO<sub>2</sub>-Dh1 drillhole)

The CO<sub>2</sub>-Dh1 drillhole was drilled down to 518 m in Longyearbyen, Svalbard (Fig. 3.13), in October 2007 and logged down to 440 m TD by NGU two months later (Elvebakk 2008).

The drilling was connected to the “Longyerbyen CO2 Lab” project led by UNIS (<http://co2-ccs.unis.no>). Thanks to Alvar Braathen (UNIS) we also got access to core material and could measure thermal conductivities. Thermal conductivities of sandstones/conglomerates and of shales/siltstones were measured on water-saturated samples at NGU and the Geological Institute of Aarhus University respectively. It is worth noting that in contrast with NGU, Aarhus uses a needle probe method to measure conductivities that usually results in slightly lower values (Kalskin Ramstad et al. 2008).



**Figure 3.13.** Location of the (1) CO<sub>2</sub>-Dh1 and (2) Sysselembreen drillholes in Svalbard (source: [http://eivind.npolar.no/Geocortex/Essentials/Web/viewer.aspx?Site=svbk\\_v01\\_no](http://eivind.npolar.no/Geocortex/Essentials/Web/viewer.aspx?Site=svbk_v01_no)).

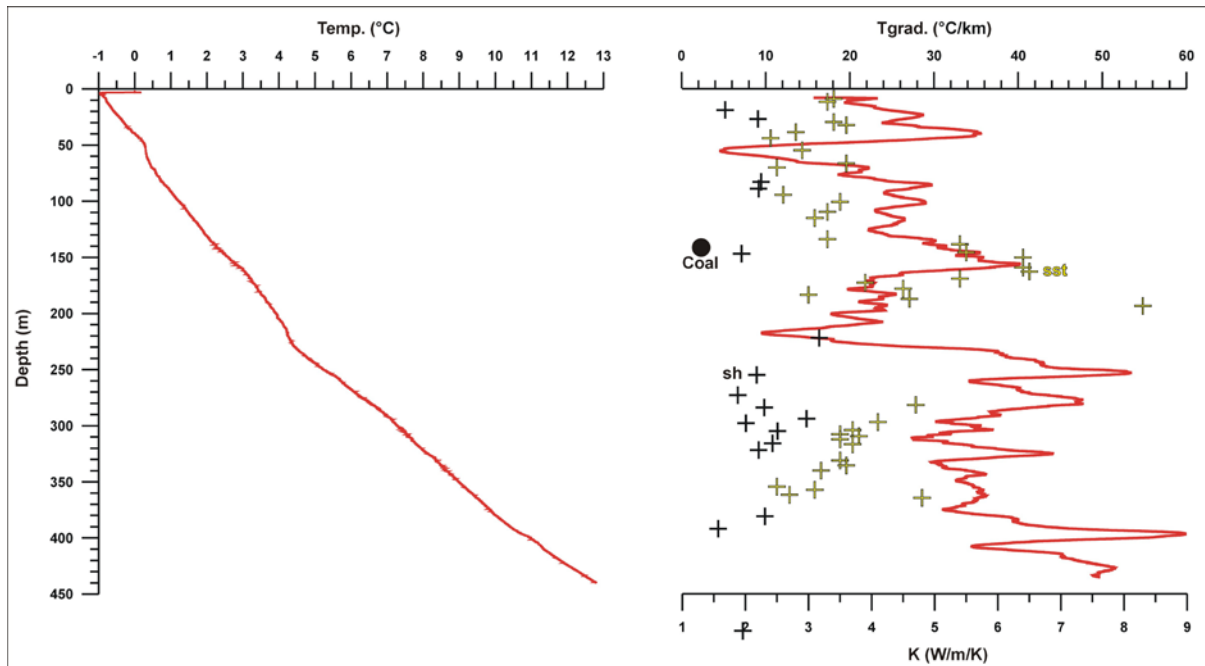


**Figure 3.14. Longyearbyen: temperature log, thermal gradient (10m moving average) and measured thermal conductivities on core samples (yellow and black crosses represent sandstones and shales respectively).**

Our temperature measurements reveal a sharp increase in geothermal gradients from 20-30°C/km to 30-40°C/km at ~230 m depth (Fig. 3.14). This increase can be partly explained by paleoclimatic disturbances and to some extent by changes in thermal conductivity (i.e. lithologies). There is surprisingly little correlation between rock type and geothermal gradient. A finer analysis of the results of thermal conductivity measurements shows that average values for shales and sandstones are 2.2 and 3.9 W/(m.K) respectively (Fig. 3.15). In general, the values measured for shales appear to fall in a reasonable range. Those measured for sandstones are up to 8.3 W/(m.K) exceeding by more than 1 W/(m.K) typical values of pure quartz (Brigaud & Vasseur 1989).

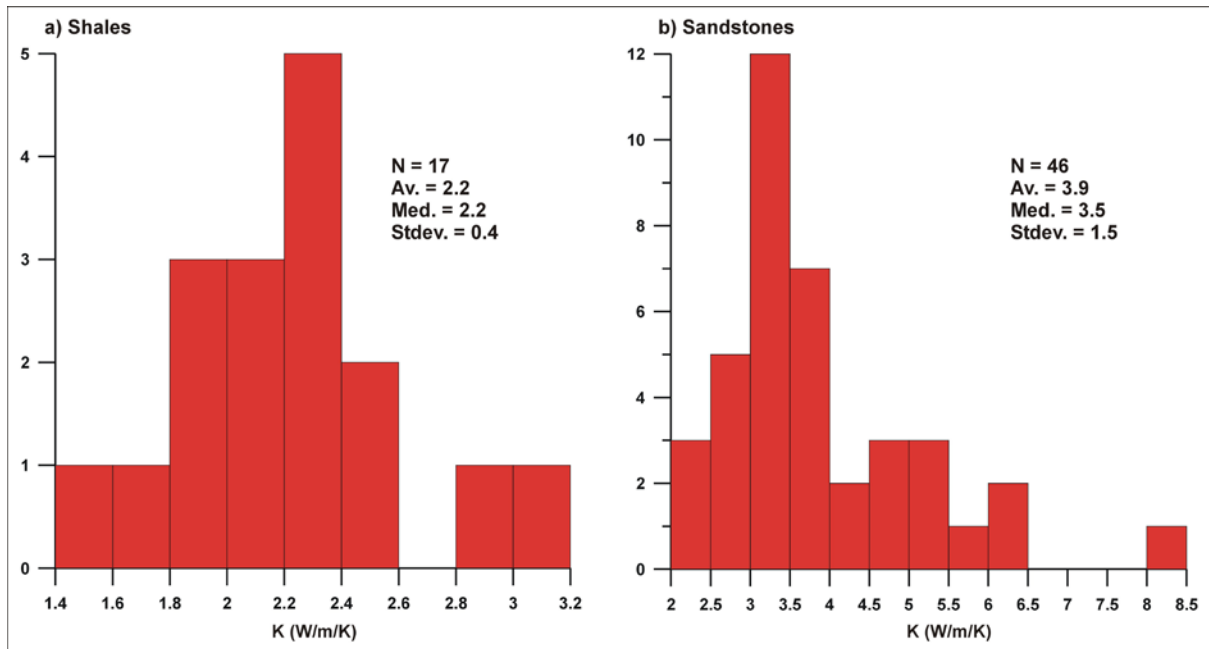


**Figure 3.15. Longyearbyen: statistical distributions of thermal conductivities measured on core samples and separated according to lithology.**

Nevertheless we attempted to estimate heat flow variations in the borehole using a similar procedure than previously. Our analysis suggests that, in general, heat flow increases with depth from  $\sim 60$  to  $\sim 90$   $\text{mW/m}^2$  (Fig. 3.16). Very sharp heat flow variations occur at  $\sim 170$  and  $\sim 350$  m depth, where values reach up to  $\sim 130$   $\text{mW/m}^2$ . According to Figure 3.16, it is obvious that these apparent heat flow anomalies result from overestimation of thermal conductivities for the sandstones.

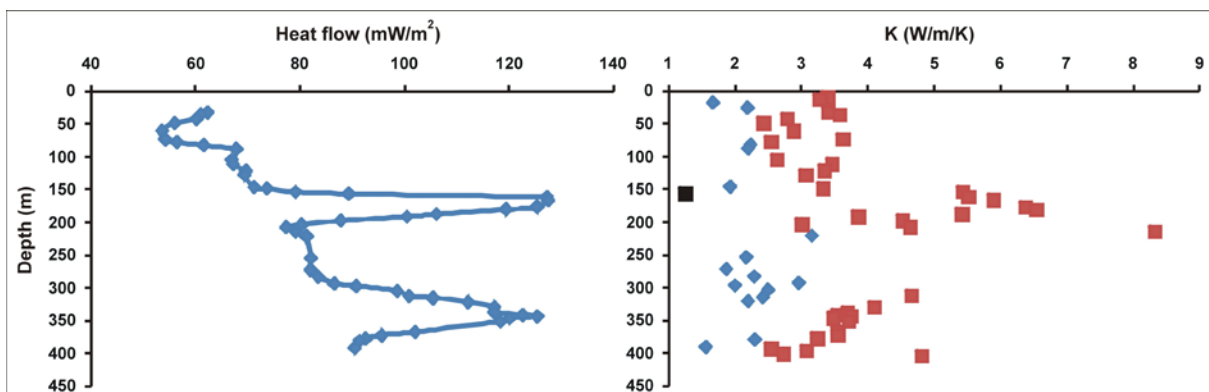


**Figure 3.16. Longyearbyen: calculated heat flow and measured thermal conductivities (red squares = sandstones, blue diamonds = shales and black square = coal). Note the two sharp peaks in heat flow values corresponding to sections in the well dominated by sandstones.**

In summary, (1) the heat flow is not stable in the  $\text{CO}_2$ -Dh1 drillhole and (2) there is an apparent bias in the measured thermal conductivities for the sandstones. Therefore, it was not



possible to derive any reliable heat flow value, however, the results at hand point towards unusually high heat flow at greater depths.

### 3.6 Sysselembreen, Svalbard

During summer 2008, a 1084 m deep borehole was drilled by Store Norske Spitsbergen Kulkompani (SNSK) and LNS Spitsbergen in the lateral ice-cored moraine of the glacier Sysselembreen in southern Spitsbergen (Fig. 3.13). The borehole was drilled in the framework of a cooperation project between the oil companies Statoil and Det norske, the Norwegian Petroleum Directorate, SNSK and NGU (Johannessen et al. 2011). Because of the quick recovery of the penetrated permafrost layer, temperature logging was done five days after drilling completion (Elvebakk et al. 2008). Although logging shortly after drilling is not ideal, we estimated that remaining temperature perturbations caused by mud circulation in the 56-66 mm diameter borehole were less than 0.1 °C (Fig. 3.17). Noteworthy our estimations are based on a simple Horner-type correction (Middleton 1982) and do not account for eventual penetration of drilling fluids in the formations.

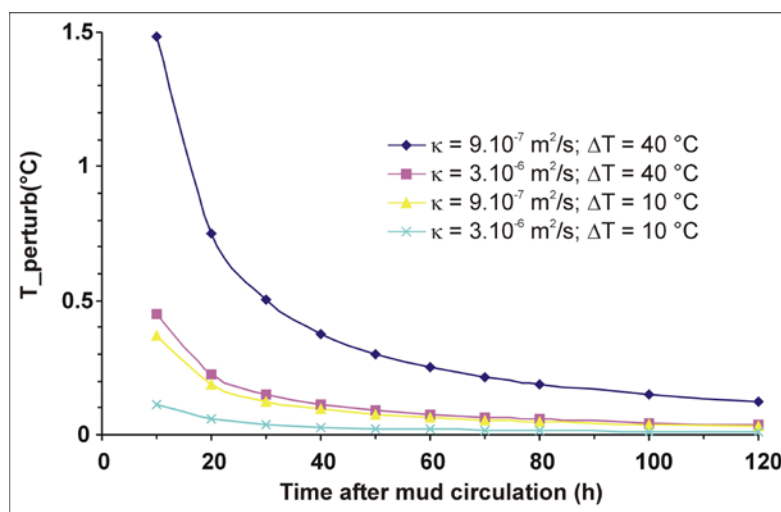


**Figure 3.17.** Calculated temperature perturbation after drilling completion for a 70 mm diameter borehole and using a Horner type of correction (Middleton 1982).  $\kappa$  and  $\Delta T$  represent rock diffusivity and temperature difference between drilling mud and borehole walls respectively. Note that the temperature perturbation induced by mud circulation is predicted to be negligible five days (i.e. 120 hours) after drilling completion.

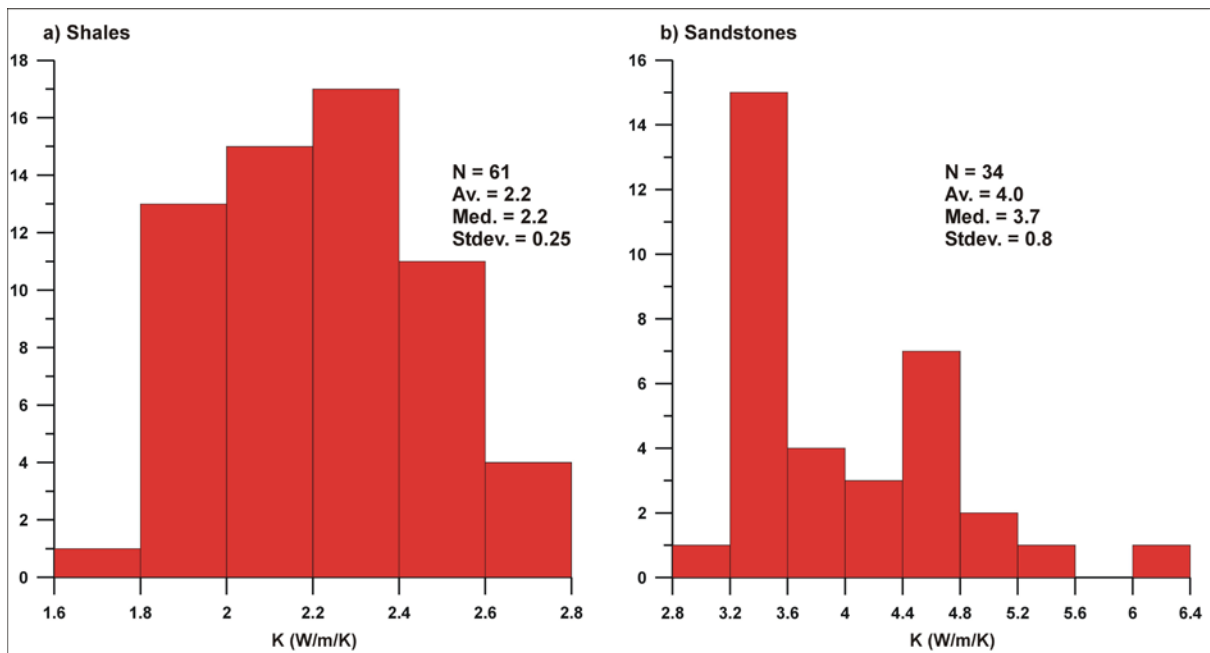


Figure 3.18. Sysselmannbreen: statistical distributions of thermal conductivities measured on core samples and separated according to lithology.

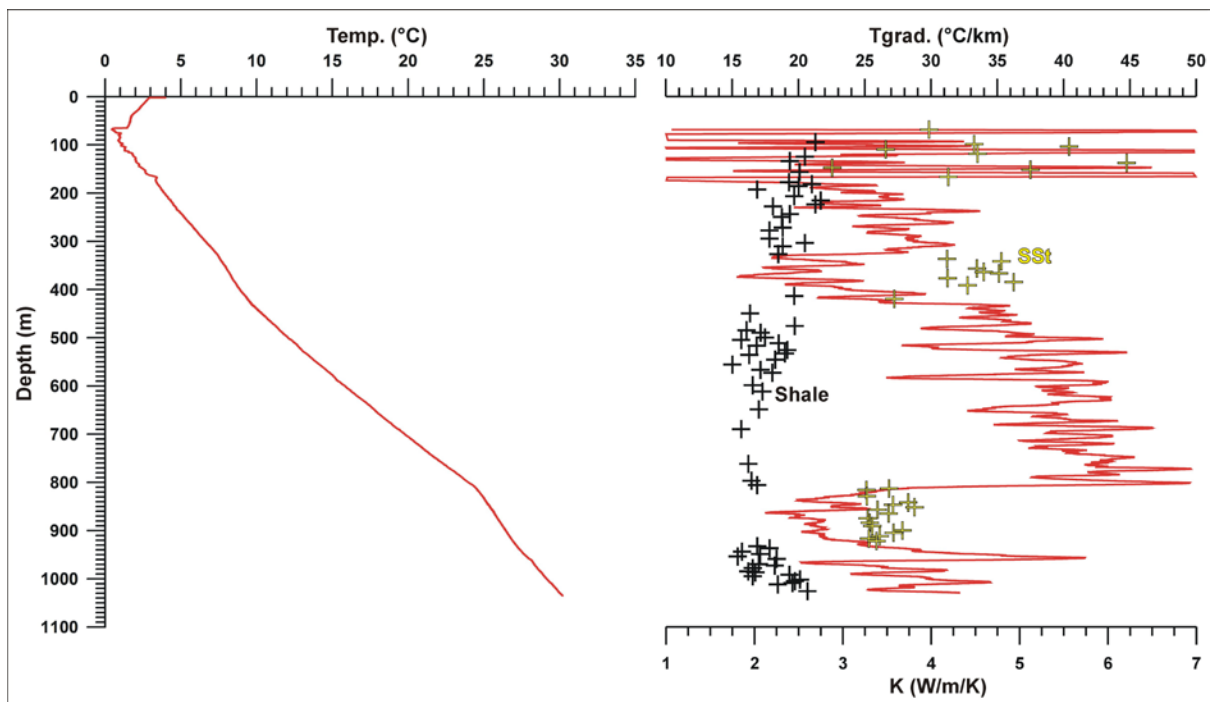


Figure 3.19. Sysselmannbreen: temperature log, thermal gradient (10m moving average) and measured thermal conductivities on core samples (yellow and black crosses represent sandstones and shales respectively).

Thermal conductivity was measured on 95 core samples evenly distributed in the borehole (Figs. 3.18 and 3.19). In detail, 61 samples of shales and siltstones were measured at the

University of Aarhus and 34 samples of sandstones at NGU (Fig. 3.18). We suspect that, like for the case of the CO<sub>2</sub>-Dh1 drillhole (see previous section), thermal conductivities for sandstones are overestimated. However, a reasonably good correspondence between variations in thermal gradient and lithology is seen in the present case (i.e. thermal gradient lows and highs appear, in general, to be correlated to sandstones and shales respectively, Fig. 3.19). The temperature log evidences an almost isothermal interval from ~65 m down to ~100m that could correspond to a melted layer of permafrost. The short-wavelength variations in temperature gradient down to ~170 m are obviously caused by alternating layers of shale and sandstones, hence rapid changes in thermal conductivity.

Heat flow was calculated using the Bullard plot technique (Fig. 3.20a) and the results were plotted as a function of depth (Fig. 3.20b). Heat flow appears to increase gradually from ~60 to ~80 mW/m<sup>2</sup> in the interval 200 to 800 m and drops back abruptly below 800 m. The two pronounced heat flow peaks at ~360 and 810 m correspond to two massive sandstone layers and are obviously the response to overestimated thermal conductivities for those sandstones. The significant heat flow drop below 800 m appears to be independent on lithology. This latter drop is problematic to interpret but a likely explanation is that drilling fluids entered the formations at the base of the borehole and cooled down it for longer times than predicted by a simple Horner analysis. In particular, this would account for the anomalously low geothermal gradients (i.e. down to 20-25 °C/km, Figs. 3.19 and 3.20b) observed in this deep part of the borehole we do not expect to be affected by significant paleoclimatic disturbances.

However, in the shale-dominated interval between ~500 and ~800 m heat flow values appear to be relatively stable. We consequently made new calculations focussed on this specific interval and created a second Bullard plot (Fig. 3.21). As expected the Bullard plot mimics a straight line and points to relatively stable heat flow values of 77-78 mW/m<sup>2</sup> on average. We estimated the impact of topography on heat flow using a 2D numerical model that follows the maximum slope of the terrain and crosses the borehole location (Fig. 3.22). In agreement, with seismic experiments (Johannessen et al. 2011), we assumed that the glacier of Sysselman is thinner than a few tens of metres in the vicinity of the borehole and neglected it in the 2D model. Our calculations show that the relief adds 3 to 5 mW/m<sup>2</sup> to the heat flow values derived from the depth interval 480 to 760 m. Paleoclimate corrections are much more difficult to conduct. Based on our corrections for the Vuoddašjav'ri borehole (Fig. 3.11) we propose that paleoclimatic variations have suppressed 5 to 10 mW/m<sup>2</sup> of the total heat flow value. In summary, a conservative and reasonable estimate for the steady-state heat flow value in the Sysselmanbreen borehole is 80 mW/m<sup>2</sup>.

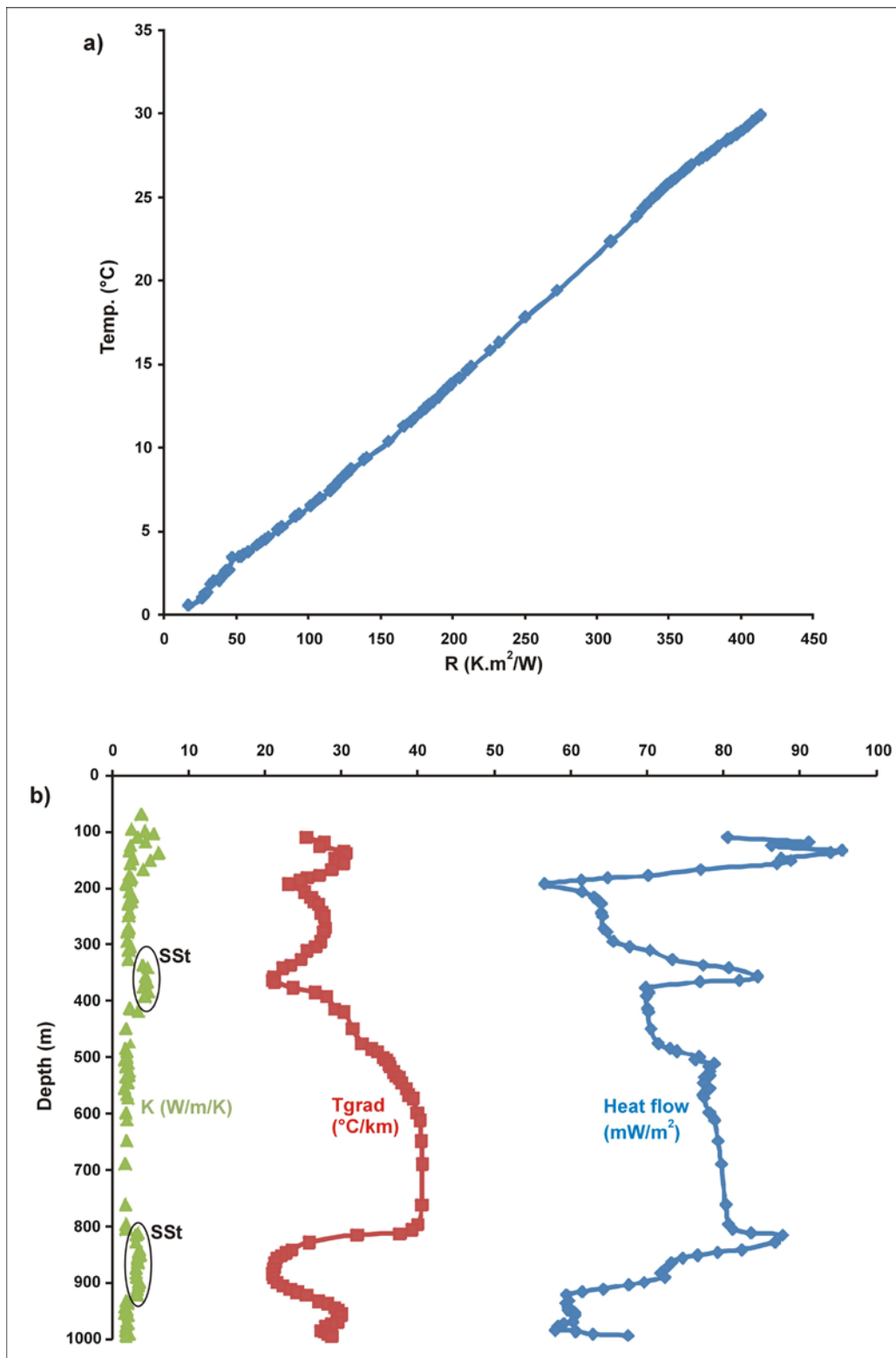


Figure 3.20. Sysselembreen: a) computed heat flow using the Bullard-plot technique, R represents thermal resistance; b) measured thermal conductivities, temperature gradient and computed heat flow, note the two sharp peaks in heat flow values corresponding to sections dominated by sandstones.

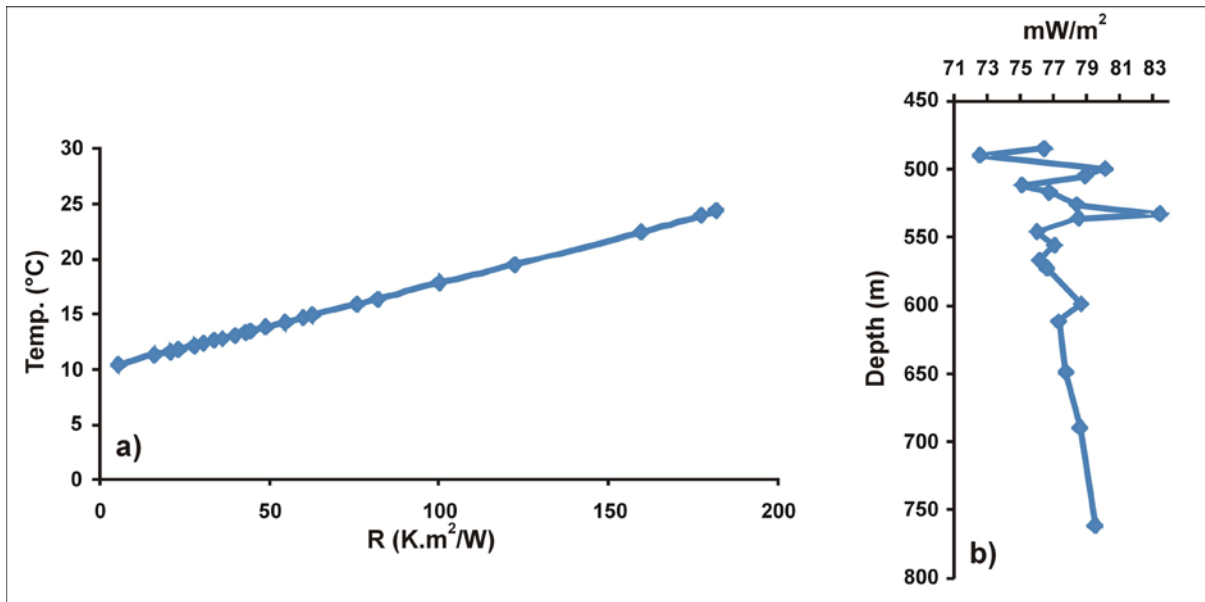


Figure 3.21. Sysselembreen: a) computed heat flow using the Bullard-plot technique for the borehole interval comprised between 480 and 760 metres depth,  $R$  represents thermal resistance; b) computed heat flow Vs depth.

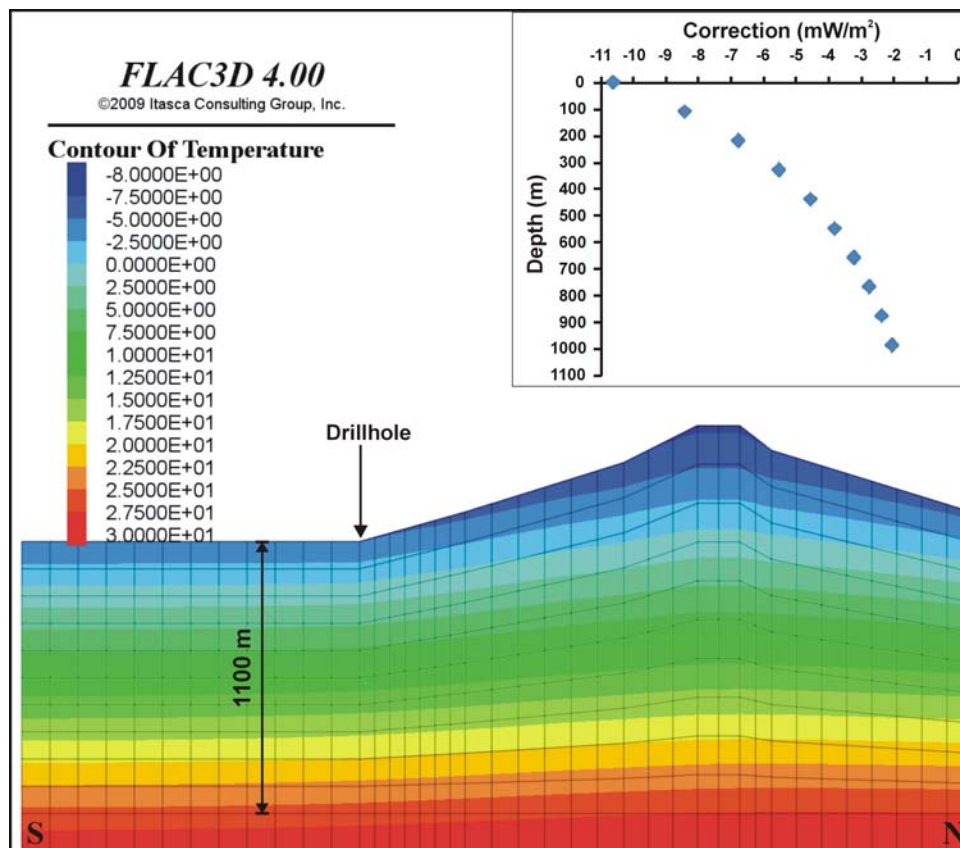


Figure 3.22. Sysselembreen: topographic corrections using a 2D numerical model. A background heat flow of  $80 mW/m^2$  and an average thermal conductivity of  $3 W/(m \cdot K)$  are assumed. No vertical exaggeration.

### 3.7 Conclusions

In the framework of the HeatBar project we studied six drillholes with the purpose of deriving steady-state heat flow values: four drillholes from Finnmark (Båtsfjordfjellet, Bjørnevatn, Bidjovagge and Vuoddašjav'ri) and two from Svalbard (Longyearbyen and Sysselmannbreen). We obtained convincing results only for two out of the six boreholes. Results from the Vuoddašjav'ri borehole suggest a steady-state heat flow value of  $\sim 40$  mW/m<sup>2</sup> in agreement with values commonly measured in Archean cratons (Nyblade & Pollack 1993). In contrast, we derived a steady-state heat flow value of  $\sim 80$  mW/m<sup>2</sup> for the Sysselmannbreen borehole. Again, this value appears to be consistent with the present-day geological context of Svalbard where hot springs and recent volcanism are both documented (Harland 1997).

## **4 RADIOGENIC HEAT PRODUCTION**

Trond Slagstad, NGU

### **4.1 Introduction**

Radiogenic heat production rates determined on rock samples from the Earth's surface, although biased towards upper crustal rocks, provide key input and constraints on thermal models of the lithosphere. A number of studies have shown lithology to be the main source of variation in radiogenic heat production rate (Kukkonen & Lahtinen 2001), but factors such as tectonic setting, tectonometamorphic history and major element composition may also play a role. Some studies indicate that heat production rates are relatively uncorrelated with the age of a particular rock type or geological province (e.g., Kukkonen & Lahtinen 2001), but there are also examples to the contrary (e.g., McLaren et al. 2003).

### **4.2 Sources of heat production data**

The heat production rate of individual samples is calculated following Rybach (1988), based on the samples' K, U and Th concentrations, and density. The chemical data used to calculate heat production come from various sources, summarised in Table 4.1. The majority of the samples have been analysed by XRF and LA-ICP-MS, thus a complete set of major and trace element data exists for each of these samples. The analytical procedure, detection limits, accuracy and precision of the LA-ICP-MS analyses are described in Flem et al. (2005). With regard to calculating heat production, K concentrations are from the XRF data whereas U and Th concentrations are from the LA-ICP-MS data. The remaining samples have been analysed by  $\gamma$ -ray spectrometry, thus for these samples we have no chemical information outside the concentration of heat producing elements. The analytical procedure, detection limits, accuracy and precision of the  $\gamma$ -ray spectrometry method are described by Raade (1973) and Killeen & Heier (1975). For several geological units, heat production data based on both XRF/LA-ICP-MS and  $\gamma$ -ray spectrometry exist. Average heat production rates for such units are similar regardless if they are based on the older  $\gamma$ -ray data or more modern XRF/LA-ICP-MS data, suggesting that the quality of the former are good. The densities of the Lito-project samples have been determined using Archimedes' principle by weighing the samples in air and immersed in water. Densities of the other samples have been assigned based on lithology, and are, where available, similar to those assigned by the original authors.

**Table 4.1. Sources of heat production data.**

<b>Source</b>	<b>No.</b>	<b>Analytical method</b>
LITO-project	2050	XRF, LA-ICP-MS
LITO-project, Finmark	348	XRF
Various NGU samples	623	XRF, LA-ICP-MS
Killeen & Heier (1975)	629	$\gamma$ -ray spectrometry
Raade (1973)	967	$\gamma$ -ray spectrometry
Ormaasen (1976)	102	$\gamma$ -ray spectrometry

### **4.3 Radiogenic heat production rates of Norwegian bedrock**

As stated in the introduction, a number of factors, of which lithology, tectonic setting, tectonometamorphic history and age are the most obvious, may influence the heat production and heat flow of a geologically distinct terrain. Furthermore, the work presented here is part of a larger effort to enhance our understanding of the geological and thermal structure of the continental margin of Norway (and the Baltic Shield). This means that heat production values must be assigned to geological terrains onshore that can be correlated offshore onto the continental margin using seismic or potential field data. With these objectives in mind, we have previously presented and discussed the heat production data in reference to specific geological units or terrains, subdivided based on lithology, tectonic setting, tectonometamorphic history and age (Figs. 4.1 and 4.2, Table 4.2, and Slagstad (2008)).

### **4.4 Summary of previous work**

The already extensive, and growing, geochemical database from Norwegian bedrock allows for comprehensive investigations into the factors that control the distribution of the heat producing elements. Since the purpose of this paper is to characterise the heat production of the main geological provinces in Norway, a major part of this discussion focuses on average heat production rates obtained from a variety of rock types that in some cases formed at different times and in different tectonic settings. However, in general the geological provinces delineated here are dominated by a small number of lithologies that display rather modest geological variation (i.e., composition, age, metamorphic grade, tectonic setting) to make such a discussion meaningful. Because granite (*sensu lato*) is the main host for the heat producing elements, the heat production of Norwegian granites is discussed in particular, emphasising the relationship between the tectonic setting in which the granite formed and its heat production rate.



## 4.5 Heat production vs. lithology, composition and tectonic setting

### 4.5.1 Lithology and chemical composition

Lithological variation is the primary factor controlling the distribution of heat production in the crust. In general, granitic rocks have relatively high heat production whereas intermediate and mafic lithologies produce less heat, however, in reality heat production within the same lithology may vary by an order of magnitude or more. To facilitate the discussion of heat production and its dependence on lithology, I have subdivided the samples for which we have a complete geochemical data set (XRF and LA-ICP-MS) into 4 lithological groups. 'Metasedimentary rocks' encompass arkose, quartzite, mica schist, phyllite and greywacke; 'Metamafic rocks' include gabbro, amphibolite, diorite and greenstone/-schist; 'Granite and granitic gneiss' and 'Granodiorite and granodioritic gneiss' are self-explanatory. As expected, the mafic rocks yield the lowest heat production with an average of  $0.74 \mu\text{W}/\text{m}^3$  and the granitic rocks the highest heat production with an average of  $2.95 \mu\text{W}/\text{m}^3$ . The granodioritic and metasedimentary rocks yield similar, intermediate heat production with averages of  $1.54$  and  $1.55 \mu\text{W}/\text{m}^3$ , respectively. These values are as expected, and the variation within each lithological group in relation to chemical composition is perhaps more interesting. Figure 4.3 shows heat production vs.  $\text{SiO}_2$ ,  $\text{Fe}_2\text{O}_3$  and total rare earth element (REE) content for the different lithological groups.  $\text{SiO}_2$  and  $\text{Fe}_2\text{O}_3$  represent the samples' major element composition and reflect the mineralogical composition of the samples, whereas Total REE represents trace elements mainly hosted by accessory phases including zircon and monazite, which are also the main hosts of the heat producing elements (e.g. Bea 1996).

**Table 4.2. Simplified geological history and heat production rates of geological provinces in Norway (Slagstad (2008), updated with new data from Finnmark).**

	Geological province	n	Age (Ma)	Lithology	Tectonic setting	Tectonometamorphic history	Heat production rate ( $\mu\text{W}/\text{m}^3$ )		Heat flow ( $\text{mW}/\text{m}^2$ )	
							Area wtd. mean <sup>1</sup>	Median $\pm 1\sigma$	Mean $\pm 1\sigma$ (n)	Median
1	Archaean gneisses	95	3000–2500	Dominantly tonalitic to granitic gneisses		Early Proterozoic (c. 2.0–1.8 Ga) amphibolite- to granulite-facies metamorphism.	1.25	$0.81 \pm 1.48$	$38 \pm 8$ (2)	38
2	Proterozoic gneissic rocks									
2a	Karasjok-Kautokeino greenstone belts, NE Norway	n.d.	2100–2000	Tholeiitic metabasalts, amphibolites and interlayered metasedimentary rocks	Continental rifting and oceanic subduction	Metamorphosed under greenschist- to amphibolite-facies conditions during obduction onto the Karelian craton at c. 1.9 Ga.	0.65	$0.46 \pm 0.52$	24 (1)	24
2b	Palaeoproterozoic gneisses	17	2000–1900	Garnet-quartz-feldspar paragneiss and hypersthene-plagioclase orthogneiss	Deposition in continental back-arc basin	High-grade metamorphism during continent-continent collision at c. 1900 Ma	1.42	$0.54 \pm 1.44$	$38 \pm 3$ (16)	38
2c	Transscandinavian Igneous Belt (TIB)	571	1810–1770	Alkali-calcic to calc-alkaline quartz monzonites to granites	Active continental margin, back-arc extension	Deformation and metamorphism at c. 1.46–1.42 and 1.0 Ga in SW Sweden. Variable Caledonian effects in NW Norway at c. 420 Ma.	2.57	$2.57 \pm 2.03$	$38 \pm 8$ (4)	38
2d	Sveconorwegian Province, S Norway	385	1500–1000	Tholeiitic to calc-alkaline, intermediate to felsic, metavolcanic and –plutonic suites	Active continental margin and continental back-arc.	Local crustal reworking at 1.26–1.16 Ga. Continent-continent collision and associated medium- to high-grade metamorphism at c. 1.0 Ga. Very low-grade Caledonian metamorphism at c. 400 Ma in western areas.	1.76	$1.73 \pm 1.45$	$43 \pm 8$ (25)	45
2e	Western Gneiss Region, W Norway	332	1750–1000	Dominantly tonalitic to granitic gneisses	Active continental margin	Sveconorwegian and Caledonian high-grade metamorphism at c. 1000 and 400 Ma, respectively.	1.36	$1.41 \pm 0.82$	$42 \pm 9$ (8)	41
3	Lofoten anorthosite-mangerite-charnockite-granite (AMCG) complex	130	1800–1790	Mangerite, smaller volumes of gabbro, anorthosite, charnockite and granite	Related to TIB 1 magmatism	Crystallised under low-P granulite-facies conditions. No significant later metamorphic events.	0.65	$0.61 \pm 0.32$	n.d.	n.d.
4	Post-Sveconorwegian granites, S Norway	473	930–920	Dominantly granite, locally grading to diorite	Extensional, post-tectonic magmatism	Generally no significant metamorphic overprinting.	4.61	$3.92 \pm 2.54$	$58 \pm 17$ (12)	59
5	Egersund anorthosite-mangerite-charnockite (AMC) complex	47	930	Massive anorthosite, lesser volumes of leuconorite, mangerite and charnockite	Extensional, post-tectonic magmatism	Very low-grade Caledonian metamorphism at c. 400 Ma.	0.57	$0.71 \pm 0.42$	21 (1)	21

Geological province	n	Age (Ma)	Lithology	Tectonic setting	Tectonometamorphic history	Heat production rate ( $\mu\text{W}/\text{m}^3$ )		Heat flow ( $\text{mW}/\text{m}^2$ )		
						Area wtd. mean <sup>1</sup>	Median $\pm 1\sigma$	Mean $\pm 1\sigma$ (n)	Median	
6	Caledonian thrust-sheets									
6a	Late Proterozoic to Palaeozoic metasedimentary and metamafic rocks	561	500–450	Metagreywacke, phyllite, mica schist, lesser volumes of marble and greenstone.	Passive margin sequences. Greenstones formed in oceanic arc / back-arc.	Low- to high-grade metamorphism during the Caledonian orogeny at c. 450–400 Ma.	1.47	1.40 $\pm$ 1.39	48 $\pm$ 8 (12)	49
6b	Caledonian intrusive rocks	167	480–430	Dominantly calc-alkaline diorite, tonalite, granodiorite and granite. Minor trondhjemitic intrusions.	Active continental margin.	Variable overprinting during the Caledonian orogeny at c. 430–410 Ma.	1.85	1.74 $\pm$ 1.85	66	66
6c	Seiland igneous province	n.d.	570–560	Gabbro, lesser volumes of ultramafic rocks and intermediate granitoid rocks.	Intracontinental rift.	Variable overprinting during the Caledonian orogeny at c. 420 Ma.	1.10	0.71 $\pm$ 0.57	n.d.	n.d.
6d	Precambrian gneissic rocks	35	1690–950	Syenitic to monzonitic gneisses, anorthosite-mangerite-charnockite-granite suites	Active continental margin. AMCG suite formed in intraplate setting (?)	Late Sveconorwegian, high-grade metamorphism at c. 930 Ma. Variable, but locally high-grade metamorphism at c. 450 Ma.	2.01	1.70 $\pm$ 1.78	41 $\pm$ 11 (4)	43
6e	Neoproterozoic metasedimentary rocks	48	1000–500	Quartzitic to arkosic sandstone, mica schist, pelite and volumetrically subordinate carbonate	Continental shelf	Variable high- to low-grade Scandian and pre-Scandian metamorphism in Finnmark. Low-grade overprinting in Lillehammer during the Scandian phase at c. 430–400 Ma.	1.35	1.31 $\pm$ 0.82	43 $\pm$ 6 (4)	42
7	Devonian sedimentary rocks	15	400–390	Fluvial sandstones, conglomerate, breccia	Post-orogenic extension	No metamorphic overprinting.	1.33	1.23 $\pm$ 0.47	n.d.	n.d.
8	Cambro–Silurian sedimentary rocks	37	540–420	Marine shales, carbonates, sandstones	Epicontinental basin, later foreland basin	Low-grade metamorphism and deformation during the Caledonian orogeny at c. 420 Ma; local contact metamorphism during formation of Oslo rift at c. 300–280 Ma.	1.89	1.56 $\pm$ 1.45	48 $\pm$ 8 (6)	51
9	Oslo Rift	1044	300–280	Tholeiitic basalts, monzonite, syenite and granite	Intracontinental rift.	No metamorphic overprinting.	2.93	2.50 $\pm$ 1.64	45 $\pm$ 8 (4)	46

See Slagstad (2008) for details and references.

<sup>1</sup>Area-weighted heat production of all map units classified within the particular geological province.

n.d. = not defined.

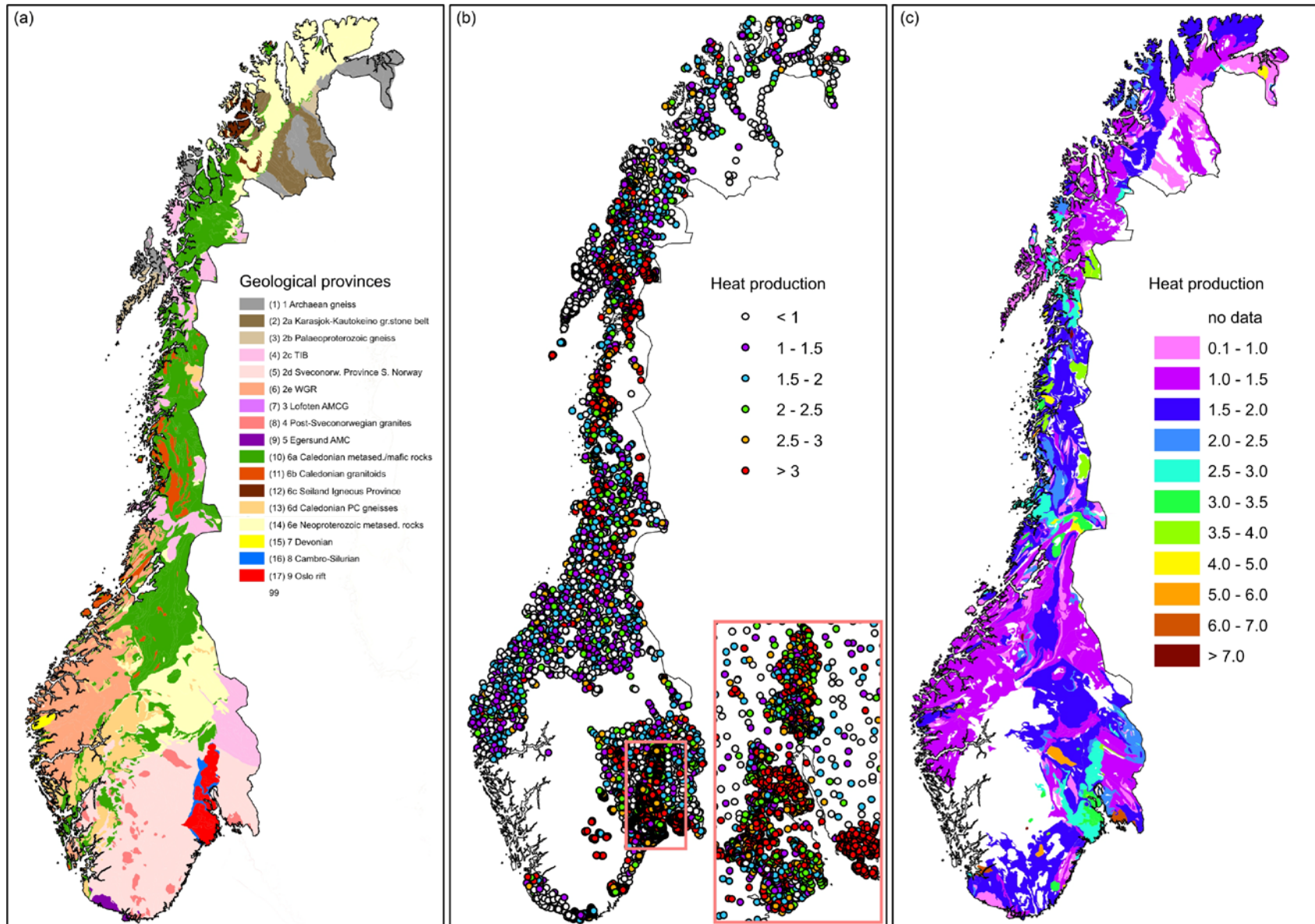
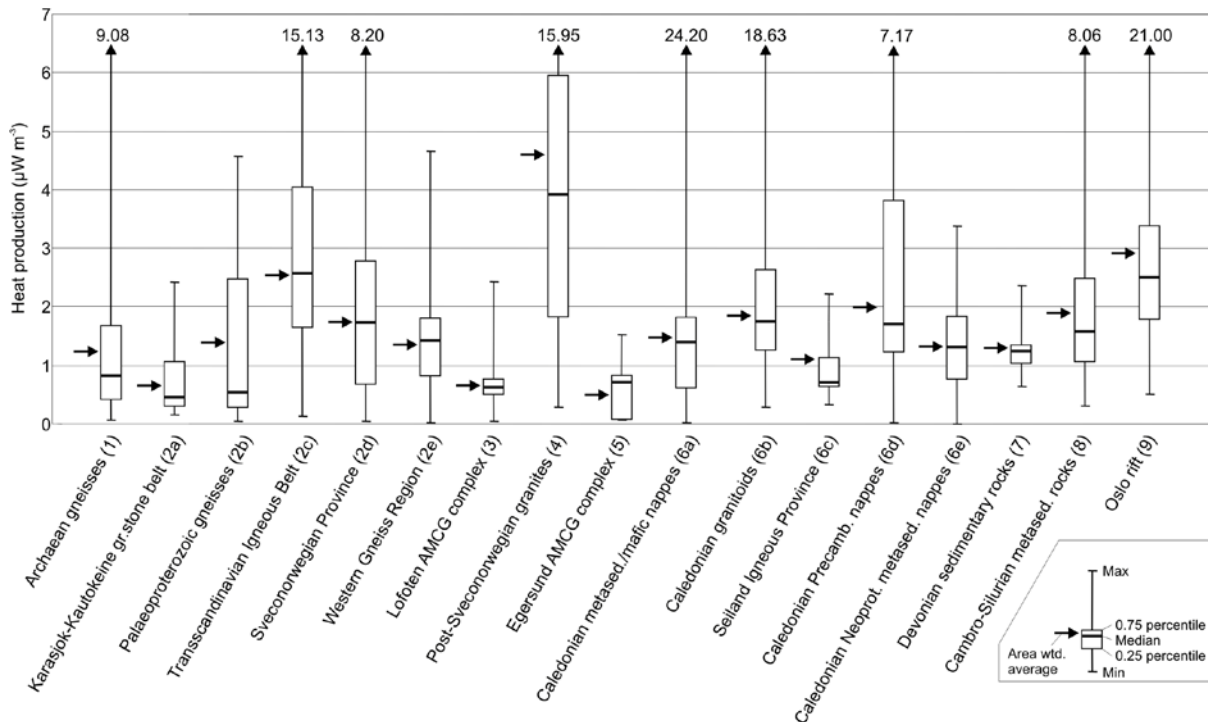


Figure 4.1. (a) Simplified geological map, modified after Sigmond (1998). (b) Heat production data. (c) Average heat production rates for geological units where data are available Figure from Slagstad (2008), updated with new data from Finnmark.



**Figure 4.2.** Heat production data from geological units presented in Table 4.2. and Fig. 4.1. (from Slagstad 2008, updated with new data from Finnmark).

The metasedimentary rocks show a small increase in heat production with increasing SiO<sub>2</sub> at low SiO<sub>2</sub>, then a gentle decrease (Fig. 4.3a). The trend is opposite with respect to Fe<sub>2</sub>O<sub>3</sub> (Fig. 4.3e). In contrast the other three groups, consisting of magmatic rocks and orthogneisses, display increasing heat production with increasing SiO<sub>2</sub> (Figs. 4.3b-d) and vice versa with respect to Fe<sub>2</sub>O<sub>3</sub> (Figs. 4.3f-h). These variations reflect different mechanisms controlling the mineralogical and major element composition of sedimentary and magmatic rocks (Kukkonen & Lahtinen 2001). The composition of sediments partly reflects their source, resulting in correlations that are similar to those observed in magmatic rocks, and partly sedimentary sorting due to variation in the size and density of different minerals. Mica-rich rocks such as schist and phyllite represent low degrees of sedimentary sorting whereas quartz-rich rocks such as arkose and quartzite represent high degrees of sorting. Since U- and Th-bearing minerals are commonly hosted by micas, sedimentary sorting results in an inverse correlation between heat production and degree of sorting. The variation in heat production with SiO<sub>2</sub> and Fe<sub>2</sub>O<sub>3</sub> in the metasedimentary rocks reflects both these processes. Between 45 and 60 wt.% SiO<sub>2</sub>, heat production increases with increasing SiO<sub>2</sub>. The rocks in this range include mica schist and phyllite, representatives of poorly sorted sediments, and the variation in heat production most likely reflects that of the source. Rocks with >60 wt.% SiO<sub>2</sub> consist of mica schist and phyllite at low SiO<sub>2</sub> and arkose and quartzite at high SiO<sub>2</sub>, representing increasing degrees of sorting, resulting in an inverse correlation between SiO<sub>2</sub> and heat production. The other lithological groups represent magmatic rocks of mafic to intermediate ('Metamafic rocks'), intermediate to felsic ('Granodioritic rocks'), and felsic ('Granitic rocks') composition. The increase in heat production with SiO<sub>2</sub> and opposite for Fe<sub>2</sub>O<sub>3</sub> is consistent with magmatic processes where low degrees of partial melting and/or high degrees of fractionation lead result in high SiO<sub>2</sub>/low Fe<sub>2</sub>O<sub>3</sub> melts with high incompatible element (including U, Th) contents and vice versa. At very high SiO<sub>2</sub> and low

Fe<sub>2</sub>O<sub>3</sub>, the relationship breaks down due to crystallisation of accessory phases that deplete the residual melt in incompatible elements; thus, further fractionation and concomitant increase and decrease in SiO<sub>2</sub> and Fe<sub>2</sub>O<sub>3</sub>, respectively, does not lead to increased levels of elements which were incompatible earlier in the fractionation process.

Figures 4.3i-l show how heat production varies with total REE content. In most rocks, REE are hosted by accessory phases and REE content may therefore be used as a proxy for the amount of accessory phases in a rock. All rock types show a relatively well-defined positive correlation between total REE content and heat production, supporting the general consensus that the heat producing elements are hosted dominantly by accessory phases (e.g., Fountain 1986, Kukkonen & Lahtinen 2001).

#### 4.5.2 Tectonic setting

Consistent differences in chemical composition have long been used to discriminate between different tectonic settings (e.g., Pearce & Cann 1973). From the above discussion on heat flow and composition, one may therefore expect similarly consistent differences in heat production. Since the purpose of this contribution is to characterise the heat production of different geological provinces, there is a certain lumping of different lithologies formed in different tectonic settings. I therefore base this discussion on 3 provinces that display rather narrow lithological variation and the tectonic setting is relatively well defined. The Palaeoproterozoic Transscandinavian Igneous Belt (TIB) consists of granitic rocks formed along the active margin of Baltica in a subduction setting, and yields a median heat production of 2.57  $\mu\text{W}/\text{m}^3$ . The Post-Sveconorwegian granites formed during the Early Neoproterozoic, following the Sveconorwegian orogeny. Although the process(es) leading to their formation is uncertain, it is clear that they formed in an intracontinental setting. The Post-Sveconorwegian granites yield a median heat production of 3.92  $\mu\text{W}/\text{m}^3$ . The Permian Oslo Rift represents magmatic rocks formed in an intracontinental rift and yields a median heat production of 2.50  $\mu\text{W}/\text{m}^3$ . However, the Oslo Rift consists of a variety of rock types including syenites and other intermediate rocks, as well as basalts. Including only Permian granites in the calculation yields a median heat production of 3.23  $\mu\text{W}/\text{m}^3$ . These results compare well with numerous investigations showing that rocks formed in continental, extensional settings, be it continental back-arcs, continental rifts, or post-orogenic extension, are enriched in incompatible elements (Frost et al. 1999, Slagstad et al. 2004, Anderson & Morrison 2005). There are probably a number of reasons for the difference in composition between rocks formed in intraplate and plate margin settings. The most obvious difference is that most plate margin magmas form by partial melting in the mantle wedge overlying a subduction zone, whereas intraplate magmas commonly form in areas where upwelling of hot asthenospheric melts induces partial melting of lower crustal rocks. Lower crustal rocks, although generally depleted relative to upper crustal rocks, are significantly more enriched in heat producing elements than the mantle wedge, thus providing a source for relatively enriched magmas. Tectonic setting can therefore be used as a rough guide to a province's heat production.

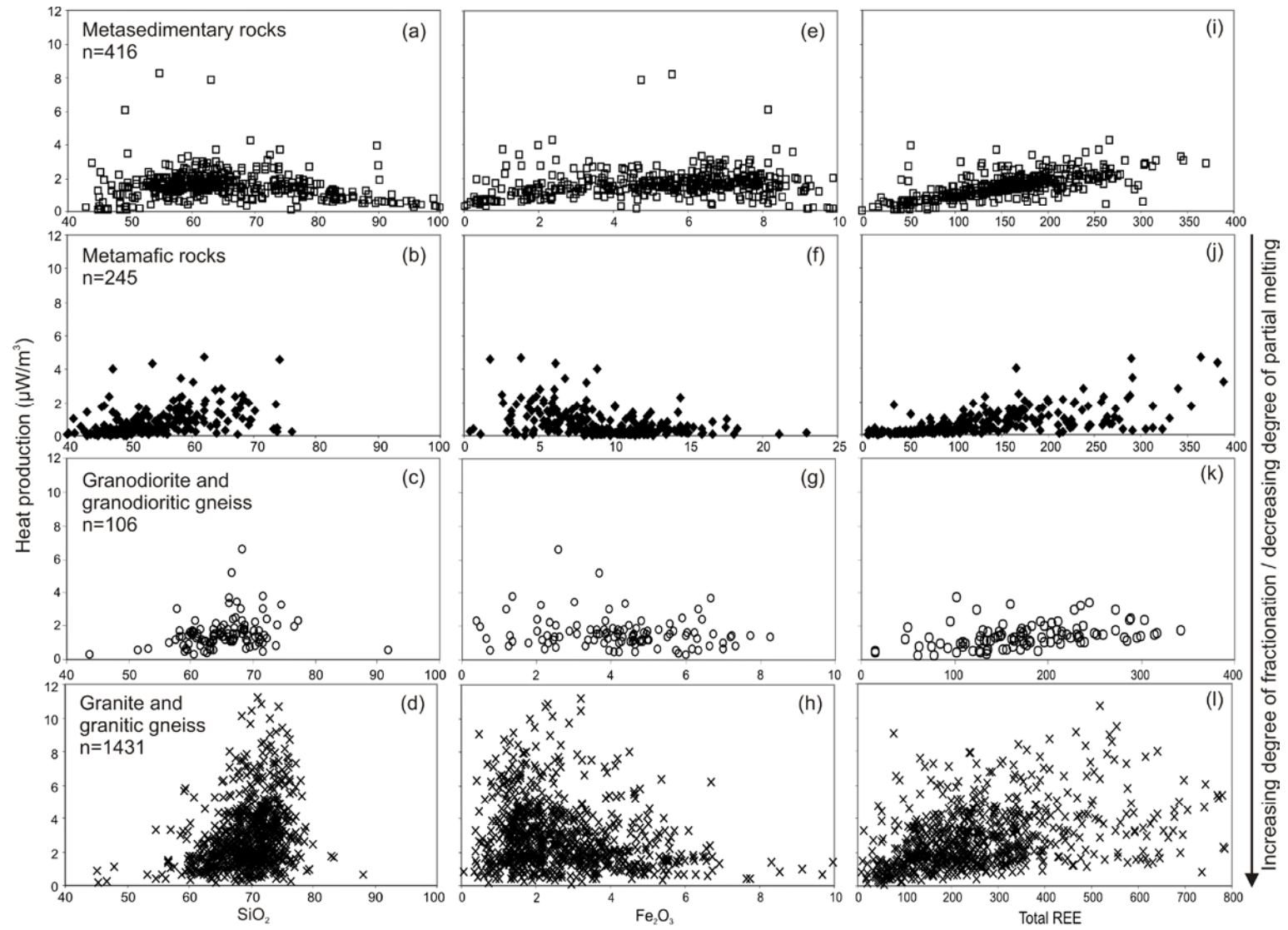


Figure 4.3. Heat production vs. chemical composition sorted by rock type.

## 4.6 Heat production vs. age and metamorphic grade

### 4.6.1 Age

Radiogenic heat production is sometimes considered to decrease with increasing age, although some studies fail to find such a correlation (e.g., Kukkonen & Lahtinen 2001). Figure 4.2 shows the heat production rates of the various geological provinces considered here, broadly arranged in chronological order. Figure 4.2 shows that there is no clear-cut relationship between geological age and heat production, despite the fact that the Archaean gneisses display relatively low heat production rates, with a median of  $0.81 \pm 1.48 \mu\text{W}/\text{m}^3$ . This is similar to that of Archaean gneisses in Finland ( $0.79 \pm 1.33 \mu\text{W}/\text{m}^3$ , Kukkonen & Lahtinen 2001). However, both the Palaeoproterozoic Lofoten and the Early Neoproterozoic Egersund AMCG complexes display significantly lower heat production rates. Notably, the two AMCG complexes display similar heat production rates despite an age difference of c. 900 million years. This shows that lithological variation exerts a first-order control on heat production. It is therefore more relevant to compare the Archaean gneisses with younger provinces with a similar lithological make up, in particular the Sveconorwegian province in South Norway and the Western Gneiss Region. These provinces consist mainly of Mesoproterozoic intermediate to felsic gneisses, not unlike the Archaean gneisses, but have heat production rates that are somewhat higher (Table 4.2, Fig. 4.2). The available data indicate that a correlation between heat production and geological age may exist, but that this correlation is weak and in most cases obscured by lithological variation. This conclusion is further supported by data from the Palaeoproterozoic Transscandinavian Igneous Belt and the Permian Oslo Rift, which both consist largely of granitoid rocks and display virtually identical heat production despite an age difference of nearly 1.5 billion years. Thus, predicting heat production rates based on geological age is clearly not feasible, a conclusion which is in line with that proposed by Kukkonen & Lathinen (2001).

### 4.6.2 Metamorphic grade (crustal depth)

Many workers assume that heat production decreases with increasing metamorphic grade or crustal depth because during orogenesis, partial melting at lower to middle crustal levels commonly form melts rich in incompatible elements, including the heat producing elements, may migrate to higher structural levels (e.g., Slagstad et al. 2005). This leads to a depletion of high producing elements at low crustal levels, and concomitant enrichment at higher crustal levels where the melts are emplaced as plutons (Sandiford & McLaren 2002, Sandiford et al. 2002). Although the concept of a rather homogeneous, low-heat producing lower crust is clearly oversimplified (cf., Flowers et al. 2006), it has long been recognised that the middle and lower crust must be depleted in heat producing elements relative to the upper crust to avoid impossibly high temperatures at depth within the crust (e.g., Morgan & Sass 1984). Unfortunately, true lower crustal rocks are exposed in only a few locations in the world, but several studies investigating the variation in heat production in vertical cross sections through the middle to upper crust have been undertaken. Ashwal et al. (1987) investigated a c. 25 km thick vertical section through amphibolite- to granulite-facies Archaean rocks in the Kapuskasing area, Superior Province, Ontario. Their work showed no relationship between vertical depth/metamorphic grade and heat production, which they



suggested could be a typical feature of rather "mafic" geological provinces, whereas more "granitic" provinces are more likely to display such a relationship. Brady et al. (2006) presented heat production data from the Sierra Nevada Batholith, California, and showed that it increased from c. 2 to 3  $\mu\text{W}/\text{m}^3$  in the uppermost 5 km, then dropped to 0.5–1  $\mu\text{W}/\text{m}^3$  at 15 km depth and remained constant at that level to the Moho. These studies show that heat production does not vary continuously or predictably with crustal depth, but that abrupt changes related to lithological variation is the norm.

The Lofoten–Vesterålen area in north Norway, including the Lofoten AMCG complex, is sometimes cited as an example of lower crustal rocks having undergone depletion in incompatible elements due to regional metamorphism (Heier & Adams 1965). However, more recent work suggests that the amphibolite- to granulite-facies transition in this area, interpreted by Heier (Heier 1960) to be a gradual metamorphic transition, could be a contact metamorphic effect (Corfu 2004). It is notable that the Lofoten AMCG complex has a heat production that is nearly identical to the unmetamorphosed Egersund AMCG complex, suggesting that the low heat production of the former is lithologically/tectonically controlled. The above discussion shows that discussions of the impact of metamorphic grade on heat production are hampered by the strong effect of lithological and chemical variation. This means that not only is comparing lithologically different high- and low-grade rocks useless, even comparing lithologically similar high- and low-grade rocks may be meaningless due to the large variation observed among similar rock types. These complexities imply that meaningful investigations into the distribution of heat producing elements and the controlling processes can only be undertaken in areas where the geological setting is particularly favourable. One such area is the Sognefjorden transect, where Caledonian folding and thrusting has resulted in the exposure of a c. 30 km vertical cross section (Milnes et al. 1997) through Sveconorwegian crust. The cross section includes Sveconorwegian granulites (source?), migmatites (melt transfer zone?) and granites (shallow crustal "deposits" of heat producing elements) (Skår & Pedersen 2003), that may reflect processes related to crustal differentiation. Syn-orogenic granites are also found elsewhere in SW Norway (Slagstad & Marker, unpub. data, 2006), suggesting that the middle to lower crust underwent relatively widespread melting during Sveconorwegian orogenesis. This evolution would have had a major impact on the distribution of heat producing elements and thus the thermal structure of the Sveconorwegian crust, which in turn may have affected its behaviour during subsequent tectonic activity.

#### **4.7 Heat production in Finnmark, northern Norway**

The geology of Finnmark (Fig. 4.4a) can briefly be summarised as consisting of an Archaean to Palaeoproterozoic gneissic basement, overlain to the north by autochthonous to parautochthonous sedimentary cover rocks, and overthrust to the west by relatively thin-skinned Caledonian nappes or thrust sheets (e.g., Sturt et al. 1975, Zwaan & Roberts 1978) that were emplaced roughly southeastwards onto the Fennoscandian Shield during the Silurian Scandian orogeny (e.g., Krill & Zwaan 1987, Kirkland et al. 2009). Here we give a brief description of the gneissic basement as well as the Caledonian nappes, focussing on lithological make-up; the most important factor determining heat production (Slagstad 2008), and present a map of radiogenic heat production in Finnmark (Fig. 4.4b).

Archaean rocks in Finnmark include the Raiseatnu and Jergol Complexes in Finnmarksvidda and large tracts of the Sør-Varanger area. Lithologically, the Raiseatnu and Jergol Complexes are rather similar and composed dominantly of medium- to high-grade orthogneisses of tonalitic, granitic and dioritic composition (Siedlecka et al. 1985), whereas the Sør-Varanger area is more varied and comprises mica schists and mica gneisses in addition to tonalitic to granitic orthogneisses (Levchenkov et al. 1993). 46 samples are available from the Jergol Complex and the Sørvaranger area, yielding a mean heat production of  $1.25 \pm 1.04 \mu\text{W}/\text{m}^3$  ( $\pm 1\sigma$ ). No samples are available from the Raiseatnu.

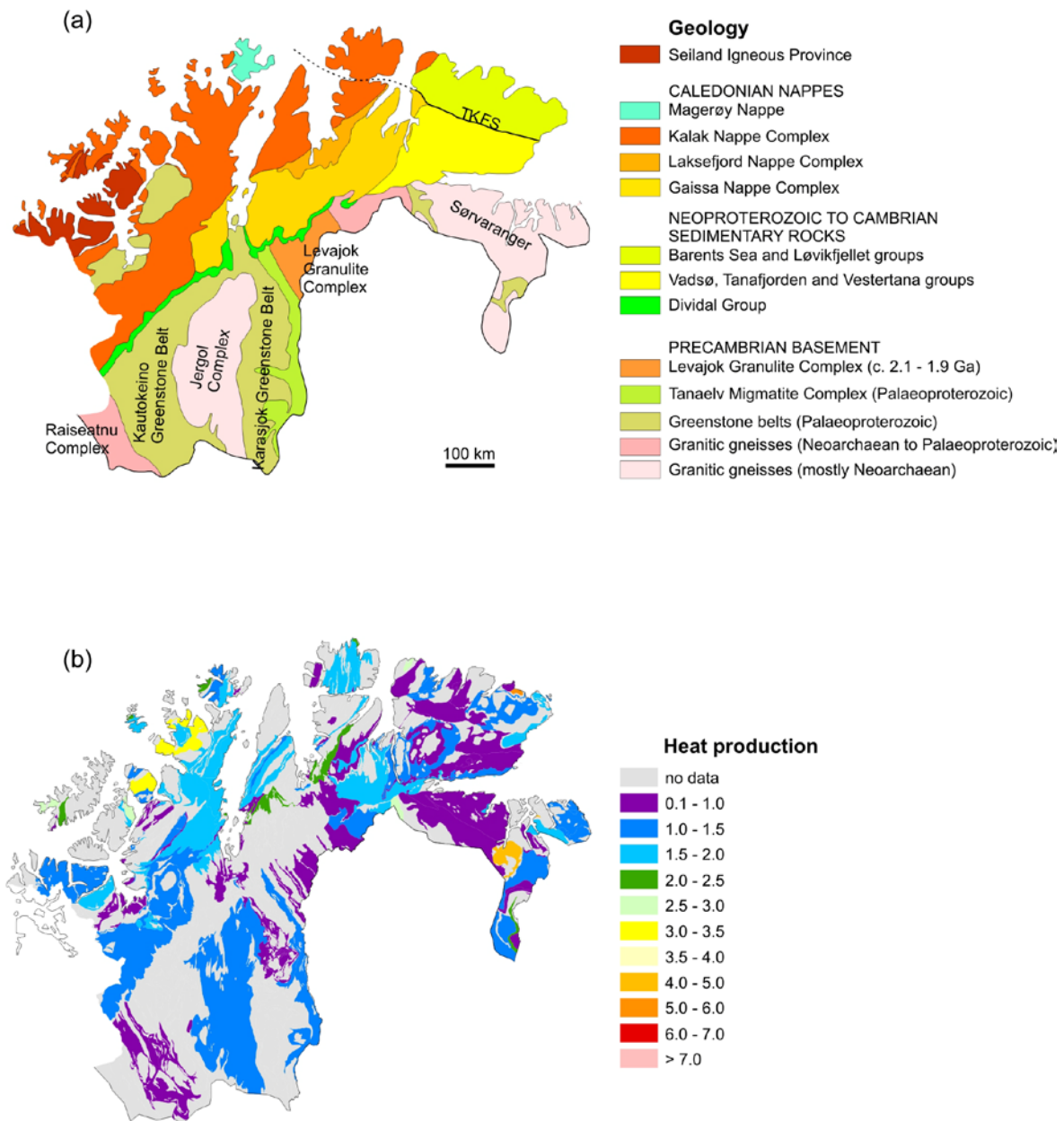


**Figure 4.4.** (a) Geological map of Finnmark, simplified from Siedlecka and Roberts (1996). (b) Radiogenic heat production in Finnmark.

The Karasjok and Kautokeino Greenstone Belts in east Finnmark (Fig. 4.4a) consist of tholeiitic metabasalts, tuffaceous greenstones and amphibolites interlayered with

metasedimentary rocks (Siedlecka et al. 1985). A Sm–Nd whole-rock age of ca. 2100 Ma from komatiites of the Karasjok Greenstone Belt was interpreted by Krill et al. (1985) to date crystallisation of the komatiite. The Greenstone Belts are believed to have formed as a result of crustal extension and/or rifting at ca. 2100 Ma, producing various mafic volcanic rocks, followed by subduction and formation of arc-related magmatic rocks at ca. 2000 Ma (Krill et al. 1985, Marker 1985). These oceanic provinces were thrust westwards onto the Archaean Karelian craton at ca. 1.9 Ga (Krill et al. 1985, Braathen & Davidsen 2000). The rocks were mostly metamorphosed under low to medium conditions (sub-greenschist to amphibolite-facies) (Siedlecka et al. 1985) during this event. 34 samples are available from the Karasjok-Kautokeino Greenstone belts, yielding a mean heat production of  $0.67 \pm 0.52 \mu\text{W}/\text{m}^3$ .

The Levajok Granulite Complex is sparsely exposed in Norway, but widens towards the east and southeast into Finland and Russia and forms a unit of regional extent; it is therefore included here as a separate unit. The granulite complex consists of two main lithologies (Marker 1985, Siedlecka et al. 1985) of which the oldest is a garnet-quartz-feldspar paragneiss that most likely represents continental back-arc basin flysch deposits. Younger, hypersthene-plagioclase orthogneisses probably represent intrusions into the paragneiss at ca. 2000–1900 Ma, possibly coeval with granulite-facies metamorphism during continent-continent collision (Bernard-Griffiths et al. 1984). 9 samples are available from the Levajok Granulite Complex, yielding a mean heat production of  $0.81 \pm 0.37 \mu\text{W}/\text{m}^3$ .

Neoproterozoic to Cambrian sedimentary assemblages on the Varanger Peninsula, northern Norway, are separated into platformal and basinal domains along the NW-SE-trending, Trollfjorden-Komagelva Fault Zone (TKFS) (Roberts et al. 2008). Platformal successions southwest of the fault range from autochthonous to allochthonous and comprise the fluvial to shallow-marine Vadsø, Tanafjord and Vestertana groups. 26 samples from the Vadsø, Tanafjord and Vestertana groups yield a mean heat production of  $1.05 \pm 0.64 \mu\text{W}/\text{m}^3$ . Northeast of the fault zone, successions are allochthonous and most have been involved in modest dextral strike-slip translation along the fault. They comprise the Barents Sea Group, the unconformably overlying Løkvikfjellet Group, and slightly higher-grade rocks of the Tanahorn Nappe. 23 samples from the allochthonous rocks northeast of the TKFS yield a mean heat production of  $1.33 \pm 1.15 \mu\text{W}/\text{m}^3$ .

The Caledonian nappes in Finnmark consist mainly of quartzitic to arkosic sandstone, mica schist, and pelite to volumetrically subordinate carbonate (Roberts 1985). Deposition mainly took place at various times beginning in the Late Mesoproterozoic and continuing through the Neoproterozoic, and in most cases the rocks appear to represent continental or shelf deposits, although the provenance and original palaeogeography of the rocks is debated (Corfu et al. 2007, Kirkland et al. 2007, Roberts 2007). The rocks were deformed and metamorphosed repeatedly during the Neoproterozoic (e.g., Kirkland et al. 2006a), and thrust into their present position during the Scandian phase of the Caledonian orogeny at ca. 430–420 Ma (Siedlecka et al. 1987, Kirkland et al. 2006b, Slagstad et al. 2006). The metamorphic grade varies from low to the east to high to the west. 113 samples from the mainly metasedimentary Caledonian nappes in Finnmark yield a mean heat production of  $1.60 \pm 0.83 \mu\text{W}/\text{m}^3$ .

The Seiland Igneous Province in western Finnmark (Fig. 4.4a) is dominated by tholeiitic, calc-alkaline and alkaline gabbros and rarer monzonitic, dioritic and ultramafic bodies (e.g., Robins & Often 1996). Recent dating of the voluminous gabbros shows that they formed in a comparatively short time interval, from ca. 570 to 560 Ma (Roberts et al. 2006), most likely

in an intracontinental rift setting (Krill & Zwaan 1987, Roberts et al. 2006). The province was subjected to Scandian deformation and medium- to high-grade metamorphism at ca. 420 Ma, and evidence of a preceding tectonic event is lacking (Krill & Zwaan 1987, Roberts et al. 2006, Slagstad et al. 2006). 9 samples from the Seiland Igneous Complex yield a mean heat production of  $0.94 \pm 0.57 \mu\text{W}/\text{m}^3$ .

## 5 GEOCHRONOLOGICAL STUDIES OF OFFSHORE BASEMENT SAMPLES

Børre Davidsen, David Roberts & Trond Slagstad, NGU

### 5.1 Overview

The geochronology work on the offshore basement drill cores, conducted under the HeatBar project forms a continuation of the work conducted under the Kontiki Project.

In total, thirty samples of basement rocks from 22 wells in the North Sea, Norwegian Sea and Barents Sea were obtained from the Norwegian Petroleum Directorate. In the Kontiki Project zircon was separated from 11 samples from the North Sea and Norwegian Sea, and analysed for Pb/U- age determination, either by laser ablation–inductively coupled plasma–mass spectrometry (LA–ICP–MS) at the Geological Survey of Norway and/or by secondary ion mass spectrometry (SIMS) at the Nordsim laboratory in Stockholm. Seven of the samples have been analysed using both techniques.

In this project, six of the remaining offshore drill cores from the Finnmark coast and Barents Sea have been processed for zircon separation. Zircons were retrieved from only three of the samples:

- 7120/12-2, Norwegian Sea: Grey, mylonitic gneiss
- 7128/4-1, Finnmark east, the Barents Sea: Laminated sandstone
- 7128/6-1, Finnmark east, the Barents Sea: Sandstone

while the remaining three were barren:

- 7120/1-1, Loppa High, Norwegian Sea: Orthogneiss/amphibolite
- 7120/2-1, Loppa High, Norwegian Sea: Diabase?
- 7226/11-1, Norsel High, Barents Sea: Biotite schist/gneiss

As there were few offshore data points, and geochronology data sets are absent for parts of the Norwegian mainland, four samples collected by David Roberts from the eastern part of Finnmark were processed as well, as a part of this project. Together with existing data from the western part of Finnmark, these samples will provide the necessary reference frame for the interpretation of the zircon age results from the offshore drill cores.

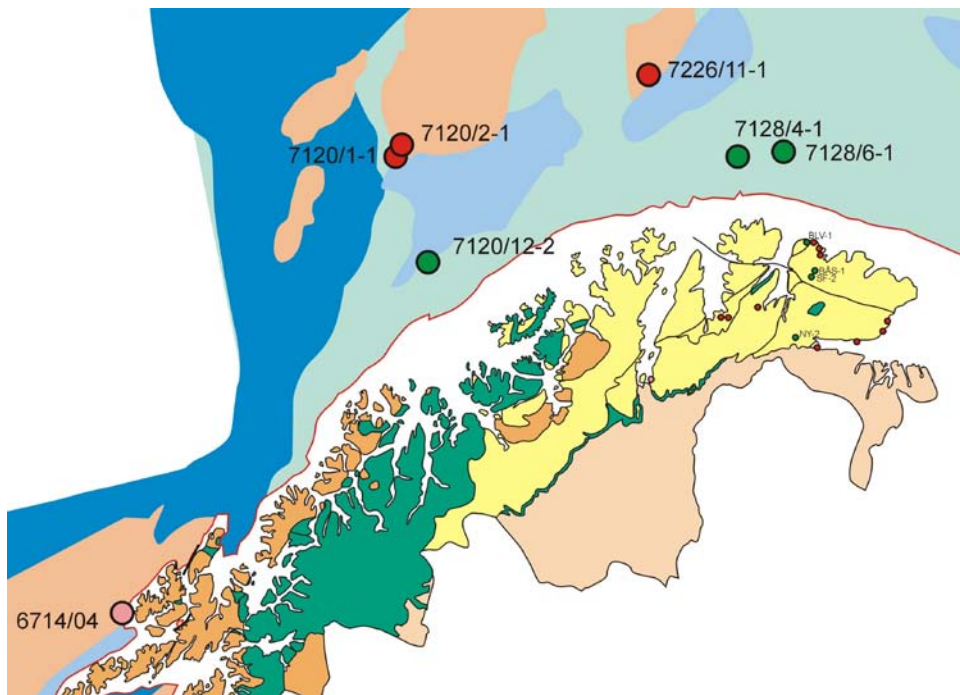


**Figure 5.1.** Location of the offshore boreholes penetrating crystalline basement. Green dots represent wells for which zircon datings were made.

## 5.2 Results

Drill core 7120/12-2, from the Norwegian Sea, penetrated a grey, mylonitic gneiss that has been sampled at 4675.8 m depth. Zircons from this sample have been dated to c. 2750-2800 Ma. The protolith most likely presents a felsic intrusive rock, now an orthogneiss. Its composition and age strongly suggests a correlation with the Archaean rocks of Ringvassøya and Vanna in Troms County. Thus, it is probably a NNE-ward continuation of the Precambrian basement present in Lofoten/Vesterålen and on the Troms islands.

The drill cores 7128/4-1 and 7128/6-1, from the Barents Sea, both sampled basement rocks in the form of (unmetamorphosed) sandstones at 2525-2540 m depth. Zircon age dating of sedimentary rocks does not provide an age of emplacement in the same way as with magmatic rocks. Rather, the zircons will display an age spread, reflecting the age of the sources supplying detritus for the sandstone. The youngest zircon in the data set also provides a maximum age for the deposition of the sandstone.

Preliminary results show the same main features for the two samples:

A multimodal spread that extends from c. 1.0 to 1.9 Ga with three groups centred at c. 1.0, around 1.2-1.3 and 1.5-1.8 Ga, with a small subsidiary group at c. 2.6 Ga.

The interpretation of these sandstones will include comparing their ages with those obtained on various sedimentary units on the neighbouring mainland, and constructing a geological history taking into account all relevant factors. This is beyond the scope of this report.

In addition, preliminary age determinations have also been obtained on four samples supplied by David Roberts from the Varanger Peninsula:

- NY-2: Nyborg Formation, Tanafjord Group
- BÅS-1 (two samples): Båsnæring Formation, Barents Sea Group.
- SF-2: Sandfjord Formation, Løkvikfjellet Group.
- BLV-1: Berlevåg Formation, Tanahorn Nappe

These samples also represent unmetamorphosed Neoproterozoic sandstones. The results have been presented at EUG in Vienna (by D. Roberts), and the submitted abstract is enclosed in Appendix A.

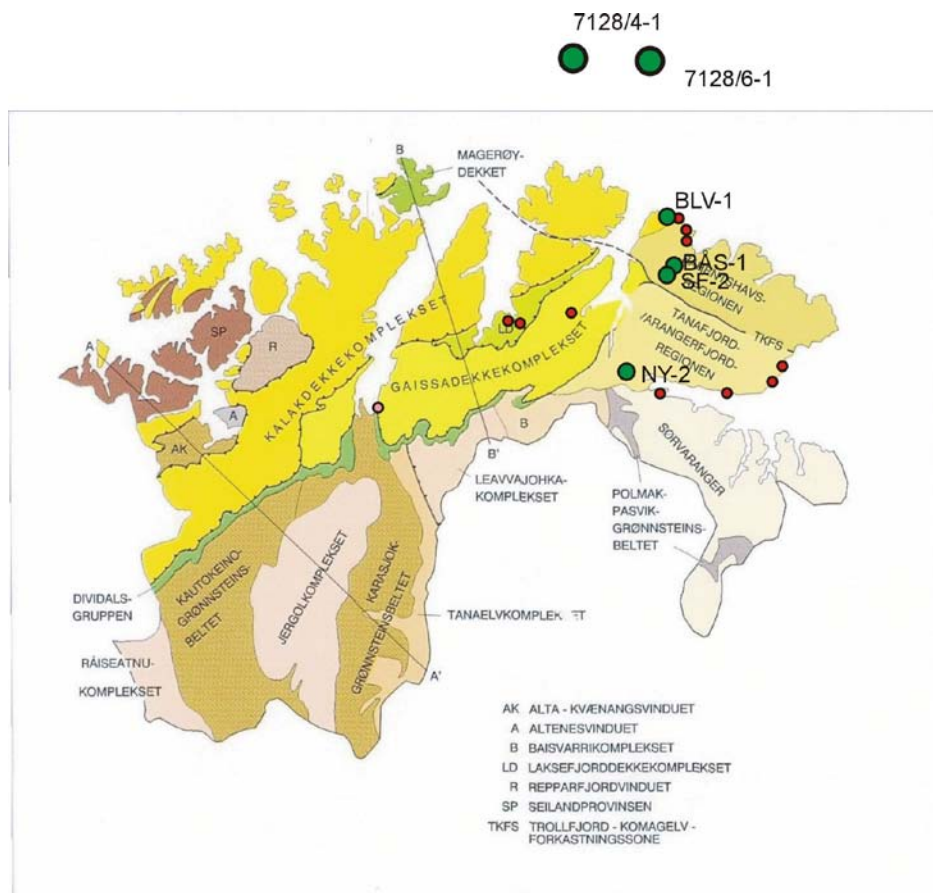


Figure 5.2. Samplig locations onshore Finnmark.





## **6 3D DENSITY AND MAGNETIC CRUSTAL CHARACTERISATION OF THE SOUTHWESTERN BARENTS SHELF**

Cécile Barrère & Jörg Ebbing, NGU

### **6.1 Introduction**

The 3D model was established as an input for the characterization of the thermal structure of the SW Barents Sea. Aeromagnetic and gravity data based on integration of multiple surveys at different scales and heights provide a main tool for mapping crustal structures both on mainland Norway and in the adjacent offshore regions. Basins in the western Barents Sea region have a depth of up to 14 km and are generally narrow compared to the broad basins in the eastern Barents Sea that have a maximum thickness of 20 km. The western Barents Sea basins are generally interpreted to be rift basins, but the distribution of different basement types is not well studied (e.g. Faleide et al. 1993, 1996); e.g. the location of the Caledonian front/suture is a matter of ongoing discussion (e.g. Ritzmann & Faleide 2007, Barrère 2009, Barrère et al. 2009). For the western Barents Sea, top basement maps have been presented previously by Johansen et al. (1992) and Skilbrei (1991, 1995). Skilbrei (1991, 1995) used magnetic depth estimates integrated with seismic profiles to construct his top basement map. The compilation by Johansen et al. (1992) is based on a similar approach and integrated further data from the Eastern Barents Sea.

In a recent study, which is reported here, Barrère (2009) modified the top basement from Skilbrei (1991, 1995), making use of a significantly improved seismic coverage (e.g. Breivik et al. 2005) and an improved aeromagnetic and gravity data base (e.g. Olesen et al. 2010). Barrère (2009) presents also a characterization of the basement lithology. The structure of the western Barents Sea shelf has a complex history imprinted in the basement structure and lithology, Using the petrophysical data from onshore Norway and following magnetic lineations from onshore to the Barents Sea, a division of different basement blocks in the western Barents Sea can be made (Barrère et al. 2009). We improve the initial model, which was based on 2D modelling in and study the different basement types and the depth to the top basement by 3D modelling (Barrère 2009). The 3D model allows also presenting the crustal structure (e.g. top basement, Moho) of the SW Barents Sea, which will be an input to thermal modelling.

*N.B.: this chapter has been copied by the second author and pasted in NGU report 2009.020*

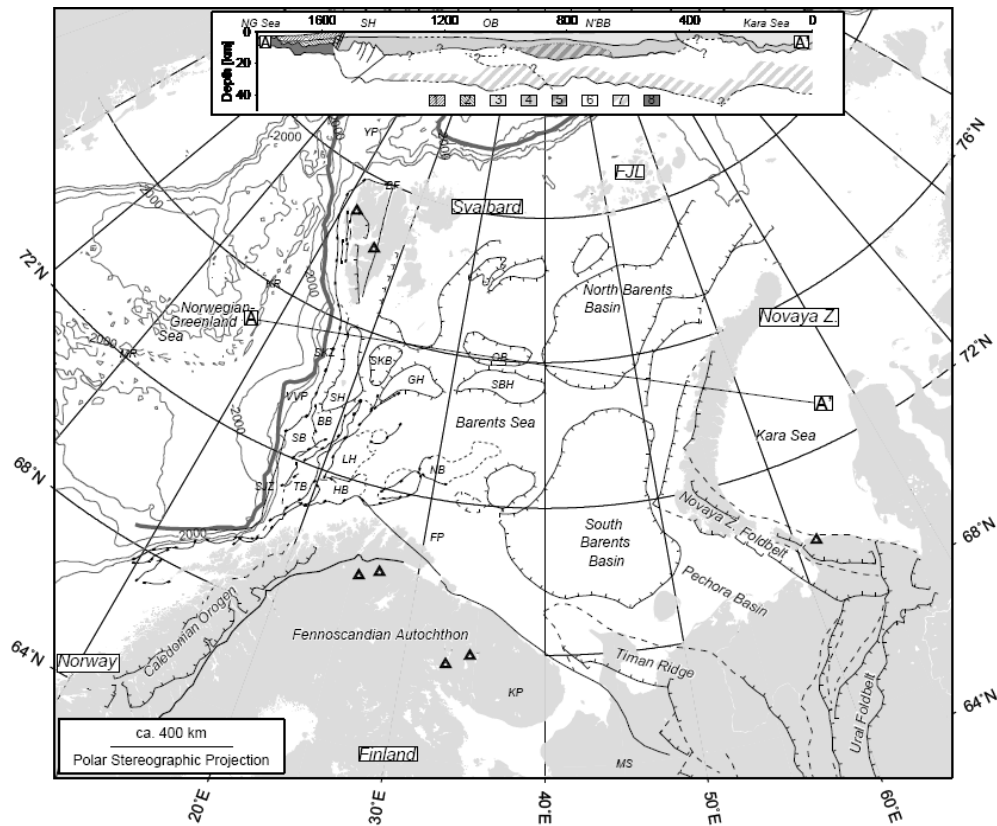


**Figure 6.1.** Overview map of the Barents Sea and surrounding regions (Ritzmann et al. 2007). BB: Bjørnøya Basin; BF: Billefjorden Fault; FP: Finnmark Platform; FJL: Franz-Josef Land; GH: Gardabanken High; HB: Hammerfest Basin; KP: Kola Peninsula; KR: Knipovich Ridge; LH: Loppa High; MR: Mohns Ridge; MS: Mezen Syncline; NB: Nordkapp Basin; OB: Olga Basin; SB: Sørvestsnaget Basin; SBH: Sentralbanken High; SH: Stappen High; SKB: Sørkapp Basin; SKZ: Sørkapp Fault Zone; SJZ: Senja Fracture Zone; TB: Tromsø Basin; VVP: Vestbakken Volcanic Province; YP: Yermak Plateau. Top insert shows a geological profile from the Knipovich Ridge to the Kara Sea (A-A').

## 6.2 Modelling concept

The SW Barents Sea margin (Fig. 6.1) is studied by 3D modelling integrating a wealth of geophysical data: seismic profiles, commercial and scientific drilling on the shelf and mainland Norway, petrophysical sampling and a dense coverage of gravity and aeromagnetic data. Magnetic depth estimates provide a good starting point for a genuine structural interpretation (e.g. an interactive modelling or a constrained inversion). Skilbrei et al. (1991) and Mørk et al. (2002) show that the susceptibilities of the basement can range between 0.005 and 0.035 SI while the susceptibilities of the overlying sediments are only in the order of 0.0003 SI, some one to two orders of magnitude lower. The range of susceptibilities for the basement is depending on composition and varies from 0.005-0.01 for Caledonian basement, 0.01-0.035 for Precambrian basement, to even higher values for mafic intruded basement (e.g. Barrère et al. 2009). Therefore, magnetic data are extremely useful to estimate the top basement.

Skilbrei & Olesen (2005) studied the accuracy and the geological meaning of the ‘magnetic basement’ on the mid-Norwegian margin. They found generally good agreement between estimates made from magnetic anomalies and the depth to the Precambrian basement. In some areas there may exist non-magnetic Devonian basins, and non-magnetic Caledonian nappes can overly the Precambrian basement. In the latter case, the true crystalline basement would lie above the ‘magnetic basement’. Comparison of magnetic depth estimates and seismic, borehole, and petrophysical data yield errors that generally vary between 5% and 15% (Skilbrei et al. 2002).

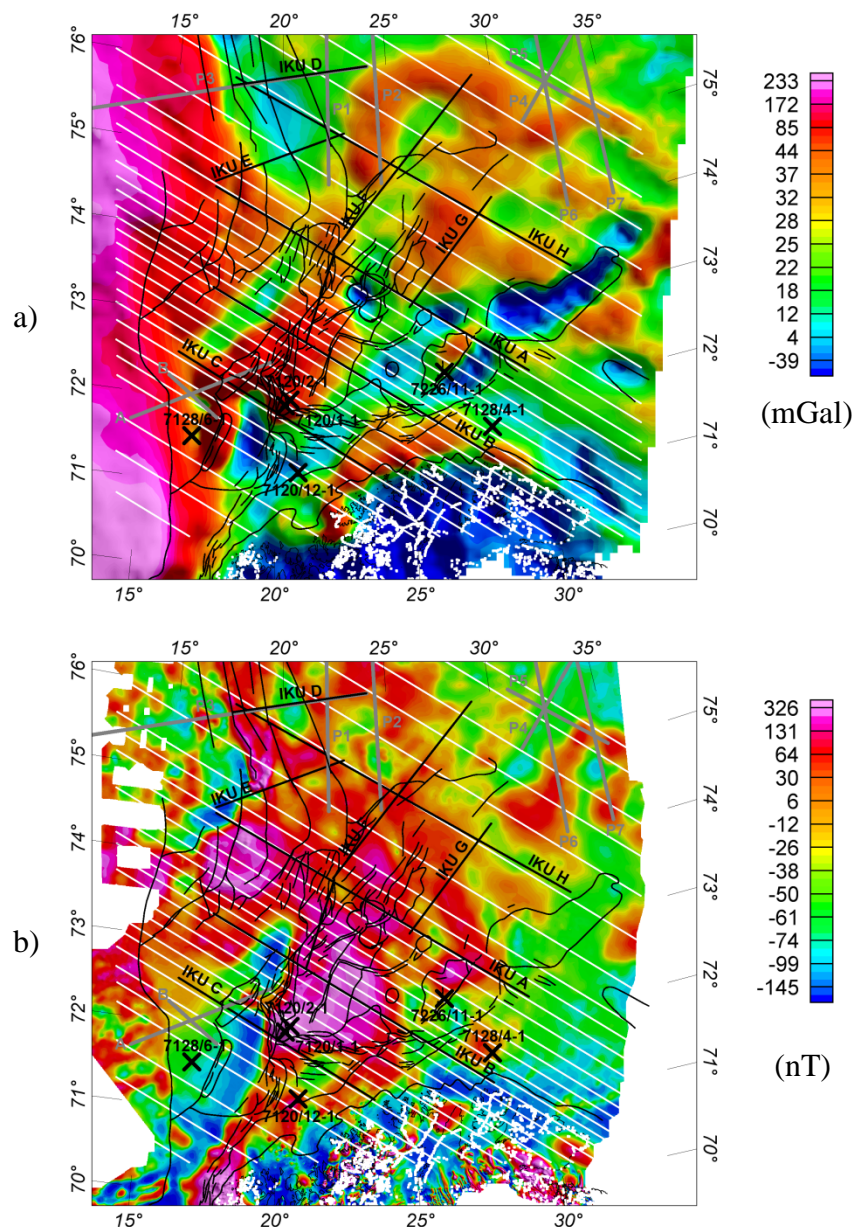


**Figure 6.2.** a) Bouguer anomaly and b) total magnetic field anomaly (reduced to the pole). White lines indicate the vertical planes defining the 3D model, thick grey lines show wide-angle data, thick black lines the IKU seismic reflection data, black crosses the wells reaching the top basement. Locations of petrophysical samples are given by white dots.

Using 3D modelling decreases the uncertainty as seismic, borehole and petrophysical data can be used directly to constrain the top basement structures, and to distinguish between different basement units. Gravity data are useful to a limited extent in the top basement mapping as due to sedimentary compaction at a depth of >5 km, the density contrast between sedimentary rocks and top basement becomes relatively small (e.g. Ramberg & Smithson 1975). The crystalline basement is also on seismic data often difficult to recognize (e.g. Hospers & Ediriweera 1991). This is a result of a decrease in the contrast in acoustic impedance between sediments and basement at greater depths, as well as a decrease in the signal-to-noise ratio. However, the amount of constraints used in constructing the 3D models leads to an overall accuracy of the depth horizons within +/- 5% depending on the reliability of the regional seismic data. At the same time, the 3D models as well as regional compilations provide also information about the base of the crust, which allows calculating total crustal thickness maps.

For the 3D modelling the software package IGMAS (Interactive Gravity and Magnetic Application System, Götze & Lahmeyer 1988) has been used. Within IGMAS the geometry is defined along parallel vertical cross-sections (white solid lines, Fig. 6.2). In our model, line spacing is ranging from 10 to 20 km kilometres depending on the complexity of the modelled structures. The geometry is automatically triangulated between the sections defining the 3D geometry. The gravity and magnetic fields are then calculated and the resulting field compared with the observed potential field.

In order to use absolute densities comparable with the petrophysical database in the modelling a reference mode has to be defined to model the Bouguer anomaly without an arbitrary shift. The densities in the model are defined with respect to reference densities representing the 'normal' crustal column at the coast:

	Depth (km)	Density (kg/m <sup>3</sup> )
upper crust	0-15	2670
lower crust	15-32	2850
mantle	32-120	3300

Magnetisation of crustal rocks is mainly related to the magnetite content in the bedrock, e.g. sedimentary rocks can be considered non-magnetic relative to basement rocks. The Curie temperature of magnetite is 580°C and at this temperature rocks lose their ability to remain magnetized. Assuming a normal thermal gradient the Curie temperature is located in the deep crust. Therefore, we can limit the extension of magnetic sources to the crust. Magnetic field calculations require the definition of an external magnetic field. We define the normal inducing magnetic field with a field strength of 53300 nT, an inclination of 79° and a declination of 4.3°. We can also use the true magnetic field over the study area, which increases the results slightly, but increases substantially the computation time. Therefore, we use the fixed magnetic field and the remanent field is modelled parallel to the induced magnetic field. To setup the 3D model information about the geometry and density/magnetization of the crustal rocks are needed. These parameters are described in the following chapter.

### 6.3 Data

The Bouguer anomaly (Figure 6.2a) is calculated from the free air anomaly compilation by Skilbrei et al. (2000). A simple Bouguer correction at sea was carried out using a bathymetric grid with a resolution of 2000 m and reduction densities of 2200 kg/m<sup>3</sup> and 2670 kg/m<sup>3</sup> for offshore and onshore, respectively. The applied bathymetric data are based on the International Bathymetric Chart of the Arctic Oceans (IBCAO; Jakobsson et al. 2000) and GTOPO30 ([http://eros.usgs.gov/#/Find\\_Data/Products\\_and\\_Data\\_Available/gtopo30\\_info](http://eros.usgs.gov/#/Find_Data/Products_and_Data_Available/gtopo30_info)) data for the onshore domain, with a resolution of 2.5 and 1 km, respectively.

Aeromagnetic data are available from a magnetic compilation (Fig. 6.2b) of the western Barents Sea most recently presented by Olesen et al. (2010). The dataset is compiled from reprocessed aeromagnetic surveys and line spacing ranges from 0.5 to 2.5 km over mainland Norway and from 3 to 8 km over the continental shelf.

In the western Barents Sea strong magnetic anomalies up to > 900 nT are associated with the Loppa and Stappen highs, which have already been recognized as basement highs by e.g. Åm (1975) and Gabrielsen et al. (1990). Within the Loppa High region two different provinces can be distinguished from the potential field data. The western part of the basement high is characterised by a Bouguer high (70 mGal) and a medium magnetic anomaly (100 nT) whereas the eastern part is marked by a decrease in Bouguer anomaly to 0 mGal and an increase in the magnetic field amplitude to 900 nT. The trend of the magnetic anomalies describes an elongated half-circle and indicates a trend from the Billefjorden Fault Zone on Svalbard across the western Barents Sea into Finnmark.

### *6.3.1 Petrophysical data*

Densities of the sedimentary layers are based on well data (Tsikalas 1992) and tables published by Ritzmann et al. (2007) based on velocity-density relationships of sedimentary units obtained from the seismic refraction and reflection/gravity studies. Bedrocks densities are based on direct onshore measurements (Olesen et al. 1990, Galitchanina et al. 1995). Deep crustal densities are based on published values from refraction data models (Breivik et al, 1998, 2002, 2003, 2005, Mjelde et al. 2002) inferred from velocity-density relationships and gravity modelling. The errors from the velocity-density relations on these densities are of the order of  $\pm 50$  kg/m<sup>3</sup> and  $\pm 100$  kg/m<sup>3</sup> for the upper crustal layers and deep crustal layers.

For the magnetic field, the magnetic susceptibility and remanence from the magnetic modelling along IKU A, B and C by Barrère et al. (2009) were used as initial parameters. Those values were derived from onshore samples (Troms and Finnmark regions) (Olesen et al. 1990, Slagstad et al. 2008). Q-ratios (the ratio between remanent and induced magnetization) were applied according to the samples and modified during the modelling. We set a homogeneous and low Q-ratio and magnetic susceptibility for the lower crust and mantle with  $Q=0.4$  and magnetic susceptibility= $1000 \cdot 10^{-5}$  (SI). Sedimentary rocks are set to  $30 \cdot 10^{-5}$  (SI) as they are very low-magnetic in comparison to basement rocks.

### *6.3.2 Geometric constraints from seismic experiments*

To constrain the sedimentary layers we got access to three industrial depth-converted seismic horizons: top Tertiary, base Cretaceous and top Permian. These horizons were produced by

depth-conversion of seismic horizons using regional velocity laws calibrated by well data. The sedimentary rocks are thus subdivided in four sedimentary units: Cenozoic, Cretaceous/Jurassic, Triassic and Palaeozoic. Six wells (black crosses, Fig. 6.2) reach the top basement in the southwestern Barents region; they were used to calibrate the modelled top basement and check the reliability of the depth-converted seismic horizons.

We set up our initial crustal structure using the Barents50 model (Ritzmann et al. 2007), a crustal velocity model with a resolution of 50 km, which also provides information along all available regional seismic profiles with 25 km sampling. The Barents50 model is a seismic-velocity model of the crust in the Barents Sea with a lateral resolution of 50 km (Fig. 6.3). The Barents50 model is based on 2D wide-angle reflection and refraction lines, passive seismological stations and, to a limited extent, potential field data (Ritzmann et al. 2007). The Barents50 compilation also provides information on the deep structure of the crust. For the crust, this compilation includes an intra-crustal horizon inferred mainly on the basis of velocity models and 2D gravity modelling because crustal reflectivity does not allow clear imaging from seismic data alone (e.g. Breivik et al. 2005).

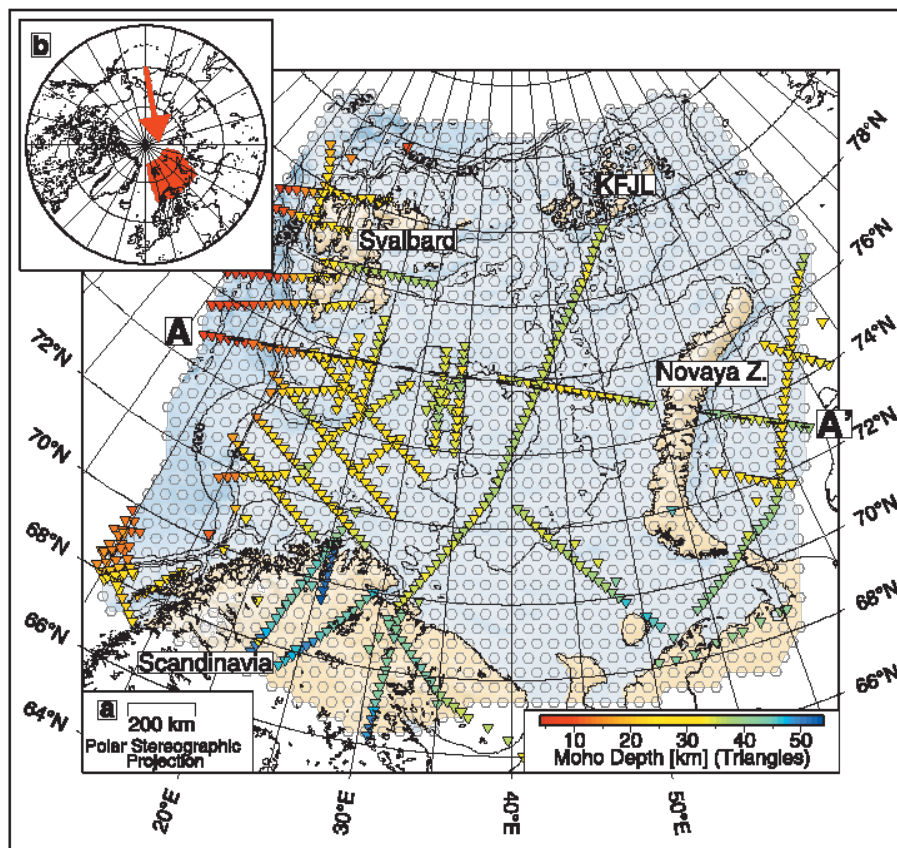


**Figure 6.3.** Presentation of the spatial resolution of the Barents50 and the utilized seismic profiles (in colour) (Ritzmann et al. 2007).

The IKU deep seismic reflections profiles and the seismic refraction data (Breivik et al. 2002, 2003, 2005, Mjelde et al. 2002) were used to constrain the crustal structure of our model. The upper-lower crustal boundary varies between 20 and 22 kilometres depending on the reflectivity along the IKU profiles and the seismic velocities from refraction seismic lines. A

recent OBS profile (Clark et al. 2009) has been used in the final step of the modelling. This profile is running along profile IKU-B, but is extended in the north-west and south-east, and includes stations located onshore Norway. Table 1 shows the published density/velocities for the southwestern Barents Sea and the initial values for our model.

**Table 6.1. Compilation of density/velocity laws applied in the Barents Sea and starting value used in this study.**

Density (kg/m <sup>3</sup> ) – Vp Velocity (km/s)										
		Mjelde et al. 2002	This Study And Barrère et al. 2008	Bungum et al. 2005 Greater Barents Sea Ritzmann and Faleide, 2007 (Southwestern Barents Sea – GM)		Breivik et al. 2003		Breivik et al. 2002		Clark et al. 2008
		Sørvestsnaget Basin;Based on well logs and Ludwig et al 1970	Southwestern Barents Sea - Onshore database and gravity modelling	(ESP velocity data from Jackson et al. 1990 (southwestern Barents Sea) & Sanner 1995)		South Svalbard OBS data and GM		Southeast Svalbard OBS data and GM		Southwestern Barents Sea Seismic refraction data
		Density	Density	Density	Vp	Density	Vp	Density	Vp	Vp
Quaternary		2050		1800	1.80	-		-		1.04-2.00
Cenozoic	Upper Tertiary	2200	2300	2050	2.25	-		-		2.00-3.00
	Lower Tertiary			2280	3.26					
Cretaceous	Upper	2350	2550	2240	2.75-3.60	-	3.50-3.60	-	3.20-3.36	3.00-4.50
	Lower	2400		2370						
Jurassic		2480	2550		4.00-5.45	-	3.80-5.00	-	3.30-4.05	-
Triassic	Upper			2380-2590			4.60-5.45		4.00-4.80	4.50-5.00
	Middle			2470-2590			5.10-5.45		4.50-4.95	
	Lower			2520-2590						
Palaeozoic	PermianCarboniferous	-	-	2640	4.50-5.90	-	5.65-5.90 5.92-5.95		5.10-5.52	5.00
	Near top Basement	2620 Salt 2150	2600	2710	5.50-6.00	-	5.97-5.99		5.80-6.00	
Upper Crust		2750	2750-2850	2770	-	-	-	-	6.3-6.8	6.00-6.50
Lower Crust	Lower Crust Standard	2820	2950	2930	-	2790-2880	-	2890-2990		6.50-7.00
	High Density Body	Vp=7.4	3100 Vp=7.2 –7.4	2980-3050	-					
Oceanic crust		2800-2850-2950	3000	-		2900-2950	-	-		-
Continental Mantle		3220	3280	3300	-	3280-3330	-	3330-3450	8.00	7.50
Oceanic Mantle		3180	3200				8.00			



## 6.4 Modelling results

The final differences between the measured and modelled gravity anomalies have a standard deviation of less than  $\pm 6.8$  mGal. This value is slightly higher than the accuracy for the gravity data, but the remaining mismatch can be explained largely as related to local structures below the resolution of our model (e.g. salt domes). The short-wavelength anomalies ( $<10$  km) onshore have not been modelled and create subsequently local deviations from the modelled Bouguer anomalies. The general pattern is comparable between the observed and modelled magnetic anomalies. The anomalies linked to basement topography (wavelength=100-200 km) are relatively well modelled compared to the short-wavelength ( $<100$  km) anomalies linked to intra-basement magnetic sources and/or shallow magnetic sources. Because of our simplified settings, the magnetic modelling is representing the general magnetic gradients but not the absolute magnetic field amplitudes.

### 6.4.1 Modelled densities

The different crustal units in the model are presented in Table 2, and Figure 6.5a. To produce Moho depth compatible with the computed isostatic Moho and the seismic Moho (Ritzmann et al. 2007), a lower crustal body (LCB) had to be introduced over the central part of the SW Barents Shelf with a density of  $3100 \text{ kg/m}^3$  (surrounding  $2950 \text{ kg/m}^3$ ).

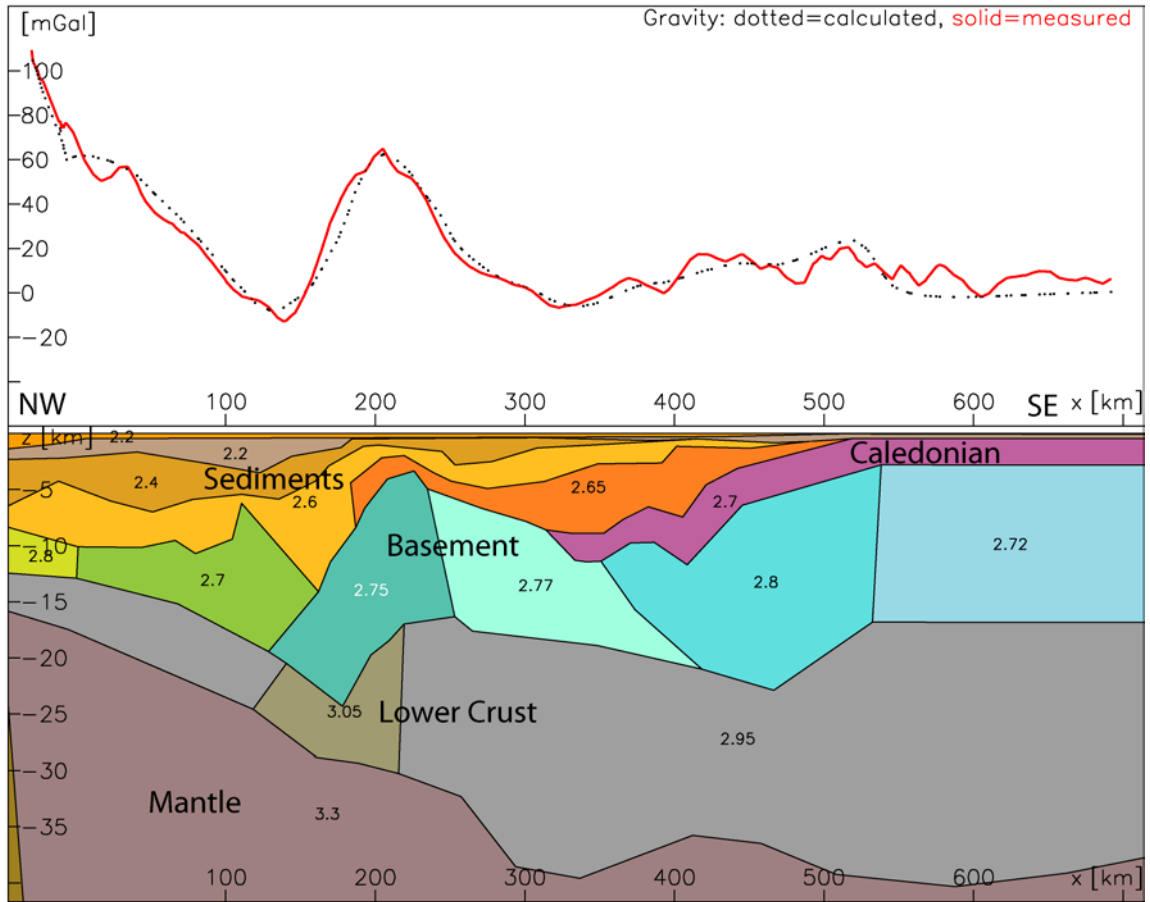
### 6.4.2 Modelled susceptibilities

The top of the magnetic sources is assumed to be the top basement and the top of the oceanic basalts obtained by density modelling, for the continental and oceanic crust, respectively. Due to the resolution of the model and lack of constraining data, no intra-basement magnetic sources are distinguished. The resulting magnetic modelling highlights therefore the main changes in magnetic properties of the upper crust. The final model shows variation of the upper crustal magnetic susceptibility values from  $500 \cdot 10^{-5}$  (SI) to  $5000 \cdot 10^{-5}$  (SI).

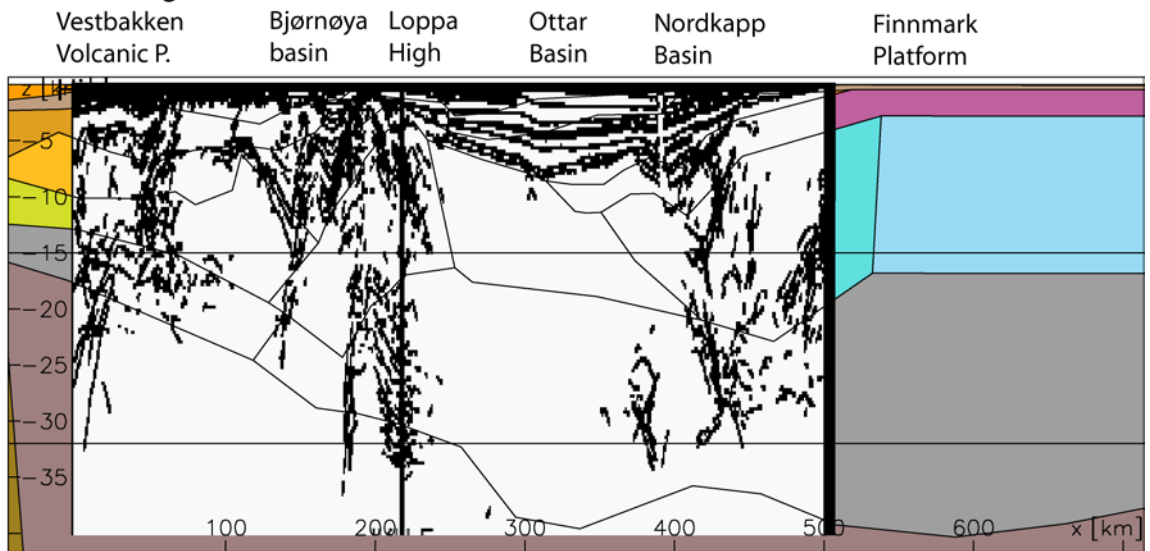
**Table 6.2. Modelling parameters (Barrère 2009): different crustal units are defined by a combination of petrophysical values obtained by density and magnetic modelling. Figure 5a shows the location of the different basement units.**

		Density (kg/m <sup>3</sup> )	Magnetic properties		
			Q-ratio	Susceptibility (.10 <sup>-5</sup> SI)	
lower crust	standard lower crust	2950	0.4	1000	
	LCB high density body	3100	0.4	1000	
oceanic crust	basalt	2950	1	2000	
upper crust	onshore zone	BAS1 onshore Fennoscandian Shield	2700-2750	0.5	1000
		Caledonian nappes – CN	2750	1	500
	costal zone	UCB high-density body	2810-2850	0.5	1000
	Loppa High zone	BAS1 Loppa High (South & west)	2750	0.6	4000
		BAS1 Loppa High (East & North)			3000
		Stappen High (South)		2850	0.5
		COT zone	MB1 Hornsund area	2850	0.5
	Sørvestnaget Basin		2850	0.5	3000
	MB2 Harstad Basin		2860	0.5	4000
	eastern zones	MB2 Vestbakken Volcanic Province	2850	0.5	3000
		BAS2 North of Nordkapp Basin	2820	0.5	2000
		BAS2 South of Nordkapp Basin	2820	0.5	1000
	northern area	MI (Norsel High, N-E Loppa High)	2750	0.6	3000
		BAS2 Stappen High North	2750	0.5	3500
		BAS2 central area		0.7	1500

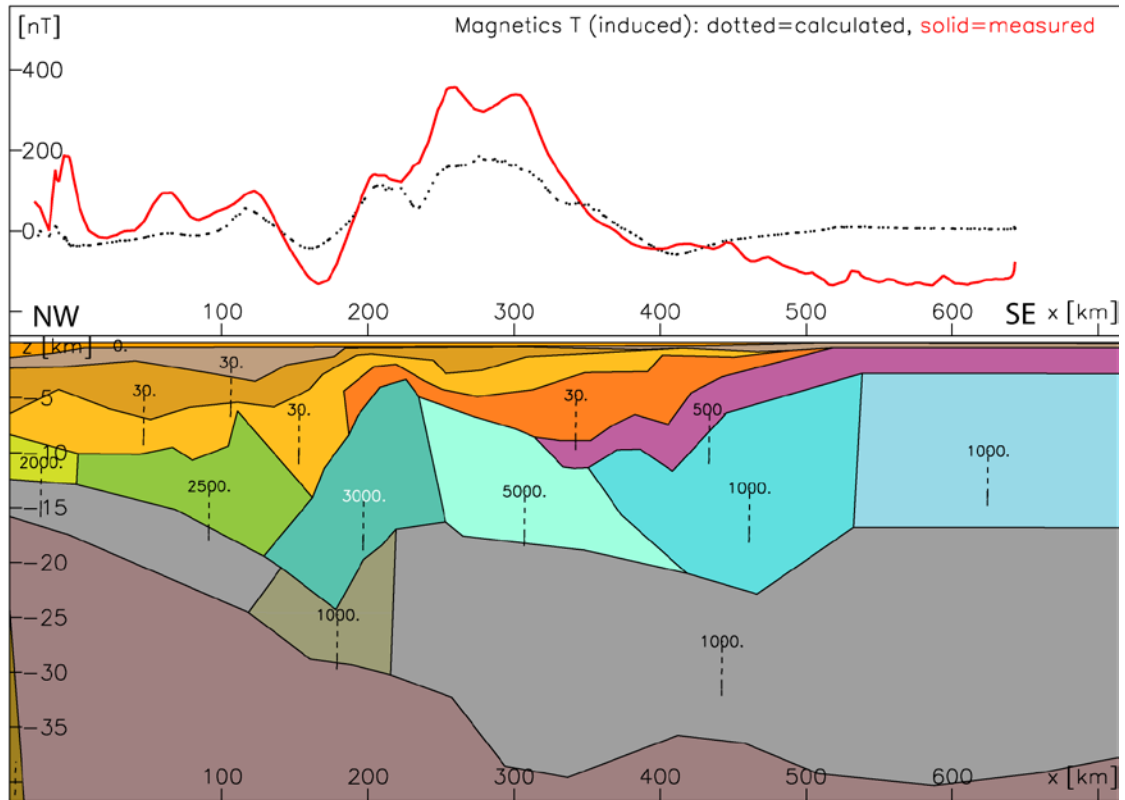
a) Bouguer anomaly and density distribution



b) Line drawing of IKU-B



c) Induced magnetic field and susceptibility distribution



d) Induced and remnant magnetic field and Q-ratio distribution

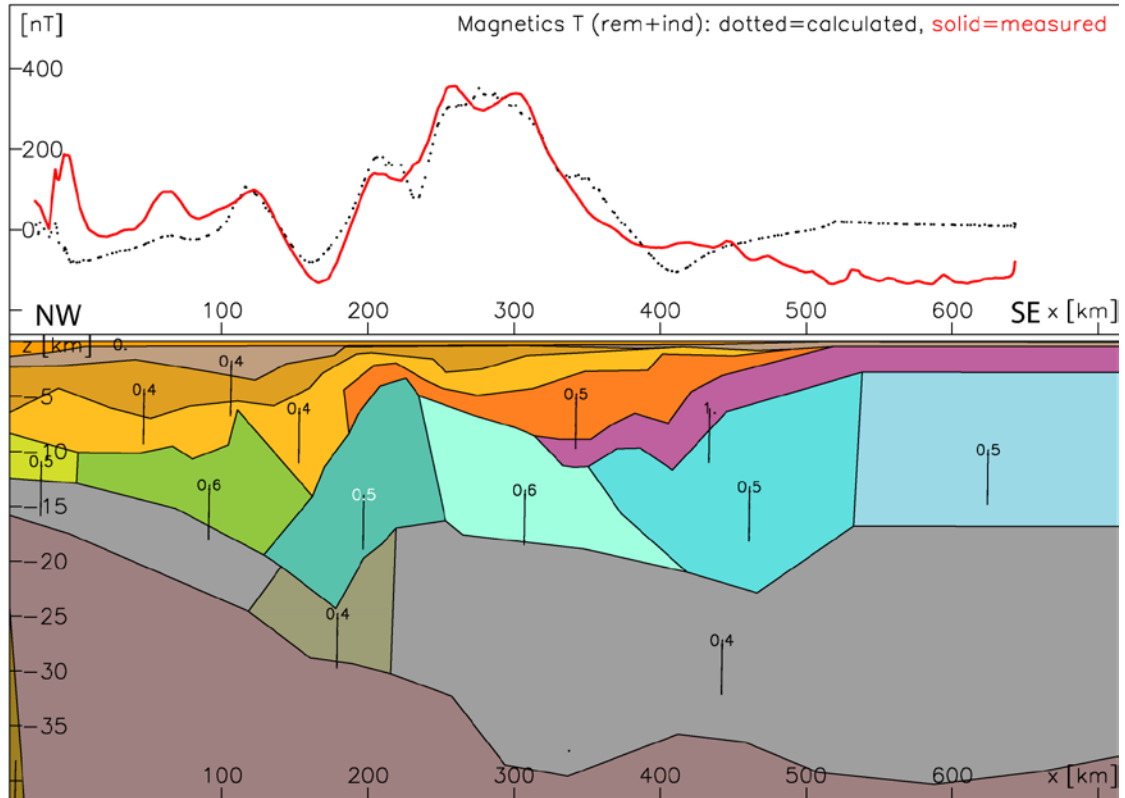


**Figure 6.4.** *NW-SE cross-section through the SW Barents Sea along profile IKU-B and Petrobar-07. a) Density structure and modelled Bouguer anomaly. Densities are given in Mg/m<sup>3</sup>. b) Reflectivity of the seismic profile IKU-B for comparison, c) Modelled induced magnetic field and susceptibility distribution (10-5 SI), d) Modelled remanent and induced magnetic field and Q-ratio distribution for the model. Remanent magnetization has to be included in the modelling to match the observed anomalies. The direction of the remanent magnetization is parallel to the induced field (Inclination: 79°, declination: 4.3°).*

#### 6.4.3 Depth to top basement

The extension of the top basement map is limited by the transition to the North Atlantic, as indicated by the Senja Fracture Zone. To the east the compilation ends at the transition between the Norwegian and Russian Barents Sea, where seismic data are sparse and where the transition from the Cenozoic rift basins of the Western Barents Sea to the deep Eastern Barents basins occurs. The density contrast between the basement and Palaeozoic sedimentary rocks is at least 50 kg/m<sup>3</sup> (Figure 6.4, Table 6.2). The top basement (Fig. 6.5a) is in our model also the top of the magnetic sources, as sedimentary rocks are considered relatively non-magnetic.

Over large parts of the shelf, the top basement is located at depths between 4 and 10 km. The shallowest basement (< 2 km) is mapped at the Gardarbanken High, north of the Stappen High and below Bjørnøya. Along the continental slope, the top basement deepens from to more than 11 km where a thick fan of Tertiary sediments is reported (Engen et al. 2006). With the depth to crystalline basement reaching 12 km the northern part of the Nordkapp Basin can be classified as a deep basin. Much deeper basins to the west of the Loppa High and south of the Stappen High are modelled with a depth to basement locally reaching >15 km.

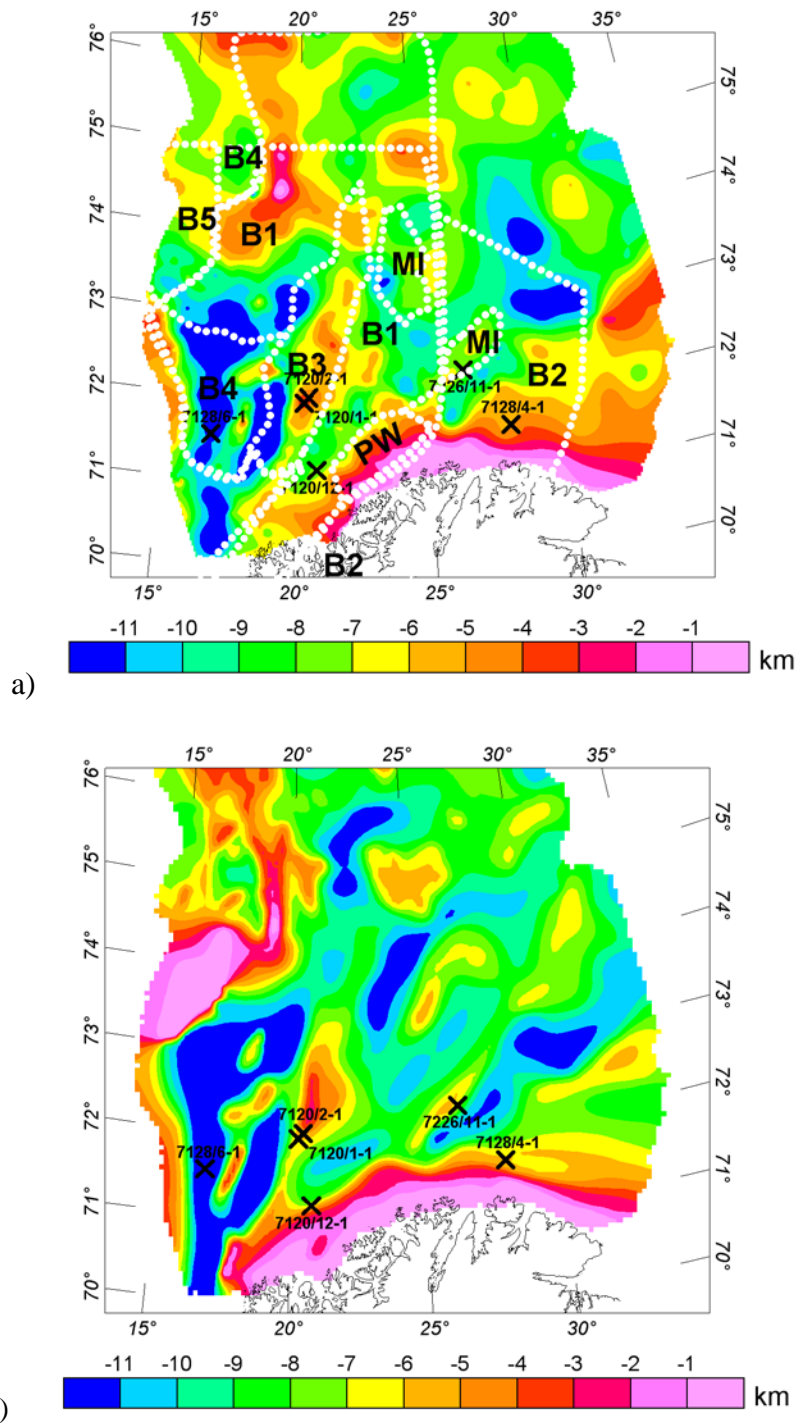


**Figure 6.5.** a) Top basement as defined in the 3D model with different basement units on top (as defined in Table 2); b) Top basement map after Skilbrei (1995) based mainly on magnetic depth estimates.

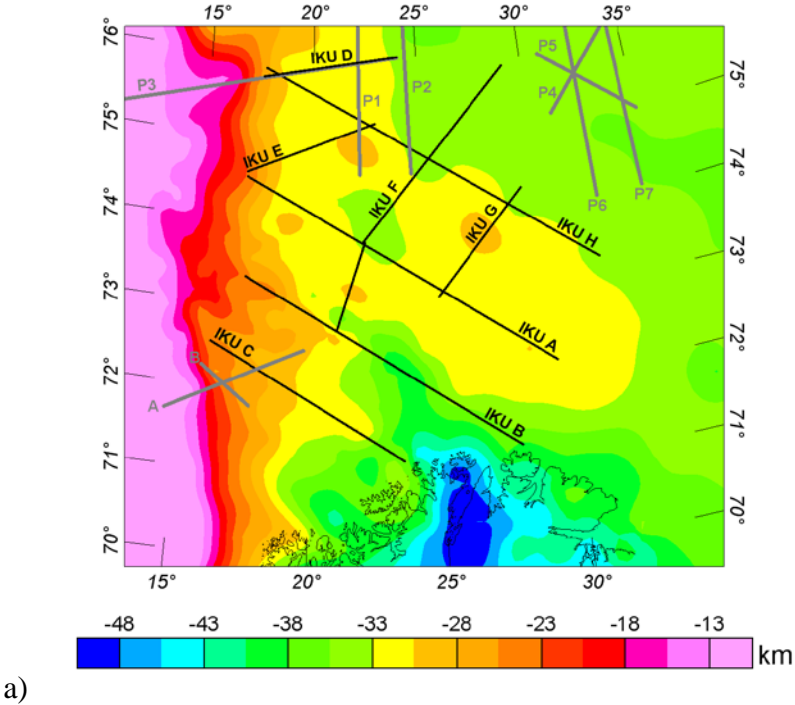
#### 6.4.4 Depth to the crust-mantle boundary

The Moho (Fig. 6.6a) is in general associated with a density contrast of  $350 \text{ kg/m}^3$  between the lower crust and the upper mantle. Only across the lower crustal body (LCB) this contrast is slightly smaller. The resulting Moho geometry reflects the Moho of the Barents50 (Fig. 6.6b) model at the continental margin and onshore. Over most of the margin the Moho is

similar to the Barents 50 model, but varies significantly in the trend of anomalies. Essentially, along existing seismic profiles the depth are the same with the exception of IKU-B, where the new OBS profile Petrobar-07 has recently been acquired and provided for the modeling (Clark et al. 2009).

The Moho undulates over the continental shelf between 20 and 35 km depths. In the central study area an E-W shallowing correlates with the location of basins and highs. We also notice a steep deepening of the Moho, from 20 km to 30 km, between the COT and the Ringvassøy-Loppa and Bjørnøyrenna fault complexes.

Interestingly, Moho depths are in the order of 30-32.5 km below the Bjarmeland Platform and northwards and show a gradual thinning from north to south.



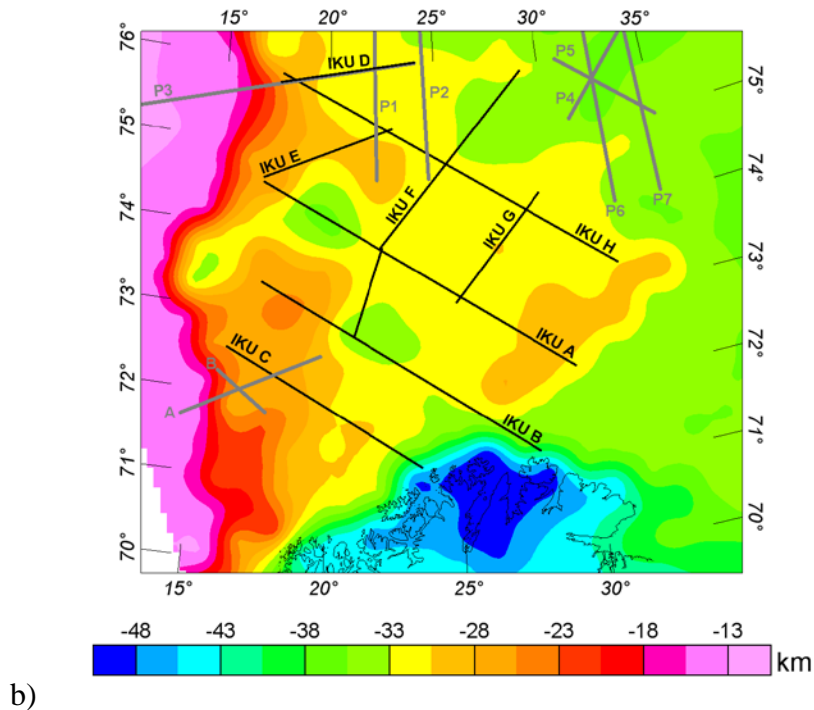


Figure 6.6. a) Depth to Moho from 3D model, b) depth to Moho from Barents 50 model. Black and grey lines show locations of seismic profiles.

## 6.5 Basement characterisation and basin characteristics

The western and eastern Barents Sea contains a series of deep sedimentary basins of more than 10 km thickness with very different characteristics, when considering the wavelengths involved: the eastern Barents Sea Basins are very large whereas the western Barents Sea basins are characterised by much smaller cross-wavelengths. This observation is an indication of a different formation history of the basins which may correlate with different crustal properties. Figure 6.5a and Table 6.2 show the different crustal domains.

On the Bjarmeland Platform; the densities are slightly higher than the  $2750 \text{ kg/m}^3$  average values usually considered for the Fennoscandian Shield (Galitchanina et al. 1995). This slight increase between the crustal units BAS1 and BAS2 was required with respect to the constraints on the Moho depth both from seismic and isostatic observations. Although the western boundary of the BAS2 crustal unit (Fig. 6.5a) is schematic in its definition of the geometry along the vertical sections, the seismic confirm the presence of both a major reflectivity change and a possible structural boundary coinciding with contrasting density/magnetization values (Barrère 2009, Barrère et al. 2009).

The densities and magnetic properties (Table 6.2) are used to distinguish different units, but resolve the Caledonian nappes only in general terms:

The Norwegian Caledonian nappes correspond to low-magnetic basement on top of an Archaean to Paleoproterozoic basement of higher magnetization properties (Olesen et al. 1990). The extension of the Caledonian nappes is based on the assumption of the offshore propagation of these nappes mapped in northern Norway (Åm 1975, Olesen et al. 1990, Skilbrei 1991, Siedlecka & Roberts 1996) and on the integrated analysis carried out by



Barrère et al. (2009). Estimation of the extension and thickness from our model are difficult as the density and magnetization contrasts between nappes and Archaean to Palaeoproterozoic basement are low. However, five crustal zones consisting of one or several units (Figure 6.5a) are distinguished: (1) an onshore zone, (2) an offshore coastal zone, (3) a zone along the COT, (4) a central zone and (5) a last zone covering the eastern and northern areas.

#### *6.5.1 Onshore*

The BAS1 onshore the Fennoscandian Shield was divided into two bodies, one of  $2750 \text{ kg/m}^3$  interpreted as Archaean to Palaeoproterozoic high-grade metamorphosed rocks (potential granulites), and the second with a slightly lower density ( $2700 \text{ kg/m}^3$ ) was interpreted as lower grade metamorphic rocks like Archaean to Palaeoproterozoic gneisses. This body may represent a prolongation of the Transscandinavian Igneous Belt (TIB) beneath the Caledonian nappes.

#### *6.5.2 Coastal area*

Offshore, along the coast, the high-density upper crustal body (UCB) of mean magnetic properties can be related to rocks within middle and upper allochthon intruded by major mafic-ultramafic, plutonic complexes such as the Vendian-age (570-520 Ma) Seiland Igneous Province (Roberts et al. 2006) and the Early Silurian, Honningsvåg Igneous Complex (Robins 1998, Corfu et al. 2006).

#### *6.5.3 COT = elongated marginal zone*

Four bodies are distinguished, which correlate to distinct structural elements: (1) the Harstad Basin, (2) the Vestbakken Volcanic Province, (3) the Sørvestsnaget Basin and (4) the Hornsund Area (west of the Stappen High). The four bodies have a high density, between  $2850 \text{ kg/m}^3$  and  $2880 \text{ kg/m}^3$  and very variable magnetic susceptibility from  $1000 \cdot 10^{-5}$  to  $3000 \cdot 10^{-5}$  (SI). The good correlation between basement units and tectonic units is interpreted as reflecting the strong link between the different basement types and the evolution of the margin.

Over the Sørvestsnaget Basin, the Bouguer anomaly high and low magnetic signatures may be comparable with a 'quiet zone' often described at the vicinity of margins (Gunn 1997). This kind of 'quiet zone' can be interpreted as attenuated crust with intermediate character between true continental and true oceanic crust developed close to the continental-oceanic transition. Such a quiet zone can also be due to a specific chronostratigraphy period of reverse polarity.

#### *6.5.4 Central zone*

This elongate zone encompasses the Loppa High, the Bjørnøya Basin and the southern part of the Stappen High. Several units with the same density value ( $2750 \text{ kg/m}^3$ ) and high susceptibility were distinguished in the upper crust. Compared to onshore geology, the relatively high susceptibility is interpreted as indicating a crust consisting of magnetic

gneisses comparable to the ones mapped and sampled onshore Norway (Olesen et al. 1990). They are regrouped under the label BAS1 linking them to the onshore Fennoscandia Shield. A high-density body (LCB) of  $3100 \text{ kg/m}^3$  is modelled in the lower crust to the west of the Loppa High. The modelling allows approximating its extension along the Ringvassøy-Loppa and Bjørnøyrenna fault complexes. Locally, it reveals the existence of a lower crustal bulge. The elongation of the high-density body suggests a close genetic link to the development of these faults. It suggests that the crustal thinning was accommodated along the Ringvassøy Loppa and/or the Bjørnøyrenna Fault Complexes comparable to the major detachments documented onshore and offshore Norway (Braathen et al. 2002, Olesen et al. 2002, Osmundsen et al. 2002). The structural and petrophysical characteristics of this LCB strengthens the interpretation as a core complex (Barrère 2009), but better seismic imaging is needed to understand how the structures are linked to each other.

#### *6.5.5 Eastern and northern zones*

East and north of the Loppa High the upper crust (BAS2) consists of two bodies different from the upper crust type BAS1. The BAS2 crust appears to be denser and has a slightly lower magnetic susceptibility ( $< 3500 \cdot 10^{-5} \text{ SI}$ ) to the east and north of the Loppa High. On a regional scale, the BAS1/BAS2 (Fig. 5a) boundary clearly separates a NE zone of platforms from a deeply rifted SW zone. In addition to changes in the reflectivity and density, the path of the boundary between BAS1 and BAS2 correlates to a striking NW-SE jump at the Moho along IKU F (Ritzmann & Faleide 2007, Barrère 2009, Barrère et al. 2009). In the East Barents Sea, the NW striking trends are related to Timanian structures formed in Late Neoproterozoic times (Ivanova 2001) and the northwestern limit of the Timanides remains unclear as well as the interactions between the Timanian and the Caledonian structures. Local mafic intrusions are interpreted (MI bodies, Fig. 6.5a); they may be emplaced between the Caledonian nappes or linked to the Mesozoic basins formation.

## **6.6 Conclusion**

We present a new 3D model of the SW Barents Shelf that gives valuable insights into the crustal architecture. Interpretation of the crustal base allows defining domains of different isostatic compensation, which correlate with the vicinity to the margin and onshore Norway. The new top basement map highlights the regional differences between the platforms, the deep basins and the transition to the North Atlantic. The 3D model further enlightens the complex 3D architecture of the SW Barents Sea and allows discussing the distribution of different basement blocks and as well the deep crustal structure of the western Barents Sea.

## 7 3D THERMAL MODELLING OF THE SW BARENTS SEA

Christophe Pascal, NGU

### 7.1 Introduction

This chapter represents the final research effort made in the framework of the HeatBar project and the work presented here benefits directly from all other project activities. The main goal of the project is to provide estimates on the relative part of the heat produced in the basement and quantify its distribution at top basement levels (Fig. 1.1). In order to estimate the relative amount of heat flowing through the chrystalline basement-sediments interface, we carried out series of 3D thermal models focused on the SW Barents Sea (Fig. 7.1).

### 7.2 Modelling strategy

The main purpose of the 3D modelling is to test the influence of the geometry of the basement on the variability of the heat flowing at the base of the sedimentary basins. We used the crustal model developed during the course of this project by Barrère and Ebbing (see Chapter 6) and concentrate on the major geological interfaces (i.e. Moho, top basement and Earth's surface). Three major rock units with distinct thermal properties (i.e. thermal conductivity and heat generation, Table 7.1) are modelled (Fig. 7.1). The modelled mantle layer is void of heat producing elements and used as a “substratum” in order to apply mantle (i.e. Moho) heat flow at its planar and horizontal base at 50 km depth below sea level. This procedure allows for simulating the expected diffusion of heat before it reaches the Moho. Thermal properties of the three rock units are meant to represent their respective bulk properties. In particular, the low thermal conductivity selected for the sediments is in agreement with a sedimentary pile dominated by shales and siltstones (Clauser & Huengens 1995). Admitely, in the sedimentary basins thermal conductivities should increase with depth following depth-dependent compaction. However, the modelling does not aim to calculate a precise temperature distribution in the sediments, which demands more detailed information, but the first-order effects of the structure of the basement on the heat flowing at the base of the sediments.

**Table 7.1. Parameters used in the thermal modelling.**

Layer	k (W/m/K)	$A_0$ ( $\mu\text{W}/\text{m}^3$ )
<i>Sediments</i>	1.5	0.5
<i>Basement</i>	2.5	1.0
<i>Mantle</i>	3.5	0.0

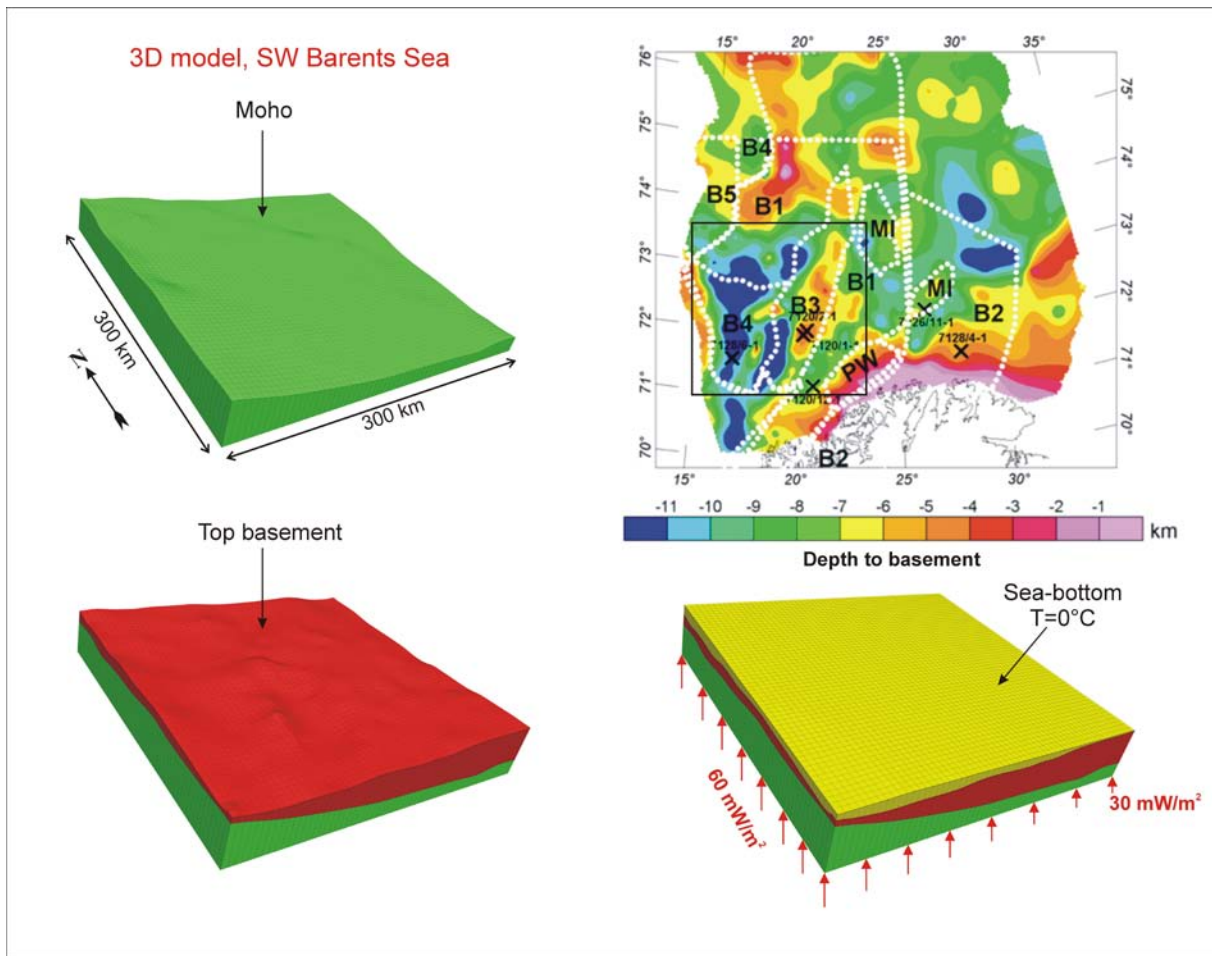


**Figure 7.1.** Setup of the 3D thermal model. The black frame on the depth to basement map (Fig. 6.5a from Barrère and Ebbing, this report) depicts the modelled area. Vertical extent of the model are ~50 km, Moho depth is given in Fig. 6.6a.

Boundary conditions consists in (1) a fixed temperature equal to  $0^{\circ}\text{C}$  at the surface of the model, (2) an applied vertical heat flow at the base of the model decreasing gradually from 60 to  $30\text{ mW/m}^2$  eastwards and (3) no heat flowing through the lateral edges of the model. The first condition is consistent with an average Quaternary temperature more appropriate to the present model, considering its characteristic dimensions, than an average present-day one. The choice of applying  $60\text{ mW/m}^2$  below the western edge of the model (i.e. continent-ocean boundary) is supported by marine heat flow data that are, furthermore, consistent with what would be predicted from the age of the adjacent oceanic basement (Sundvor et al. 2000). A value of  $30\text{ mW/m}^2$  below the eastern edge is somewhat more uncertain but resulted in reasonable heat flow values at the surface. A gradual eastwards decrease in Moho heat flow is suggested by heat flow measurements (e.g. Pascal et al. 2009), gravity gradients (Breivik et al. 1999) and seismic data (Levshin et al. 2007).

The computations were carried out using the commercial software FLAC3D 4.00 ([www.itascacg.com/flac3d](http://www.itascacg.com/flac3d)). FLAC3D is a modelling code designed to calculate large deformations and involves different types of rheologies but can also be used for static thermal

computations. The code utilises an explicit finite difference formulation. In the present case, we used FLAC3D to solve the three dimensional form of the steady-state heat equation:

$$q = -k \cdot \frac{\partial T}{\partial z} \quad (1)$$

where  $q$  is heat flow,  $k$  thermal conductivity,  $T$  temperature and  $z$  depth (positive downwards). Equation (1) is solved considering the boundary conditions described above and considering internal sources of heat (i.e.  $A_0$ , rocks' heat generation).

### 7.3 Modelling results

The computed top basement heat flow is shown in Fig. 7.2. Heat flow data are scarce in the studied area and a proper calibration of the model is, at the present, out of reach. However, the few data points at hand (Fig. 7.2, see also Sundvor et al. 2000) support our modelling results that suggest that heat flow values drop when crossing the ocean-continent transition zone from west to east. The relatively low value devised by Løseth et al. (1992) appears also to be consistent with our modelled values.

According to the applied basal heat flow condition (i.e. eastward decrease in Moho heat flow, Fig. 7.1) one should expect a gradual eastwards decrease in heat flow values. However, the applied gradual decrease in Moho heat flow appears to be balanced by the gradual increase in crustal heat flow (i.e. eastwards thickening of the crystalline crust from ~10 to 30-40 km), resulting in a weak eastward decrease at top basement levels.

In turn, the heat flow distribution is strongly controlled by basement topography, heat flow values being up to ~20 mW/m<sup>2</sup> higher at basement highs (e.g. Senja Ridge, Velesmøy High, Fig. 7.2) than at deep sedimentary basins (e.g. Sørvestsnaget and Tromsø basins). This effect is mainly explained by heat refraction below the sedimentary basins and channelling of the heat through the basement highs. Thermal conductivity values of sediments are lower than those of basement rocks or, conversely, sediments show higher resistance to heat transfer than basement. As a consequence, heat flows following basement highs that represent paths of minimum thermal resistance. In addition, the crystalline crust being attenuated below the sedimentary basins, less crustal heat is produced below them as compared to the basement highs.

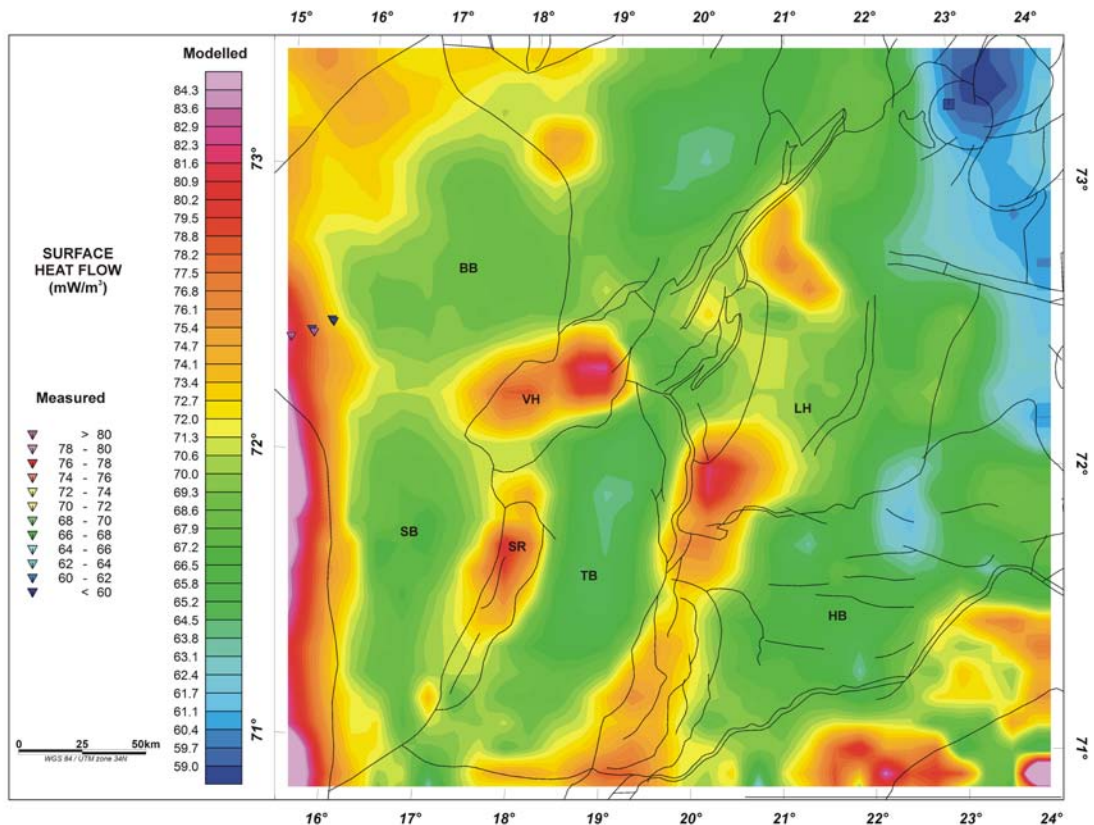


**Figure 7.2.** Computed heat flow at top basement using the 3D model in Fig. 7.1 and main structural elements from NPD ([www.npd.no](http://www.npd.no)). Note strong heat flow variations induced by basement topography, heat flow being enhanced at basement highs. From west to east: BB=Bjørnøya Basin, SB=Sørvestsnaget Basin, VH=Veslemøy High, SR =Senja Ridge, TB= Tromsø Basin, LH= Loppa High, HB=Hammerfest Basin. Inverted triangles are marine heat flow measurements from Sundvor et al. (2000), the square located at the NE corner represents one heat flow determination from shallow drilling (Løseth et al. 1992).

Modelled subcrustal temperatures show a clear decrease from west to east (Fig. 7.3). This trend was expected as a direct consequence of assuming decaying mantle heat flow values eastwards (Fig. 7.1). Furthermore, higher temperatures by the continent-ocean transition zone are consistent with observed reduction in shear wave velocities (Levshin et al. 2007) and regional gravity anomalies (Breivik et al. 1999). In detail our simulated isotherms differ from those of the thermal model advanced by Breivik et al. (1999), maximum temperatures being predicted at the COB. In the present case, maximum temperatures are predicted below the very deep (i.e. ~10 km deep, Fig. 6.5a) Sørvestsnaget Basin as a natural consequence of thermal blanketing in combination with relatively high heat flow from the mantle.

Modelled temperatures in the sedimentary basins remain indicative as long as finer details on their structure are not considered in the modelling. Nevertheless, the model appears to simulate the first-order geothermal gradients of ~40 °C/km that are derived from DST temperatures in exploration wells (e.g. Pascal et al. 2009).

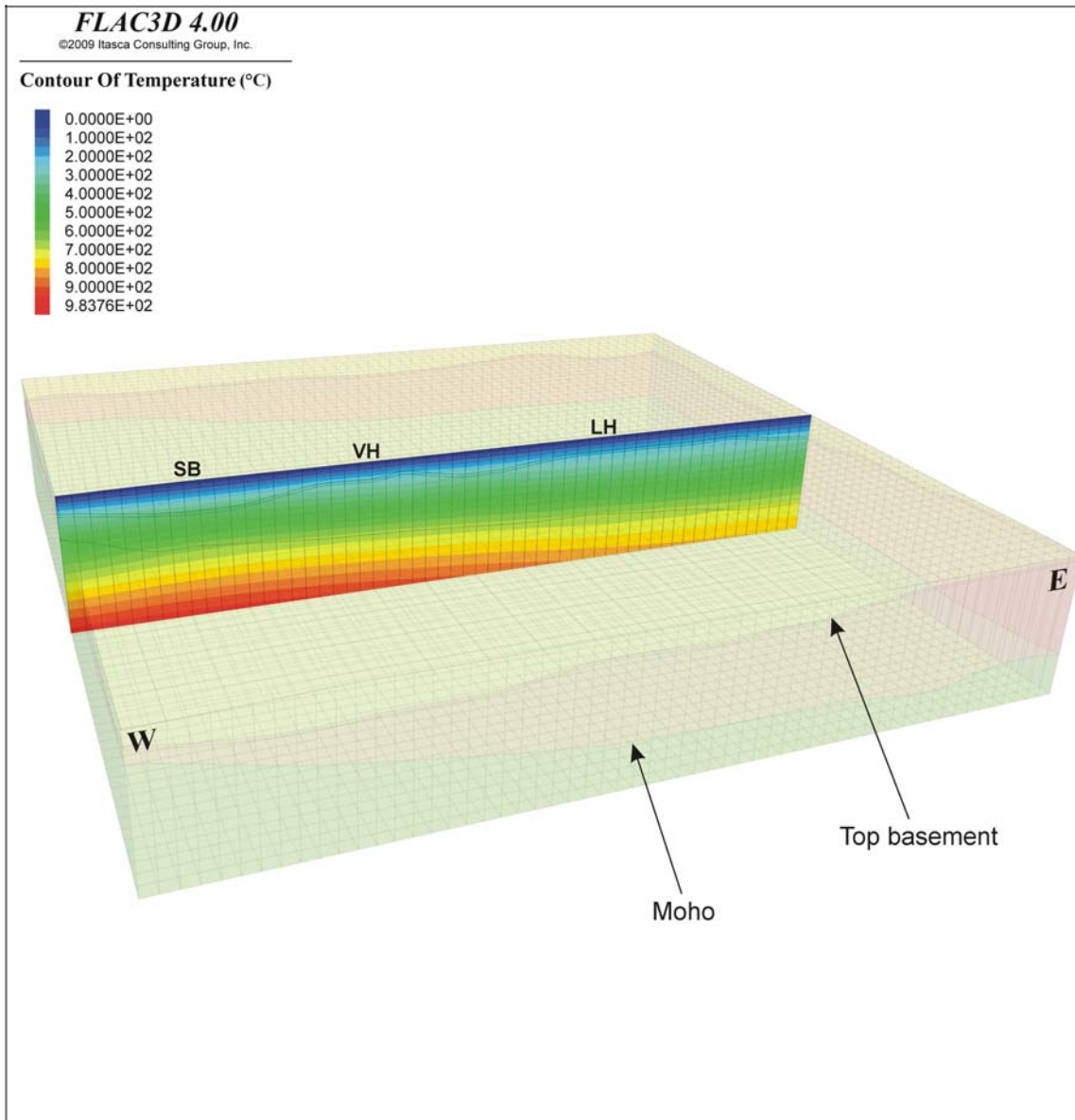


**Figure 7.3.** *Computed temperatures along an E-W vertical section by the middle of the modelled domain. Note the general decrease in mantle temperatures from west to east, maximum mantle temperatures being predicted not at the continent-ocean boundary but below the Sørvestsnaget Basin. SB=Sørvestsnaget Basin, VH=Velesmøy High, LH= Loppa High.*

Additional modelling tests involving constant mantle heat flow and/or different heat generation rates for the basement than that given in Table 7.1, resulted in similar heat flow patterns at top basement levels with maxima located at basement highs. In brief, basement topography exerts a primary control on heat transfer in the modelled domain and the heat flow pattern depicted in Fig. 7.2, but admittedly not the absolute heat flow values, remains a very robust result of the modelling.

## 7.4 Summary

We used the geophysical 3D crustal model from Barrère and Ebbing (chapter 6) together with available thermal constraints in order to build a thermal model of the SW Barents Sea. Although absolute temperature and heat flow values remain uncertain in the modelling, two first-order conclusions can be drawn. Firstly, subcrustal temperatures appear to increase when approaching the continent-ocean boundary. This result is in agreement with other independent geophysical data (i.e. gravity and seismic tomography). The most robust result of the modelling is the strong control that basement topography exerts on the heat flow pattern, maxima and minima being predicted at basement highs and sedimentary basins respectively. Our modelling suggests that a difference of up to  $\sim 20$  mW/m<sup>2</sup> can exist depending on basement topography. It is thus recommended that variation of basement heat flow according to basement topography is used instead of assuming constant basement heat flow in basin modelling studies.



## 8 CONCLUSIONS

The HeatBar project aimed to determine the relative proportion of heat originating in the basement of the western Barents Sea and, as such, followed the methodologies and scientific approach developed in the course of the 2005-2008 Kontiki Project. Our ultimate goal was to shed new lights on the thermal state of the basins of the western Barents Sea by (1) determining the heat flow and the relative content in heat-producing elements of the basement onshore northern Norway, (2) building 3D structural models of the basement offshore based on extensive geophysical information and (3) building 3D thermal models of the basins offshore.

We studied six drillholes with the purpose of deriving steady-state heat flow values: four drillholes from Finnmark (Båtsfjordfjellet, Bjørnevatn, Bidjovagge and Vuoddašjav'ri) and two from Svalbard (Longyearbyen and Sysselmannbreen). We obtained convincing results only for two out of the six boreholes. Results from the Vuoddašjav'ri borehole suggest a steady-state heat flow value of  $\sim 40 \text{ mW/m}^2$  in agreement with values commonly measured in Archean cratons (Nyblade & Pollack 1993). In contrast, we derived a steady-state heat flow value of  $\sim 80 \text{ mW/m}^2$  for the Sysselmannbreen borehole. Again, this value appears to be consistent with the present-day geological context of Svalbard where hot springs and recent volcanism are both documented (Harland 1997).

Geochemical analyses were conducted on an extensive sample collection from Finnmark in order to derive the relative content in radioactive elements and calculate the amount of heat produced by the encountered types of basement. Our results show that heat generation values are, in general, higher for the Caledonian nappes than for the autochthonous Archean to Paleoproterozoic basement. Heat generation values usually range from 0.1 to  $1\text{-}2 \mu\text{W/m}^3$ .

We presented a new 3D model of the SW Barents Shelf that gives valuable insights into the crustal architecture. Interpretation of the crustal base allowed for defining domains of different isostatic compensation. The new top basement map highlights the regional differences between the platforms, the deep basins and the transition to the North Atlantic. The 3D model further shows the complex architecture of the SW Barents Sea and allows for discussing the distribution of different basement blocks and the deep crustal structure of the western Barents Sea.

We used the geophysical crustal model together with available thermal constraints in order to build a 3D thermal model of the SW Barents Sea. Although absolute temperature and heat flow values remain unconstrained, two first-order conclusions can be drawn. Firstly, subcrustal temperatures appear to increase when approaching the continent-ocean boundary. This result is in agreement with other independent geophysical data (i.e. gravity and seismic tomography). The most robust result of the modelling is the strong control that basement topography exerts on the heat flow pattern, maxima and minima being predicted at basement highs and sedimentary basins respectively. Our modelling suggests that a difference of up to  $\sim 20 \text{ mW/m}^2$  can exist depending on basement topography. It is thus recommended that variation of basement heat flow according to basement topography is used instead of assuming constant basement heat flow in basin modelling studies.

## 9 REFERENCES

- Anderson, J.L. & Morrison, J. 2005: Ilmenite, magnetite, and peraluminous Mesoproterozoic anorogenic granites of Laurentia and Baltica. *Lithos* 80, 45-60.
- Ashwal, L.D., Morgan, P., Kelley, S.A. & Percival, J.A. 1987: Heat production in an Archean crustal profile and implications for heat flow and mobilization of heat-producing elements. *Earth and Planetary Science Letters* 85, 439-450.
- Barrère, C. 2009: Integrated geophysical modeling and tectonic evolution of the western Barents Sea. Doctoral theses, Norwegian University of Science and Technology, Trondheim, 2009:267.
- Barrère, C., Ebbing, J. & Gernigon, L. 2009: Offshore prolongation of Caledonian structure and basement characterisation in the western Barents Sea from geophysical modeling. *Tectonophysics* 470, 71-88.
- Bea, F. 1996: Residence of REE, Y, Th, and U in granites and crustal protoliths: Implications for the chemistry of crustal melts. *Journal of Petrology* 37, 521-552.
- Beardsmore, G.R. & Cull, J.P. 2001: *Crustal Heat Flow, a guide to measurement and modelling*, Cambridge University Press, 324 pp.
- Bernard-Griffiths, J., Peucat, J. J., Postaire, B., Vidal, P., Convert, J. & Moreau, B. 1984: Isotopic data (U-Pb, Rb-Sr, Pb-Pb, Sm-Nd) on mafic granulites from Finnish Lapland. *Precambrian Research* 23, 325-348.
- Braathen, A. & Davidsen, B. 2000: Structure and stratigraphy of the Palaeoproterozoic Karasjok Greenstone Belt, north Norway - regional implications. *Norsk Geologisk Tidsskrift* 80, 33-50.
- Braathen, A., Osmundsen, P.T., Nordgulen, Ø, Roberts, D. & Meyer, G.B. 2002: Orogen-parallel extension of the Caledonides in northern Central Norway: an overview. *Norwegian Journal of Geology* 82, 225-241.
- Brady, R. J., Ducea, M.N., Kidder, S.B. & Saleeby, J.B. 2006: The distribution of radiogenic heat production as a function of depth in the Sierra Nevada Batholith, California. *Lithos*, 86, 229-244.
- Breivik, A.J., Faleide, J.I. & Gudlaugsson, S.T. 1998: Southwestern Barents Sea margin: late Mesozoic sedimentary basins and crustal extension. *Tectonophysics*, 293, 21-44.
- Breivik, A.J., Verhoef, J. & Faleide, J.I. 1999: Effect of thermal contrasts on gravity modeling at passive margins; results from the western Barents Sea. *Journal of Geophysical Research*, 104, 15293-15311.
- Breivik, A.J., Mjelde, R., Grogan, P., Shimamura, H., Murai, Y., Nishimura, Y. & Kuwano, A. 2002: A possible Caledonide arm through the Barents Sea imaged by OBS data. *Tectonophysics*, 355, 67-97.
- Breivik, A.J. Mjelde, R., Grogan, P., Shimamura, H., Murai, Y. & Nishimura, Y. 2003: Crustal structure and transform margin development south of Svalbard based on ocean bottom seismometer data. *Tectonophysics*, 369, 37-70.
- Breivik, A.J. Mjelde, R., Grogan, P., Shimamura, H., Murai, Y. & Nishimura, Y. 2005: Caledonide development offshore-onshore Svalbard based on ocean bottom seismometer, conventional seismic, and potential field data. *Tectonophysics*, 401, 79-117.
- Brigaud, F. & Vasseur, G. 1989: Mineralogy, porosity and fluid control on thermal conductivity of sedimentary rocks. *Geophysical Journal*, 98, 525-542.
- Bullard, E.C. 1939: Heat flow in South Africa, *Proceedings of the Royal Society of London A*, 173, 474-503.

- Bungum, H., Ritzmann, O., Maercklin, N., Faleide, J., Mooney, W.D. & Detweiler, S.T. 2005: Three-dimensional model for the crust and upper mantle in the Barents sea region. *EOS* 86(16), doi:10.1029/2005EO160003.
- Carslaw, H.S. & Jaeger, J.C. 1959: *Conduction of heat in solids*, London, Oxford University Press, 386 pp.
- Clark, S. A., Faleide, J.I., Ritzmann, O. & Mjelde, R. 2009: Multi-stage rift evolution of the SW Barents Sea from wide-angle seismic velocity modeling. *Geophysical Research Abstracts* 11, EGU2009-12559.
- Clauser C. & Huengens, E. 1995: Thermal conductivity of rocks and minerals. In: Ahrens, T. J. (ed.) *Rock Physics and Phase Relations - a Handbook of Physical Constants*, AGU Reference Shelf, Vol. 3, pp. 105-126, American Geophysical Union, Washington.
- Corfu, F. 2004: U-Pb age, setting and tectonic significance of the anorthosite-mangerite-charnockite suite, Lofoten-Vesterålen, Norway. *Journal of Petrology* 45, 1799-1819.
- Corfu, F., Torsvik, T.H., Andersen, T.B., Ashwal, L.D., Ramsay, D.M. & Roberts, R.J. 2006: Early Silurian mafic-ultramafic and granitic plutonism in contemporaneous flysch, Magerøy, northern Norway: U-Pb ages and regional significance. *Journal of the Geological Society* 163, 291-301.
- Corfu, F., Roberts, R. J., Torsvik, T. H., Ashwal, L. D. & Ramsay, D. M. 2007: Peri-Gondwanan elements in the Caledonian nappes of Finnmark, northern Norway: implications for the paleogeographic framework of the Scandinavian Caledonides. *American Journal of Science* 307, 434-458.
- Elvebakk, H. 2008: Results of borehole logging in CO<sub>2</sub> wells, Dh1-CO<sub>2</sub>-07 and Dh2-CO<sub>2</sub>-07, Longyearbyen, Svalbard. NGU Report 2008.054, 25 pp.
- Elvebakk, H., Rønning, J.S., Jochmann, M., Henningsen, T., Johannessen, E.P., Bering, D. & Elvebakk, G. 2008: Geophysical borehole logging in Dh 10-2008 at Sysselembreen, Svalbard. NGU Report 2008.090, 45 pp (confidential).
- Engen, O., Frazer, L.N., Wessel, P. & Faleide, J.I. 2006: Prediction of sediment thickness in the Norwegian-Greenland Sea from gravity inversion. *Journal of Geophysical Research-Solid Earth* 111, B11403.
- Faleide, J.I., Vagnes, E. & Gudlaugsson, S.T. 1993: Late Mesozoic-Cenozoic Evolution of the South-Western Barents Sea in a Regional Rift Shear Tectonic Setting. *Marine and Petroleum Geology*, 10, 186-214.
- Faleide, J.I., Solheim, A., Fiedler, A., Hjelstuen, B.O., Andersen, E.S. & Vanneste, K 1996: Late Cenozoic evolution of the western Barents Sea-Svalbard continental margin. *Global and Planetary Change*, 12, 53-74.
- Flem, B., Grimstvedt, A., Slagstad, T. & Skår, Ø. 2005: Bulkanalyse av Th og U i bergartsprøver med LA-ICP-MS. Metodebeskrivelse.
- Flowers, R.M., Mahan, K.H., Bowering, S.A., Williams, M.L., Pringle, M.S. & Hodges, K.V. 2006: Multistage exhumation and juxtaposition of lower continental crust in the western Canadian Shield: Linking high-resolution U-Pb and <sup>40</sup>Ar/<sup>39</sup>Ar thermochronometry with pressure-temperature-deformation paths. *Tectonics* 25, doi:10.1029/2005TC001912.
- Fountain, D.M. 1986: Is there a relationship between seismic velocity and heat production for crustal rocks? *Earth and Planetary Science Letters* 79, 145-150.
- Frost, C.D., Frost, B.R., Chamberlain, K.R. & Edwards, B.R. 1999: Petrogenesis of the 1.43 Ga Sherman batholith, SE Wyoming, USA: A reduced, rapakivi-type anorogenic granite. *Journal of Petrology* 40, 1771-1802.
- Gabrielsen, R.H., Færseth, R.B., Jensen, L.N., Kalheim, J.E. & Riis, F. 1990: Structural elements of the Norwegian continental shelf. Part I: The Barents Sea Region. *Norwegian Petroleum Directorate Bulletin*, 6, 33.

- Galitchanina, L.D., Glaznev, V.N., Mitrofanov, F.P. & Olesen, O. 1995: Surface density characteristics of the Baltic Shield and adjacent territories. *Norwegian Journal of Geology, Special Publication*, 349-354.
- Gunn, P.J. 1997: Application of aeromagnetic surveys to sedimentary basin studies. *Journal of Australian Geology & Geophysics* 17, 133-144.
- Götze, H.J. & Lahmeyer, B. 1988: Application of 3-Dimensional Interactive Modeling in Gravity and Magnetics. *Geophysics* 53, 1096-1108.
- Harland, W. B. 1997: *The Geology of Svalbard*. Geological Society of London, Memoir No. 17, 521 p.
- Heier, K.S. 1960: Petrology and chemistry of high-grade metamorphic and igneous rocks on Langøy, Northern Norway. *Norges geologiske undersøkelse* 207, 1-246.
- Heier, K.S. & Adams, J.A.S. 1965: Concentration of radioactive elements in deep crustal material. *Geochimica et Cosmochimica Acta* 29, 53-61.
- Hospers, J. & Ediriweera, K.K. 1991: Depth and configuration of the crystalline basement in the Viking Graben area, Northern North Sea. *Journal of the Geological Society, London* 148, 261-265.
- Ivanova, N.M. 2001: The geological structure and petroleum potential of the Kola-Kanin Monocline, Russian Barents Sea. *Petroleum Geoscience* 7, 343-350.
- Jackson, H.R., Faleide, J.I. & Eldholm, O. 1990: Crustal structure of the sheared southwestern Barents Sea continental margin. *Marine Geology*, 93, 119– 146.
- Jakobsson, M., Cherkis, N.Z., Woodward, J., Macnab, R. & Coakley, B. 2000: New grid of Arctic bathymetry aids scientists and mapmakers. *Eos, Transactions, American Geophysical Union* 81, 89-96.
- Johannessen, E.P., Henningsen, T., Bakke, N.E., Johansen, T.A., Ruud, B.O., Riste, P., Elvebakk, H., Jochmann, M., Elvebakk, G. & Woldengen, M.S. 2011: Palaeogene clinoforn succession on Svalbard expressed in outcrops, seismic data, logs and cores. *First Break* 29, 35-44.
- Johansen, S.E., Ostist, B.K., Birkeland, Ø., Fedorovsky, Y.F., Martirosjan, V.N., Christensen, O.B., Cheredeev, S.I., Ignatenko, E.A. & Margulis, L.S. 1992: Hydrocarbon potential in the Barents Sea region: play distribution and potential. In: *Arctic Geology and Petroleum Potential* (Vorren, T.O., Bergsager, E., Dahl-Stammes, Ø.A., Holter, E., Johansen, B., Lie, E. & Lund, T.B. eds.). NPF Special Publication 2, 273-320. Elsevier, Amsterdam.
- Kalskin Ramstad, R., de Beer, H., Midttømme, K., Koziel, J. & Wissing, B. 2008: Status of thermal diffusivity equipment – method development 2005-2008. NGU Report 2008.050, 38 pp.
- Killeen, P.G. & Heier, K.S. 1975: Radioelement distribution and heat production in Precambrian granitic rocks, southern Norway. *Det Norske Videnskaps-Akademi, I. Mat.-Naturv. Klasse. Skrifter, Ny Serie* 35, 1-32.
- Kirkland, C. L., Daly, J. S. & Whitehouse, M. J. 2006a: Granitic magmatism of Grenvillian and late Neoproterozoic age in Finnmark, Arctic Norway - Constraining pre-Scandian deformation in the Kalak Nappe Complex. *Precambrian Research* 145, 24-52.
- Kirkland, C. L., Daly, J. S., Eide, E. A. & Whitehouse, M. J. 2006b: The structure and timing of lateral escape during the Scandian Orogeny: A combined strain and geochronological investigation in Finnmark, Arctic Norwegian Caledonides. *Tectonophysics* 425, 159-189.
- Kirkland, C. L., Daly, J. S. & Whitehouse, M. J. 2007: Provenance and terrane evolution of the Kalak Nappe Complex, Norwegian Caledonides: Implications for Neoproterozoic Paleogeography and tectonics. *Journal of Geology* 115, 21-41.

- Kirkland, C. L., Whitehouse, M. J. & Slagstad, T. 2009: Fluid-assisted zircon and monazite growth within a shear zone: a case study from Finnmark, Arctic Norway. *Contributions to Mineralogy and Petrology*, doi:10.1007/s00410-009-0401-x.
- Krill, A. G. & Zwaan, B. K. 1987: Reinterpretation of Finnmarkian deformation on western Sørøy, northern Norway. *Norsk Geologisk Tidsskrift* 67, 15-24.
- Krill, A. G., Bergh, S., Lindahl, I., Mearns, E. W., Often, M., Olerud, S., Olesen, O., Sandstad, J. S., Siedlecka, A. & Solli, A. 1985: Rb-Sr, U-Pb and Sm-Nd isotopic dates from Precambrian rocks of Finnmark. *Norges geologiske undersøkelse Bulletin* 403, 37-54.
- Kukkonen, I.T. & Lahtinen, R. 2001: Variation of radiogenic heat production rate in 2.8-1.8 Ga old rocks in the central Fennoscandian shield. *Physics of the Earth and Planetary Interiors* 126, 279-294.
- Lachenbruch, A. 1968: Rapid estimation of the topographic disturbance to superficial thermal gradients. *Reviews of Geophysics*, 6, 365-400.
- Levchenkov, O. A., Levsky, L. K., Nordgulen, Ø., Dobrzhinskaya, L. F., Vetrin, V. R., Cobbing, J., Nilsson, L. P. & Sturt, B. A. 1993: U-Pb zircon ages from Sørvaranger, Norway, and the western part of the Kola Peninsula, Russia. *Norges geologiske undersøkelse Special Publication* 7, 29-47.
- Levshin, A.L., Schweitzer, J., Weidle, C., Shapiro, N.M. & Ritzwoller, M.H. 2007: Surface wave tomography of the Barents Sea and surrounding regions. *Geophys. J. Int.* 170, 441-459.
- Ludwig, W.I., Nafe, J.E. & Drake C.L. 1970: Seismic refraction. *Sea* 4 (1), 53-84.
- Løseth, H., Lippard, S. J., Sættem, J., Fanavoll, S., Fjerdingsstad, V., Leith, T. L., Ritter, U., Smelror, M., & Sylta, Ø. 1992: Cenozoic uplift and erosion of the Barents Sea-evidence from the Svalis Dome area. In Vorren, T. et al. (eds.): *Arctic Geology and Petroleum Potential*. NPF Special Publication 2, 643-664.
- Marker, M. 1985: Early Proterozoic (c. 2000-1900 Ma) crustal structure of the northeastern Baltic Shield: Tectonic division and tectogenesis. *Norges geologiske undersøkelse Bulletin* 403, 55-74.
- McLaren, S., Sandiford, M., Neumann, N., Wyborn, L. & Bastrakova, I. 2003: The hot southern continent: Heat flow and heat production in Australian Proterozoic terranes *Geological Society of Australia Special Publication*. 22, 151-161.
- Middleton, M.F. 1982: Bottom-hole temperature stabilization with continued circulation of drilling mud. *Geophysics*, 47, 1716-1723.
- Middleton, M. 1993: A transient method of measuring the thermal properties of rocks. *Geophysics*, 58, 357-365.
- Milnes, A.G., Wennberg, O.P., Skår, Ø. & Koestler, A.G. 1997: Contraction, extension and timing in the South Norwegian Caledonides: The Sognefjord transect. In: Burg, J.-P. & M. Ford (eds.) *Orogeny Through Time*. Geological Society Special Publication 121, 123-148.
- Mjelde, R., Breivik, A.J., Elstad, H., Ryseth, A.E., Skilbrei, J.R., Opsal, J.G., Shimamura, H., Murai, Y. & Nishimura, Y. 2002: Geological development of the Sorvestsnaget Basin, SW Barents Sea, from ocean bottom seismic, surface seismic and gravity data. *Norwegian Journal of Geology*, 82, 183-202.
- Morgan, P. & Sass, J.H. 1984: Thermal regime of the continental lithosphere. *Journal of Geodynamics* 1, 143-166.
- Mottaghy, D., Popov, Y. A., Schellschmidt, R., Clauser, C., Kukkonen, I. T., Nover, G., Milanovsky, S., & Romushkevich, R. A. 2005: New heat flow data from the immediate vicinity of the Kola superdeep borehole: Vertical variation in heat flow density confirmed, *Tectonophysics*, 401, 119-142.

- Mørk M.B.E., McEnroe S.A. & Olesen O. 2002: Magnetic susceptibility of Mesozoic and Cenozoic sediments off Mid Norway and the role of siderite: implications for interpretation of high-resolution aeromagnetic anomalies. *Marine and Petroleum Geology* 19, 1115-1126.
- Nyblade, A.A. & Pollack, H.N. 1993: A global analysis of heat flow from Precambrian terrains: implications for the thermal structure of Archean and Proterozoic lithosphere. *J. Geophys. Res.* 98, 12207–12218.
- Olesen, O., Roberts, D., Henkel, H., Lile, B.L. & Torsvik, T.H. 1990: Aeromagnetic and gravimetric interpretation of regional structural features in the Caledonides of West Finnmark and North Troms, northern Norway. *Norges geologiske undersøkelse Bulletin* 419, 1-24.
- Olesen, O., Lundin, E., Nordgulen, Ø., Osmundsen, P.T., Skilbrei, J.R., Smethurst, M.A., Solli, A. & Fichler, C. 2002: Bridging the gap between the onshore and offshore geology in Nordland, northern Norway. *Norwegian Journal of Geology* 82, 243-262.
- Olesen, O., + 18 co-authors 2007: *Kontiki Final Report, Continental Crust and Heat Generation in 3D*. NGU Report 2007.042 (confidential), 438 pp.
- Olesen, O., Brønner, M., Ebbing, J., Gellein, J., Gernigon, L., Koziel, J., Lauritsen, T., Myklebust, R., Sand, M., Solheim, D. & Usov, S. 2010: New aeromagnetic and gravity compilations from Norway and adjacent areas – methods and applications. 7th Petroleum Conference Proceedings, in press.
- Ormaasen, D.E. 1976: Geochemistry and petrology of the mangeritic rocks in Lofoten-Vesterålen Cand. real./M.Sc. thesis, University of Oslo.
- Osmundsen, P.T., Sommaruga, A., Skilbrei, J.R. & Olesen, O. 2002: Deep structure of the Mid Norway rifted margin. *Norwegian Journal of Geology* 82, 205-224.
- Pascal, C., + 11 co-authors 2008: HeatBar progress report 2008, Basement heat generation and heat flow in the western Barents Sea – importance for hydrocarbon systems. NGU Report 2008.072, 64 pp.
- Pascal, C., Litvinova, T., and Negrov, O.B. 2009: Heat flow of the Barents Sea. In: *Geological History of the Barents Sea*, Smelror, M., et al. (Eds.), Geological Survey of Norway, Trondheim.
- Pearce, J.A. & Cann, J.R. 1973: Tectonic setting of basic volcanic rocks determined using trace element analyses. *Earth and Planetary Science Letters* 19, 290-300.
- Powell, W.G., Chapman, D.S., Balling N., & Beck A.E. 1988: Continental heat flow density, in *Handbook of Terrestrial Heat-Flow Density Determination*, R. Haenel, L. Stegena, and L. Rybach (eds.), 167-222, Kluwer Acad.
- Raade, G. 1973: Distribution of radioactive elements in the plutonic rocks of the Oslo region [Hovedoppgave/M.Sc. thesis], Universitetet i Oslo, 162 pp.
- Ramberg, I.B. & Smithson, S.B. 1975: Geophysical Interpretation of Crustal Structure along the Southeastern Coast of Norway and Skagerrak. *GSA Bulletin* 86(6), 769-774.
- Rath, V. & Mottaghy, D. 2007: Smooth inversion for ground surface temperature histories: estimating the optimum regularization parameter by generalised crossvalidation, *Geophysical Journal International*, 171, 1440–1448.
- Ritter, U., Zielinski, G.R., Weiss, H.M., Zielinski, R.L.B., & Sættem, J. 2004: Heat flow in the Vøring Basin, Mid-Norwegian Shelf. *Petroleum Geoscience* 10, 353-365.
- Ritzmann, O. & Faleide, J.I. 2007: The Caledonian basement of the western Barents Sea. *Tectonics*, 26, doi:10.1029/2006TC002059.
- Ritzmann, O., Maercklin, N., Faleide, J.I., Bungum, H., Mooney, W.D. & Detweiler, S.T. 2007: A three-dimensional geophysical model of the crust in the Barents Sea region: Model construction and basement characterization. *Geophysical Journal International* 170, 417-435.

- Roberts, D. 1985: The Caledonian fold belt in Finnmark: A synopsis. *Norges geologiske undersøkelse bulletin 403*, 161-177.
- Roberts, D. 2007: Palaeocurrent data from the Kalak Nappe Complex, northern Norway: a key element in models of terrane affiliation. *Norwegian Journal of Geology 87*, 319-328.
- Roberts, R. J., Corfu, F., Torsvik, T. H., Ashwal, L. D. & Ramsay, D. M. 2006: Short-lived mafic magmatism at 560-570 Ma in the northern Norwegian Caledonides: U-Pb zircon ages from the Seiland Igneous Province. *Geological Magazine*.
- Roberts, D., Davidsen, B. & Slagstad, T., 2008, Detrital zircon age record of platformal and basal Neoproterozoic sandstones from Varanger Peninsula, North Norway: a preliminary study, abstract at EGU 2008, Vienna.
- Robins, B. 1998: The mode of emplacement of the Honningsvåg Intrusive Suite, Magerøya, northern Norway. *Geological Magazine 135*, 231-244.
- Robins, B. & Often, M. 1996: The Seiland Igneous Province, North Norway. Field Trip Guidebook, IGCP project 336, NGU Report 96.127.
- Rybach, L. 1988: Determination of heat production rate. In Hänel, R., L. Rybach & L. Stegena (eds.) *Handbook of Terrestrial Heat-Flow Determination*. Dordrecht, Kluwer Academic Publishers, 125-142.
- Sandiford, M. & McLaren, S. 2002: Tectonic feedback and the ordering of heat producing elements within the continental lithosphere. *Earth and Planetary Science Letters 204*, 133-150.
- Sandiford, M., McLaren, S. & Neumann, N. 2002: Long-term thermal consequences of the redistribution of heat-producing elements associated with large-scale granitic complexes. *Journal of Metamorphic Geology 20*, 87-98.
- Sanner, S. 1995: Et seismisk hastighetsstudium i Barentshavet Cand. real./M.Sc. thesis, University of Oslo.
- Siedlecka, A. & Roberts, D. 1996: Finnmark Fylke. Berggrunnsgeologi, M 1:500,000, Norges geologiske undersøkelse.
- Siedlecka, A., Nystuen, J. P., Englund, J. O. & Hossack, J. R. 1987: Lillehammer - berggrunnskart M. 1:250,000, Norges geologiske undersøkelse.
- Siedlecka, A., Iversen, E., Krill, A. G., Lieungh, B., Often, M., Sandstad, J. S. & Solli, A. 1985: Lithostratigraphy and correlation of the Archean and Early Proterozoic rocks of Finnmarksvidda and the Sørvaranger district. *Norges geologiske undersøkelse Bulletin 403*, 7-36.
- Sigmond, E.M.O. 1998: Geologisk kart over Norge. Berggrunnsgeologisk kart ODDA, M 1: 250 000. *Norges geologiske undersøkelse, Trondheim*.
- Skilbrei, J.R. 1991: Interpretation of depth to the magnetic basement in the northern Barents Sea (south of Svalbard). *Tectonophysics 200*, 127-141.
- Skilbrei, J.R.. 1995: Aspects of the geology of the southwestern Barents Sea from aeromagnetic data. *NGU Bulletin 427*, 64-67.
- Skilbrei, J.R. & Olesen, O. 2005: Deep structure of the Mid-Norwegian shelf and onshore-offshore correlations: Insight from potential field data. In: B.T.G. Wandås, E.A. Eide, F. Gradstein, & J.P. Nystuen (Eds), *Onshore-Offshore relationships on the North Atlantic Margin*. Norwegian Petroleum Society (NPF), Special Publication 12, 43-68.
- Skilbrei, J.R., Skyseth, T. & Olesen, O. 1991: Petrophysical Data and Opaque Mineralogy of High-Grade and Retrogressed Lithologies - Implications for the Interpretation of Aeromagnetic Anomalies in Northern Vestranden, Central Norway. *Tectonophysics 192*, 21-31.

- Skilbrei J.R., Kihle O., Olesen O., Gellein J., Sindre A., Solheim D. & Nyland B. 2000: Gravity anomaly map Norway and adjacent ocean areas, 1:3 Million. Geological Survey of Norway (NGU), Trondheim.
- Skilbrei, J.R., Olesen, O., Osmundsen, P.T., Kihle, O., Aaro, S. & Fjellanger E. 2002: A study of basement structures and onshore-offshore correlations in Central Norway. *Norwegian Journal of Geology* 82, 263-279.
- Skår, Ø. & Pedersen, R.B. 2003: Relations between granitoid magmatism and migmatization: U-Pb geochronological evidence from the Western Gneiss Complex, Norway. *Journal of the Geological Society of London* 160, 935-946.
- Slagstad, T. 2008: Radiogenic heat production of Archaean to Permian geological provinces in Norway. *Norwegian Journal of Geology* 88, 149-166.
- Slagstad, T., Culshaw, N.G., Jamieson, R.A. & Ketchum, J.W.F. 2004: Early Mesoproterozoic tectonic history of the southwestern Grenville Province, Ontario: Constraints from geochemistry and geochronology of high-grade gneisses. In: Tollo, R. P., L. Corriveau, J. McLelland & M. J. Bartholomew eds. *Proterozoic tectonic evolution of the Grenville orogen in North America*. Geological Society of America, Memoir 197, 209-241.
- Slagstad, T., Jamieson, R.A. & Culshaw, N.G. 2005: Formation, crystallisation, and migration of melt in the mid-orogenic crust: Muskoka domain migmatites, Grenville Province, Ontario. *Journal of Petrology* 46, 893-919.
- Slagstad, T., Melezhik, V. A., Kirkland, C. L., Zwaan, K. B., Roberts, D., Gorokhov, I. M. & Fallick, A. E. 2006: Carbonate isotope chemostratigraphy suggests revisions to the geological history of the West Finnmark Caledonides, North Norway. *Journal of the Geological Society of London* 163, 277-289.
- Slagstad, T., Barrère, C., Davidsen, B. & Ramstad, R.K. 2008: Petrophysical and thermal properties of pre-Devonian basement rocks on the Norwegian continental margin. *Geological Survey of Norway Bulletin*, 448, 1-6.
- Sturt, B. A., Pringle, I. R. & Roberts, D. 1975: Caledonian nappe sequence of Finnmark, northern Norway and the timing of orogenic deformation and metamorphism. *Geological Society of America Bulletin* 86, 710-718.
- Sundvor, E., Eldholm, O., Gladchenko, T.P. & Planke, S. 2000: Norwegian–Greenland Sea thermal field. In: Nøttvedt, A., Larsen, B.T., Gabrielsen, R.H., Olaussen, S., Brekke, H. & Tørudbakken, B. (eds) *Dynamics of the Norwegian Margin*. Geological Society, London, Special Publications, 167, 397–410.
- Tsikalas, F. 1992: *A study of seismic velocity, density and porosity in Barents Sea wells (N. Noway)* [Hovedoppgave/M.Sc. thesis], Universitetet i Oslo.
- Zwaan, K. B. & Roberts, D. 1978: Tectonostratigraphic succession and development of the Finnmarkian nappe sequence, North Norway. *Norges geologiske undersøkelse* 343, 53-71.
- Åm, K. 1975: Aeromagnetic basement complex mapping north of latitude 62 N, Norway. *Norges geologiske undersøkelse* 316, 351-374.





## 10 APPENDIX A

### **Detrital zircon age record of platformal and basinal Neoproterozoic sandstones from Varanger Peninsula, North Norway: a preliminary study**

*D. Roberts, B. Davidsen and T. Slagstad*

*Geological Survey of Norway, 7491 Trondheim, Norway.*

Neoproterozoic to Cambrian sedimentary assemblages on Varanger Peninsula, northern Norway, are separated into platformal and basinal domains along the NW-SE-trending, Trollfjorden-Komagelva Fault Zone (TKFZ). Platformal successions southwest of the fault range from autochthonous to allochthonous and comprise the fluvial to shallow-marine Vadsø, Tanafjord and Vestertana groups. Northeast of the fault zone, successions are allochthonous and most have been involved in modest dextral strike-slip translation along the fault. They comprise the Barents Sea Group, the unconformably overlying Løkvikfjellet Group, and slightly higher-grade rocks of the Tanahorn Nappe.

In an ongoing detrital zircon provenance study of several formations from Varanger Peninsula and adjacent areas, we have carried out LA-ICP-MS, U-Pb analyses on five samples from four representative sandstone units. One formation, the inter-tillite, Vendian, Nyborg Formation, is from south of the TKFZ, and two (Båsnæring and Sandfjord formations) from north of the fault. The fourth sandstone unit analysed is from the Berlevåg Formation in the Tanahorn Nappe. Preliminary results obtained from these formations show the following main features of the detrital zircon populations:

1. *Nyborg Formation, Tanafjord Group (sample NY2)*: one group dominates the probability plot at 2.0-1.7 Ga with a minor spread of mostly discordant grains between 3.0 and 2.5 Ga.
2. *Båsnæring Formation, Barents Sea Group (BÅS1; two samples)*: a multimodal spread extends from c. 2.1 to 1.0 Ga with three peaks of concordant grains at around 1.80-1.65, 1.45-1.40 and 1.2-1.0 Ga, and subsidiary peaks at c. 2.0 and 2.9-2.6 Ga.
3. *Sandfjord Formation, Løkvikfjellet Group (SF2)*: two principal groups at 2.0-1.7 and 2.9-2.6 Ga with a subsidiary group ranging from 1.6 to c. 1.0 Ga.
4. *Berlevåg Formation, Tanahorn Nappe (BLV1)*: one major group at 1.9-1.7 Ga and a minor group at 2.9-2.6 Ga.

A feature common to all these analyses is the presence of a detrital population peak at c. 2.0-1.7 and a subsidiary peak at 2.9-2.6 Ga. From the known stratigraphical and sedimentological picture, with palaeocurrent data indicating that detritus in both the pericratonic and basinal (submarine fan and deltaic) domains came largely from southerly source regions, this is consistent with derivation from the Fennoscandian Shield. Northern parts of this craton are dominated by Neoproterozoic complexes and, just to the south, also by terranes of Palaeoproterozoic age deformed during the 1.9-1.8 Ga Svecofennian orogeny. The fact that even the Berlevåg Formation (in a thrust sheet correlated with the Kalak Nappe Complex) shows these typically Baltican detrital populations are of special interest here.

An apparent anomaly in our data is seen in the subsidiary peaks ranging from c. 1.45 to c. 1.0 Ga in formations north of the TKFZ, in the dextrally translated, allochthonous basinal domain. Such Mesoproterozoic ages have hitherto not been reported from the exposed basement of this northern part of the Fennoscandian Shield, and could be attributed to Laurentian sources. However, it is perfectly conceivable that rock complexes of Mesoproterozoic age (associated with Grenvillian magmatism) may be present in the *concealed* Baltican basement, i.e., beneath the Caledonian nappes and parts of the continental shelf, and thus provided some of the detritus in the fluvial to deltaic formations now forming the allochthon northeast of the TKFZ. An alternative interpretation would be that parts of the hidden pericraton beneath the nappes may belong to an exotic microcontinental block welded onto Baltica prior to the inception of Neoproterozoic basinal sedimentation.